

DISSERTATION

DESIGN AND APPLICATION OF STRONGLY REDUCING PHOTOREDOX CATALYSTS
FOR SMALL MOLECULE AND MACROMOLECULAR SYNTHESIS

Submitted by

Ryan Michael Pearson

Department of Chemistry

In partial fulfillment of the requirements

For the Degree of Doctor of Philosophy

Colorado State University

Fort Collins, Colorado

Summer 2019

Doctoral Committee:

Advisor: Garret Miyake

Andy McNally
Grzegorz Szamel
Yan (Vivian) Li

Copyright by Ryan Michael Pearson 2019

All Rights Reserved

ABSTRACT

DESIGN AND APPLICATION OF STRONGLY REDUCING PHOTOREDOX CATALYSTS FOR SMALL MOLECULE AND MACROMOLECULAR SYNTHESIS

The synthesis and application of new families of strongly reducing organic photoredox catalysts are described in this dissertation. These compounds provide a platform on which catalytically relevant properties including redox potentials and absorption profiles can be tuned, as well as predicted *in silico*. The critical photophysical and electrochemical characteristics have been established for both dihydrophenazine and phenoxazine catalysts which enable their ability to be used as green alternatives to commonly used transition metal photocatalysts. Specifically, phenoxazines have been utilized to mediate organocatalyzed atom transfer radical polymerization (O-ATRP) for the production of well-defined polymers using visible light. To this end, a catalyst system able to synthesize acrylic polymers with predictable molecular weights and dispersities less than 1.10 has been developed. In addition, dihydrophenazines were shown to mediate trifluoromethylation and atom transfer radical addition reactions, while phenoxazines were able to mediate C-N and C-S cross coupling reactions in the presence of a nickel co-catalyst.

TABLE OF CONTENTS

ABSTRACT.....	ii
Chapter 1 – Introduction	1
Motivations.....	1
References.....	6
Chapter 2 – Synthesis and Characterization of Core-Modified Benzo[ghi]perylene Monoimides.....	7
Overview.....	7
Introduction	7
Results and Discussion	9
Conclusion.....	14
Experimental.....	14
References.....	21
Chapter 3 – Organocatalyzed Atom Transfer Radical Polymerization Using N-Aryl Phenoxazines as Photoredox Catalysts	24
Overview.....	24
Introduction	24
Results and Discussion	28
Conclusion.....	42
Experimental.....	42
References.....	83
Chapter 4 – Impact of Light Intensity on Control of Photoinduced Organocatalyzed Atom Transfer Radical Polymerization with Phenoxazine Catalysts	88
Overview.....	88
Introduction	88
Results and Discussion	92
Conclusion.....	96
Experimental.....	96
References.....	102
Chapter 5 – Highly Reducing Organic Photocatalysts for Small Molecule Synthesis	107
Overview.....	107
Introduction	108

Results and Discussion	110
Conclusion.....	119
Experimental.....	119
References.....	167
Chapter 6 – Summary	174
References.....	177
Appendix I – List of Publications by RMP.....	178

Chapter 1 – Introduction

This dissertation is written in a journal-format style. The chapters discussed herein are modeled off of first-authored publications that have appeared in the *Journal of the American Chemical Society*, *Macromolecules*, *Chemistry-A European Journal*, and a manuscript that has been prepared for future submission. In the broadest sense, the theme of this dissertation is toward the synthesis and design of macromolecules and small molecules as well as their application. The scope of topics covered in this thesis are presented in four chapters:

1. Synthesis and Characterization of Core-Modified Benzo[ghi]perylene Monoimides
2. Organocatalyzed Atom Transfer Radical Polymerization Using *N*-Aryl Phenoxazines as Photoredox Catalysts
3. Impact of Light Intensity on Control of Photoinduced Organocatalyzed Atom Transfer Radical Polymerization with Phenoxazine Catalysts
4. Highly Reducing Organic Photocatalysts for Small Molecule Synthesis

Motivations

In chapter 2, the synthesis and characterization of a new class of perylene derivatives is described. This work was inspired by our group's seminal work from 2014 which used perylene in one of the first reported organo-catalyzed atom transfer polymerization mediated by a visible-light absorbing photocatalyst.¹ To expand on this work, novel and previously reported perylene diimides (PDIs) were synthesized to investigate this family of compounds as candidates for O-ATRP. We hypothesized that through modification of the perylene "bay" region, or one of the two imides, the redox potentials could be tuned and catalyst loading (due to altered solubility) could be changed from the parent perylene compound through addition of various functional groups. To

this end, multiple PDIs were synthesized (Figure 1.1). Ultimately, these PDIs were unsuccessful in controlling O-ATRP, which we posit is due to the strong withdrawing effects the imide group on the perylene core, resulting in a less strongly reducing excited state for these catalysts which decreases the thermodynamic driving force for initiation and activation in O-ATRP.

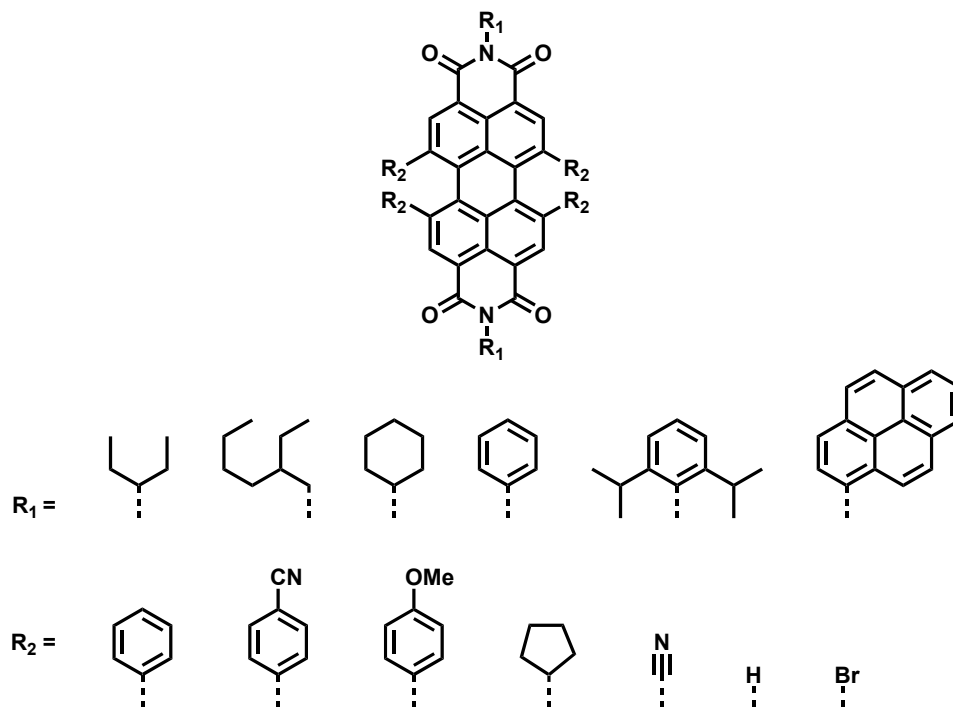


Figure 1.1. Perylenediimides synthesized for use in O-ATRP

The poor performance of the PDIs led us to hypothesize that other polyaromatic hydrocarbons (PAHs) with more strongly reducing excited states may be required for efficient polymerization via O-ATRP. For example, we envisioned that application of coronene, which has a higher triplet reduction potential (-1.37 V vs. SCE) than perylene (-0.76 V vs. SCE), could offer insight into the importance of excited state reduction potential for O-ATRP catalysts. Surprisingly, application of coronene led to the synthesis of acrylic polymers with low dispersities (<1.05), rivaling the performance of our best catalysts at the time. However, coronene catalyzed O-ATRP

with low initiator efficiency (< 30%) and relatively slow polymerization rates (>24 hours) (Figure 1.2).

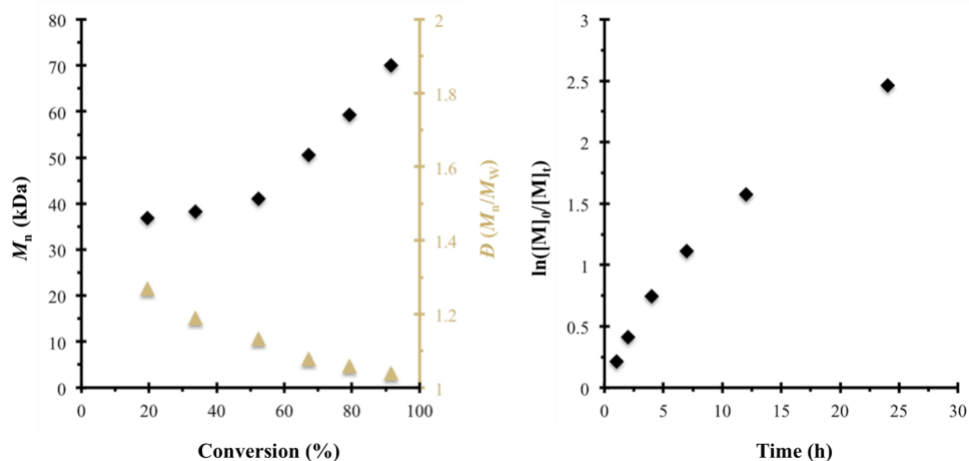


Figure 1.2. Plot of M_n (black diamonds) and \bar{D} (gold triangles) as a function of monomer conversion for the O-ATRP of Methyl Methacrylate by coronene using white light LEDs (left). Plot of the natural log of monomer consumption as a function of time for the O-ATRP catalyzed by coronene using white-light LEDs (right).

While we were excited with the improvement over the perylene system, we wanted to find a system that enabled us to systematically tune the photophysical and redox properties to investigate their effects on O-ATRP. As such, it was hypothesized that benzo[ghi]perylene monoimide derivatives would provide similar handles for chemical functionalization compared to the PDIs without the presence of the diimide functionality, which was observed to lessen the reducing power of the excited state. A new synthetic route was devised to selectively brominate the benzo[ghi]perylene core to install electron withdrawing and donating groups via cross-coupling reactions, similar to our work with PDIs. The synthesis of these compounds is highlighted in chapter 2. The performance of these catalysts was similarly as poor as their PDI counterparts which motivated us to explore drastically different chemical scaffolds.

In pursuit of organic photoredox catalysts with strongly reducing excited states, we report *N*-aryl phenoxazines as photocatalysts for O-ATRP (Chapter 3). In this investigation, we systematically tune the redox properties of the *N*-aryl phenoxazines and use density functional theory to predict the geometries and charge densities of the ground and excited states which further informed our catalyst design. Based on trends observed with the phenoxazine catalysts, and similar families of photocatalysts such as *N,N*-diarylphenazines, and *N*-aryl phenothiazines, we demonstrated the importance of O-ATRP catalysts to access intramolecular charge transfer excited states and exhibit low reorganization energies between the ground state, excited state, and radical cation species for excellent performance in O-ATRP. Modification of the phenoxazine core with aryl groups at the 3- and 7- positions enabled the absorption profiles of these catalysts to red-shift from absorbing exclusively in the UV regime to the visible light regime as well as increasing the molar absorptivity 3-fold.

Improving the ability of phenoxazine catalysts to absorb visible light through core modification was partially responsible for a significant improvement in the catalytic performance of these molecules in O-ATRP compared with their parent compounds. As such, we were interested in whether the performance of this catalyst could withstand modification of the photo reactors used. Chapter 4 addresses how the intensity of light impacts control over O-ATRP. In this study perylene and phenoxazine photocatalysts were employed in O-ATRP using a photo reactor that could be systematically dimmed. While the original co-first authored work between Ryan Pearson and Matthew Ryan discussed a significant improvement of the original perylene system through a systematic study of the mechanism and the active catalyst species in O-ATRP, only the work on phenoxazines is reported in this dissertation.

After our group demonstrated that *N*-aryl phenoxazines and *N,N*-diaryl dihydrophenazines effectively mediate O-ATRP with better control over the polymer molecular weight, initiator efficiency, and dispersity than ruthenium- and iridium- containing transition metal catalysis, we turned to implementing these photocatalysts for small molecule syntheses (chapter 5). To do this, we chose previously reported reactions such as a trifluoromethylation and atom transfer radical addition reported by Stevenson and co-workers, as well as dual-catalytic system developed independently by the MacMillan and Johannes groups.

Chapter 6 provides a brief summary of the work presented in this dissertation, as well as work where the author of this dissertation is not the lead author. Lastly, vertical themes and future directions are discussed. For reference, a list of publications and oral presentations as a result of work completed during the course of this dissertation can be found in Appendix I and II respectively.

References

- (1) Miyake, G.; Theriot, J. *Macromolecules*, 2014, 47, 23, 8255-8261.

Overview

The synthesis of 6,8,11 tri-substituted benzo[ghi]perylene monoimides was carried out in a 4-step synthesis with up to a 56% total yield providing a new scaffold for highly tunable perylene derivatives. A cyclization, imidization, and bromination were performed to synthesize the tribrominated benzoperylene core from perylene. Next, a Suzuki-Miyaura coupling was performed to install aryl substituents and obtain the target benzoperylene derivatives. DFT calculations were performed to visualize the HOMO and LUMO orbitals of these molecules, which was predictive of intramolecular charge transfer for all species in the excited state. Charge transfer characteristics were confirmed experimentally via large solvatochromic shifts, which in the case of the derivative possessing 4-methoxy phenyl substituents spanned an emission of 518-613 nm (0.37 eV) in hexanes to DMSO when excited with 365nm light. With the addition of biphenyl groups, molar absorptivity at the maximum wavelength of absorbance, was increased from 51,000 M⁻¹ cm in the parent compound to 59,600 M⁻¹ cm. Overall, installation of the aryl groups led to an increase in absorption of visible light and higher fluorescence quantum yields. The synthesis reported here provides entry to a new perylene scaffold that could be applied for a broad range of imaging, display, or electronic applications.

Introduction

Perylene dyes have garnered significant attention over the past century due to their chemical, thermal, and photophysical properties¹ which allow for their successful application in industrial pigments,² laser dyes,³ organic LEDs,⁴ light harvesting solar cells,⁵ liquid crystals,⁶

biological markers,⁷ supramolecular architectures,⁸ and photoredox catalysis.⁹ In particular, perylene diimides (PDIs) have become an intensely studied class of perylene dyes due to increased solubility and readily modifiable structure.¹⁰ For instance, attachment of branched alkyl chains or aromatic groups to the *N*-position of the imide group(s) enhances solubility.¹¹ Additionally, the imide group allows for a tether point to attach macromolecular or biologically relevant compounds that can then be used in fluorescence imaging applications.¹² Lastly, the PDI's perylene core, typically referred to as the “bay region” (1,6,7,12 positions), can be broadly modified to add substituents which greatly alter the photophysical, optical, and electrochemical properties.¹³

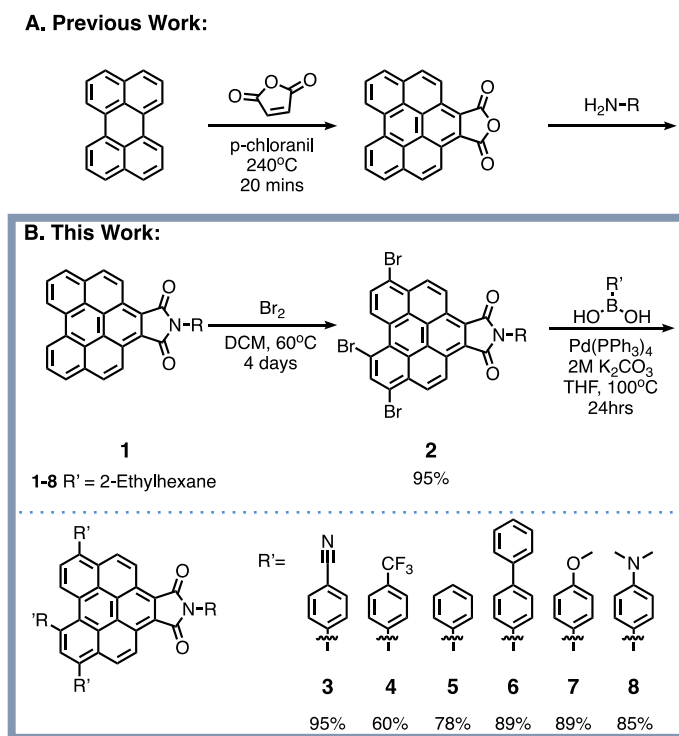


Figure 2.1. (A) Previous work toward the synthesis of benzo[ghi]perylene imides. (B) This work toward the synthesis of tri-bromo and tri-aryl substituted BPIs.

Benzo[ghi]perylene monoimides (BPIs) constitute a lesser-studied subset of perylene derivatives with few variants explored to date.¹⁴ Due to the interesting photophysical characteristics of BPIs and its structural parallels to PDIs, we were motivated to develop a method

to modify the BPI core that would enable tuning of the photophysical and electrochemical properties of these molecules. To the best of our knowledge, there have been no reports for the direct substitution of the BPI core. Herein, we report the selective bromination at the 6-, 8-, and 11- positions on the benzoperylene core, which provides a synthetic approach for modification of BPIs and allows for selective tuning of the photophysical properties.

Results and Discussion

Benzo[*ghi*]perylene-1,12-dicarboxylic anhydride was synthesized *via* a benzogenic oxidative Diels-Alder reaction between perylene and maleic anhydride. The resulting benzoperylene anhydride can undergo a condensation reaction with a primary amine to form a BPI (Figure 2.1A).^{14d} Here, 2-ethylhexyl amine was chosen due to the known ability of this motif to improve the solubility of molecules.¹⁵ To enable core functionalization, bromide groups were installed at the 6-, 8-, and 11- positions of the benzoperylene core by reacting the BPI with elemental bromine to synthesize **2** in a 91% yield (Figure 2.1B). This bromination was reliant upon imide formation, as it was unsuccessful on the parent anhydride. Lastly, Suzuki coupling was carried out with five different aryl boronic acids to give a family of BPIs bearing electron withdrawing groups (EWG): 4-cyanophenyl (**3**) and 4-trifluoromethylphenyl (**4**), neutral groups: phenyl (**5**) and biphenyl (**6**), as well as electron donating groups (EDG): 4-methoxy phenyl (**7**) and 4-(dimethylamino)phenyl (**8**). Cross coupling yields remained consistently high (60-95%) despite strain on the benzoperylene core imposed by the newly installed substituents (Figure 2.2). Groups at the 6- and 11- positions were not predicted to induce any significant strain to the BPI core.

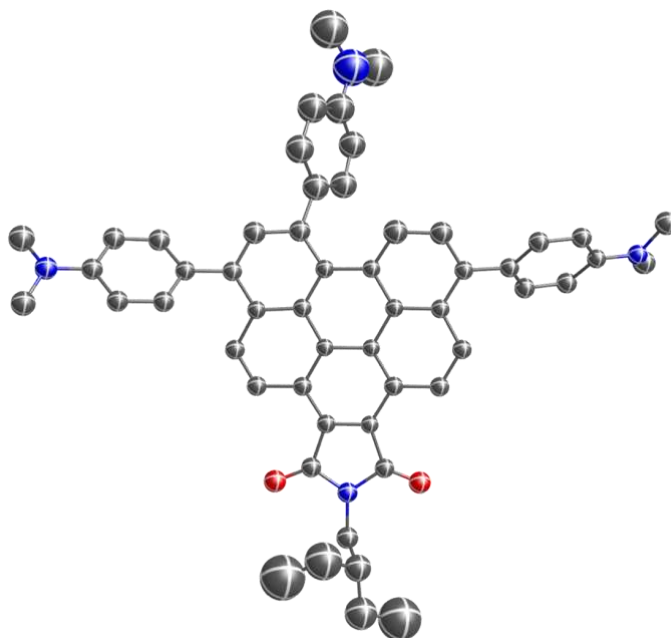


Figure 2.2. *Crystal structure of (8)*

Density functional theory calculations were then used to gain insight into the photophysical properties of these BPIs. The highest occupied molecular orbitals (HOMOs) and lowest unoccupied molecular orbitals (LUMOs) were visualized using a single point energy calculation (M06/6-31G(d,p)) (Figure 2.2B). Similar to the case of **1**, compounds **3-7** contain their HOMO residing on the benzoperylene core donor moiety and the LUMO localized to the maleimide acceptor moiety. The spatial separation of the HOMO (donor) and LUMO (acceptor) orbitals in the ground state is predictive of intramolecular charge-transfer (IMCT) a trait commonly seen in OLEDs and organo photoredox catalysis.¹⁶ This phenomenon can be seen experimentally by fluorescence studies, wherein the excited state emission is solvatochromically red-shifted with respect to increasing stabilization of the more polar IMCT species from more polar solvents.¹⁷

The newly synthesized BPIs were characterized using UV-Vis and fluorescence spectroscopy to study the effects of aryl substitution on the photophysical properties of these

molecules. The absorbance was redshifted in all aryl substituted BPIs compared to the parent molecule, likely due to the lowering of the LUMO energy from the net increased π conjugation (Figure 2.3A). The maximum wavelength of absorption ($\lambda_{\text{Max abs.}}$) was red-shifted by 15 nm (0.15 eV) from that of the parent compound **1** (340nm) to the most redshifted species **6** & **7** (355nm). Molar absorptivity (ϵ_{max}) at the $\lambda_{\text{max abs.}}$ of phenyl substituted **5** ($\epsilon_{\text{max}} = 3,800 \text{ M}^{-1} \text{ cm}$) was less than that of **1** ($\epsilon_{\text{max}} = 51,000 \text{ M}^{-1} \text{ cm}$). Compared to **5**, compounds **3** and **4** ($\epsilon_{\text{max}} = 53,400 \text{ M}^{-1} \text{ cm}$, and $48,700 \text{ M}^{-1} \text{ cm}$, respectively) bearing aryl EWG possess higher ϵ_{max} values whereas **7** ($\epsilon_{\text{max}} = 40,400 \text{ M}^{-1} \text{ cm}$), bearing an EDG, had a ϵ_{max} value less than **5**. The increased conjugation provided by the biphenyl substituents in **6** provided the derivative with the largest molar absorptivity ($\epsilon_{\text{max}} = 59,600 \text{ M}^{-1} \text{ cm}^{-1}$).

Substitution of the parent molecule with aryl groups consistently improved the ability of compounds **3-7** to absorb lower energy visible light (>400 nm) (Figure 2.3 Table). Two local maxima ($\lambda_{\text{Local Max Abs}}$) in and near the visible regime (390-425 nm and 481-507 nm) were compared between parent compound **1** and aryl substituted compounds **3-7**. At the first local maximum ($\lambda = 390\text{-}425 \text{ nm}$), addition of phenyl groups increased the molar absorptivity at the local maximum ($\epsilon_{\text{Local max}}$) by 36% and red-shifted the absorbance 0.21eV from **1** ($\lambda = 390 \text{ nm}$, $\epsilon_{\text{local max}} = 15,100 \text{ M}^{-1} \text{ cm}$) to **5** ($\lambda = 417 \text{ nm}$, $\epsilon_{\text{local max}} = 20,500 \text{ M}^{-1} \text{ cm}$). At the second most red-shifted local maximum ($\lambda = 481\text{-}507 \text{ nm}$) a similar increase of 23% was observed in the $\epsilon_{\text{Local max}}$ in addition to a red-shift of 0.10 eV from **1** ($\lambda = 481 \text{ nm}$, $\epsilon_{\text{local max}} = 5,700 \text{ M}^{-1} \text{ cm}$) to **5** ($\lambda = 501 \text{ nm}$, $\epsilon_{\text{local max}} = 7,000 \text{ M}^{-1} \text{ cm}$). Similar redshifts and greater increases in $\epsilon_{\text{Local max}}$ were seen with compounds **3**, **4**, **6**, and **7**.

Compound	λ_{Max} Absorption (nm)	ϵ_{Max} ($\text{M}^{-1} \text{cm}^{-1}$)	$\lambda_{\text{Local Max}}$ Absorption (nm)	ϵ_{Max} ($\text{M}^{-1} \text{cm}^{-1}$)	$\lambda_{\text{Local Max}}$ Absorption (nm)	ϵ_{Max} ($\text{M}^{-1} \text{cm}^{-1}$)	$\lambda_{\text{Max Emission}}$ (Hexanes) (nm)	$\lambda_{\text{Max Emission}}$ (Chloroform) (nm)	$\lambda_{\text{Max Emission}}$ (DMSO) (nm)	Φ_f^a
1	340	51,100	390	15,100	481	5,700	470	523	532	0.15
2	347	53,600	406	22,200	485	5,500	-----	-----	-----	-----
3	352	53,400	419	26,000	489	7,500	485	539	548	0.34
4	351	48,700	415	22,600	492	6,700	487	541	554	0.25
5	352	43,800	417	20,500	501	7,000	501	566	577	0.18
6	355	59,600	423	34,000	505	9,500	508	579	588	0.26
7	355	40,400	425	23,300	507	7,700	518	595	613	0.21

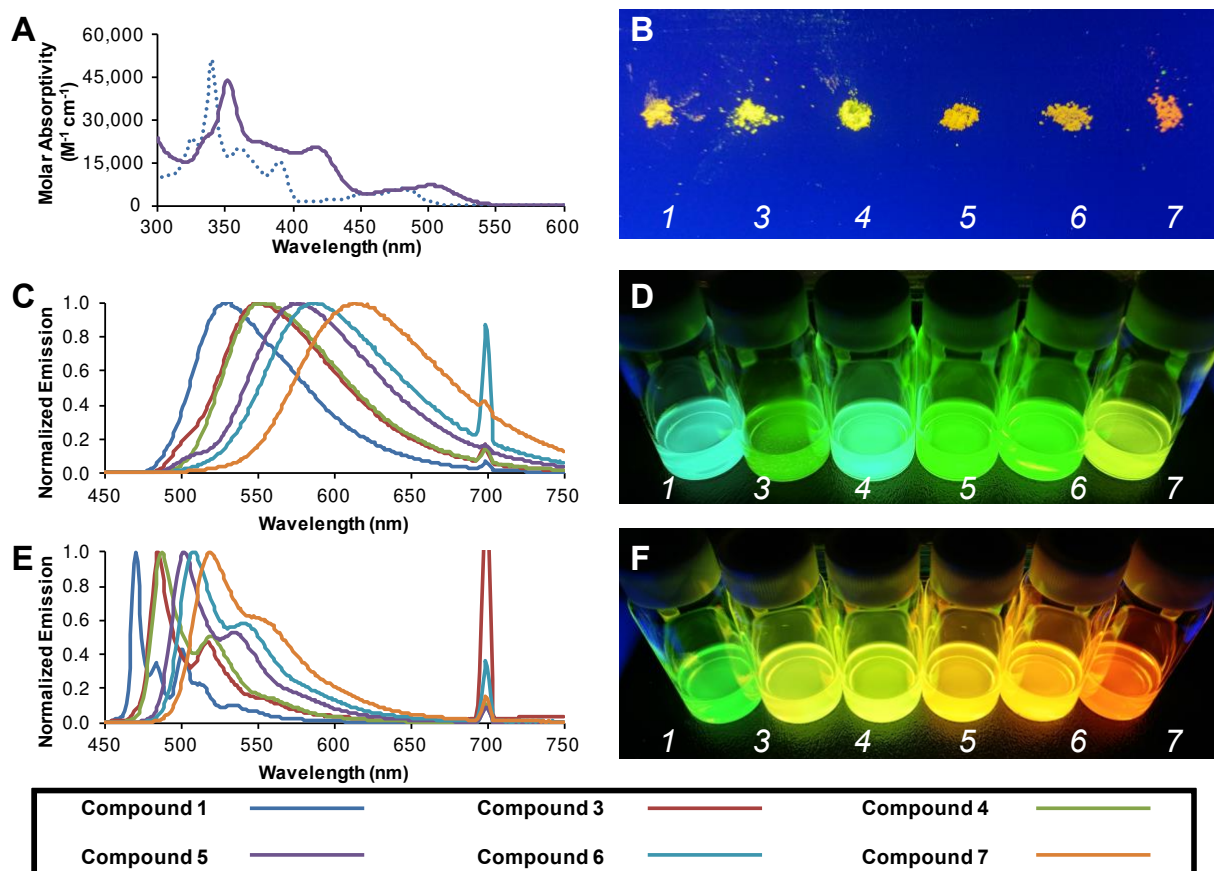


Figure 2.3. (Table) Emission data obtained from excitation with 355 nm light in chloroform. ^aQuantum yields obtained by comparing a fluorescence standard in 0.10M NaOH against compounds **1**, **3-7** were taken in chloroform excited at 340nm (see SI). (A) Molar absorptivity vs. wavelength for compounds **1** (dotted blue line) and **5** (solid purple line) taken in chloroform. Photographs of compounds **1** & **3-7** in the solid state on a matte black surface (B), dissolved in 5 mL of hexanes in a 20 mL scintillation vial (D), and dissolved in 5 mL of DMSO in a 20 mL scintillation vial (F), all of which are excited by 365 nm light. Emission spectra of compounds **1**

& **3-7** taken in hexanes with dielectric constant (ϵ) = 1.882 (C), and in DMSO, ϵ = 46.70, (E) excited at 350 nm.

A previous report, which investigated a non-core-substituted BPI with a different *N*-alkyl group (1-hexylheptyl), showed nearly identical results to **1**, with a solvatochromic shift of 62 nm (Δ = 0.30 eV) from the maximum wavelength of emission ($\lambda_{\text{max emission}}$) in hexanes (470 nm) to DMSO (532 nm).^{14d} After the installation of bromine onto parent compound **1**, **2** no longer fluoresced. A larger bathochromic shift is seen in the emission of compounds **3-7** in hexanes, with dielectric constant (ϵ) = 1.882 (Figure 2.3 C and D), to DMSO, with ϵ = 46.70 (Figure 2.3 E and F). Similar to the absorption profiles, core modifications red-shifts the emission of the derivatives relative to **1**, regardless of EDG or EWGs on the aryl substituents. The two derivatives bearing EWGs exhibit the smallest red-shift in their emission compared to **1**. In DMSO compared to **1**, **3** exhibits a change in the maximum wavelength of emission ($\Delta\lambda_{\text{max emission}}$) of 16 nm (0.08 eV) while a $\Delta\lambda_{\text{max emission}}$ of 22 nm (0.10 eV) is observed for **4**. In contrast, the derivative bearing an EDG (**7**) exhibits the most red-shifted emission with a $\Delta\lambda_{\text{max emission}}$ from **1** of 95nm (0.32 eV) in DMSO. It is possible that aryl groups on the core stabilize the IMCT excited state yielding a lower energy, red-shifted emission spectra. Additionally, these compounds were observed to emit in the solid state (Figure 2.3B), a phenomenon which has seen successful use in OLEDs, data recording storage, and security printing.¹⁸

Using the comparative method to measure the fluorescence quantum yields (ϕ_f), compounds **1**, **3-7** were dissolved in chloroform and compared against a fluoroscene standard which was dissolved in 0.1M NaOH.¹⁹ With the addition of phenyl groups, the ϕ_f improved by 20% relative to non-core modified **1** and in some cases, such as **3**, gave an increase in the ϕ_f from 0.15 to 0.34. Overall, addition of aryl groups increased the ϕ_f of the BPIs.

Conclusion

In sum, the BPI core was brominated at the 6-, 8- and 11- positions, allowing for further synthetic manipulations to modulate the photophysical properties of the BPI. Five different aryl groups were installed via a Suzuki cross coupling to yield compounds with larger molar extinction coefficients and fluorescence quantum yields than the parent compound. The HOMO and LUMO orbitals of each of the synthesized compounds was computationally predicted to be spatially separated, which was further confirmed experimentally via fluorescence solvatochromism. Ultimately, the BPIs could be tuned to span an emission profile across 470-613 nm (0.62 eV) wavelengths when dissolved in solvents of different polarity. We foresee that our new synthetic route will enable this class of perylene derivative to find broad use in imaging based applications.

Experimental

Materials and Methods. Perylene and 4-(trifluoromethyl)phenylboronic acid were purchased from TCI. 4-Biphenyl boronic acid was purchased from Oxchem. Maleic anhydride, xylenes, p-chloranil, bromine, phenylboronic acid, and 4-cyanophenylboronic acid were purchased from Alfa Aesar. All other reagents were purchased from Sigma Aldrich. THF was purified using an MBraun MB-SPS-800 solvent purification system and kept under nitrogen atmosphere.

NMR spectra were recorded on a Varian 300 MHz, 400 MHz, or 500MHz NMR Spectrometer as noted for all characterizations. All ^1H NMR are reported in δ units (parts per million – ppm) and were measured relative to the signals found in residual chloroform (7.26 ppm). All ^{13}C NMR were measured relative to CDCl_3 (77.16 ppm). Ultraviolet-visible spectroscopy was performed on a Cary 5000 spectrophotometer using chloroform as the solvent scanning from 200-800 nm at a scan rate of 600 nm/min. Emission spectroscopy was performed on a SLM 8000C

spectrofluorometer using hexanes or DMSO as the solvent. Emission data was collected exciting the compounds near lambda max of 350 nm scanning 400-750nm for hexanes and 400-800nm for DMSO all with an integration time of 0.50 seconds. Fluorescence quantum yield (Φ_f) was obtained in chloroform with the same spectrofluorometer exciting at 340nm. The internal standard used for Φ_f was fluorescein in 0.1M NaOH using the literature value of $\Phi_f = 0.79$.²⁰

Computational Methods. Calculations were performed in CPCM-chloroform. The geometry and frequencies were optimized at M06/6-31+g(d,p), except for compound **6** wherein the frequency was performed with M06/6-31g(d,p) due to the size of the structure. All energies were computed with M06/6-311+g(d,p). Single point energy calculations were performed using M06/6-31g(d,p) to visualize the HOMO/LUMO orbitals.

Synthesis of Substrates

Benzo[ghi]perylene-1,2-dicarboxylic Anhydride The anhydride was synthesized according to a previously reported procedure.^{14d}

2-(2-ethylhexyl)-1H-peryleno[1,12-efg]isoindole-1,3(2H)-dione (1) Benzo[ghi]perylene-1,2-dicarboxylic Anhydride (300 mg, 0.866 mmol, 1.00 eq) and a stir bar was added to a 250 mL round bottom flask followed by 50 mL of DMF. 2-Ethyl-1-hexylamine (0.213 mL, 1.30 mmol, 1.50 eq.) was added and the reaction was heated to 175 °C for 16 hours. After which the reaction was cooled down and 20 mL of concentrated HCl was added to the solution and a yellow-brown solid precipitated from solution. The solid was filtered and then washed with 100 ml of 1M KOH solution, followed by deionized water until a neutral pH was obtained to give an orange powder

(301 mg, 76% yield). A recrystallization can be carried out by dissolving the solid in DCM, adding 10% methanol while the solution is still hot and allowing the solution to cool in the freezer. ^1H NMR (300 MHz, Chloroform-*d*) δ = 8.23-8.16 (m, 4H), 7.61-7.55 (m, 4H), 7.34 (d, J = 9.0 Hz, 2H), 3.60 (d, J = 7.1 Hz, 2H), 1.97-1.85 (m, 1H), 1.55-1.35 (m, 8H), 1.05 (t, J = 7.3 Hz, 3H), 0.98 (t, J = 6.7 Hz, 3H). ^{13}C NMR (300 MHz, Chloroform-*d*) δ = 169.28, 130.55, 128.45, 128.20, 126.20, 124.43, 122.35, 122.21, 121.79, 121.36, 120.22, 41.57, 39.10, 30.88, 28.86, 24.16, 23.33, 14.36, 10.71 DART: Calculated for $\text{C}_{32}\text{H}_{27}\text{NO}_2$ ($[\text{M}+\text{H}^+]$) 458.2115, found 458.2118

6,8,11-tribromo-2-(2-ethylhexyl)-1H-peryleno[1,12-efg]isoindole -1,3(2H)-dione (2). To a 100 mL thick walled flask was added **1** (600 mg, 1.31 mmol, 1.00 eq.) and stir bar. Dichloromethane (DCM) was added to the solids then heated up to 60 °C until the solid was fully dissolved (~40 mL). After which bromine (2.02 mL, 39.3 mmol, 30.0 eq.) was added. The bomb flask was capped and the reaction went from orange to a dark red. After 4 days, the reaction was concentrated and the bromine blown off. The product was recrystallized in DCM and filtered and washed further with hexanes to give a yellow solid (824 mg, 91% yield). ^1H NMR (300 MHz, Chloroform-*d*) δ = 8.42 (d, J = 8.7 Hz, 1H), 8.01 (d, J = 8.9 Hz, 1H), 7.98 (d, J = 8.9, 1H), 7.66 (s, Hz, 1H), 7.45 (d, J = 9.0 Hz, 1H), 7.30 (d, J = 9.0 Hz, 1H), 7.24 (d, J = 8.8 Hz, 1H), 3.56 (d, J = 7.1 Hz, 2H), 1.93-1.77 (m, 1H), 1.55-1.33 (m, 8H), 1.07-0.93 (m, 6H). ^{13}C NMR (75 MHz, Chloroform-*d*) δ = 168.26, 168.17, 138.05, 129.08, 127.39, 127.32, 127.23, 126.64, 124.80, 124.44, 124.29, 123.94, 122.97, 122.84, 122.69, 122.56, 122.46, 122.22, 121.98, 121.71, 121.55, 120.99, 116.33, 42.08, 38.94, 30.85, 28.80, 24.14, 23.35, 14.39, 10.70. HRMS (ESI): Calculated for $\text{C}_{32}\text{H}_{24}\text{Br}_3\text{NO}_2$ ($[\text{M}^+]$) 694.9321, found 694.9332

General Procedure for the Synthesis of TriAryl Substituted BPIs. To a 100 mL storage flask was added **2** (225 mg, 0.324 mmol, 1.00 eq.) and boronic acid (1.95 mmol, 6.00 eq.). The storage flask was put under vacuum and back filled with nitrogen, this process was repeated 2 additional times. After which ~15mL of THF was added followed by 6.2 mL of 2M potassium carbonate solution. The solution was heated to 60 °C for 15 minutes wherein palladium tetrakis (57 mg, 0.0049 mmol, 15% mol) was added in 20mL of THF (the solution turns red immediately upon addition of palladium). The reaction was then heated to 100 °C for 24 hours. DCM was added to the mixture and washed with water 3 times and washed a total of 3 times with water, then brine and dried with MgSO₄. All compounds were purified by recrystallization in DCM/Methanol.

4,4',4''-(2-(2-ethylhexyl)-1,3-dioxo-2,3-dihydro-1H-peryleno[1,12-efg]isoindole-6,8,11-triyl)tribenzonitrile (3). The general procedure was followed exactly using 4-cyanophenylboronic acid (286 mg, 6.00 eq.). After recrystallization in DCM/Methanol the product was filtered and washed sparingly with methanol to give a bright yellow solid (234 mg, 95% yield). ¹H NMR (300 MHz, Chloroform-*d*) δ = 9.37 (d, *J* = 9.3 Hz, 1H), 9.30 (d, *J* = 9.4 Hz, 1H), 8.31-8.25(m, 3H), 7.95 (s, 1H), 7.93-7.71 (m, 12H), 7.61 (d, *J* = 8.3 Hz, 1H), 3.73 (d, *J* = 7.2 Hz, 2H), 1.98 (m, 1H), 1.41 (m, 8H), 0.98 (t, *J* = 7.4 Hz, 3H), 0.90 (t, *J* = 6.8 Hz, 3H). ¹³C NMR (75 MHz, Chloroform-*d*) δ = 169.88, 169.82, 149.34, 144.55, 144.28, 138.10, 137.63, 137.11, 133.78, 132.59, 132.44, 131.15, 131.13, 130.13, 129.44, 129.23, 129.13, 129.08, 128.35, 127.52, 127.37, 127.07, 126.51, 124.75, 124.64, 124.49, 124.38, 123.72, 118.60, 118.52, 112.22, 111.98, 111.82, 42.07, 38.60, 30.66, 28.62, 24.02, 23.04, 14.08, 10.53. HRMS (ESI): Calculated for C₅₃H₃₆N₄O₂ ([M⁺]) 760.2833, found 760.2822

2-(2-ethylhexyl)-6,8,11-tris(4-(trifluoromethyl)phenyl)-1H-peryleno[1,12-efg]isoindole-

1,3(2H)-dione (4). The general procedure was followed exactly using 4-(trifluoromethyl)phenylboronic acid (237.0 mg, 6.00 eq.). The compound was purified with a column eluting with 10% hexanes in DCM. It was then recrystallized in DCM/Methanol, the product was filtered and washed sparingly with methanol to give yellow orange solid (173 mg, 60% yield). ¹H NMR (300 MHz, Chloroform-*d*) δ = 9.10 (d, *J* = 9.3 Hz, 1H), 8.97 (d, *J* = 9.3 Hz, 1H), 8.23 (d, *J* = 8.4 Hz, 1H), 8.20 (d, *J* = 9.3 Hz, 1H), 8.14 (d, *J* = 9.3 Hz, 1H), 7.95 (s, 1H), 7.92-7.66 (m, 12H), 7.56 (d, *J* = 8.3 Hz, 1H), 3.58 (d, *J* = 7.3 Hz, 2H), 1.97-1.83 (m, 1H), 1.50-1.27 (m, 8H), 0.96 (t, *J* = 7.4, 3H), 0.89 (t, *J* = 7.0 Hz, 3H). ¹³C NMR (101 MHz, Chloroform-*d*) δ = 169.81, 169.74, 148.61, 143.66, 143.45, 138.36, 138.04, 137.68, 133.35, 130.93, 130.86, 130.62, 130.38, 130.30, 130.06, 129.97, 129.72, 129.36, 129.24, 129.06, 128.93, 128.08, 127.65, 127.57, 127.55, 127.45, 127.32, 127.09, 127.05, 126.82, 126.27, 125.89, 125.86, 125.75, 125.71, 125.70, 124.39, 124.24, 124.19, 124.01, 123.88, 123.15, 122.97, 42.02, 38.71, 30.78, 28.77, 24.12, 23.20, 14.23, 10.66. ¹⁹F NMR (282 MHz, Chloroform-*d*) δ = -62.40(3F), -62.43(3F), -62.45(3F). HRMS (ESI): Calculated for C₅₃H₃₆F₉NO₂ ([M+]) 775.3298, found 775.3287

2-(2-ethylhexyl)-6,8,11-triphenyl-1H-peryleno[1,12-efg]isoindole -1,3(2H)-dione (5). The general procedure was followed exactly using phenylboronic acid (237 mg, 6.00 eq.). After recrystallization in DCM/Methanol the product was filtered and washed sparingly with methanol to give an orange/red fluffy crystalline solid (173 mg, 78% yield). ¹H NMR (300 MHz, Chloroform-*d*) δ = 9.16 (d, *J* = 9.3 Hz, 1H), 9.07 (d, *J* = 9.4 Hz, 1H), 8.34 (d, *J* = 9.2 Hz, 1H), 8.31 (d, *J* = 8.1 Hz 1H), 8.29 (d, *J* = 9.4 Hz, 1H), 8.02 (s, 1H), 7.77-7.65 (m, 2H), 7.64-7.36 (m, 14H), 3.68 (d, *J* = 7.2 Hz, 2H), 2.09-1.78 (m, 1H), 1.52-1.21 (m, 8H), 0.98 (t, *J* = 7.4 Hz, 3H), 0.90 (t, *J*

= 6.8 Hz, 3H). ¹³C NMR (75 MHz, Chloroform-*d*) δ = 169.89, 169.83, 145.29, 140.30, 140.17, 139.22, 139.07, 139.04, 133.77, 130.68, 130.59, 129.92, 129.25, 129.04, 128.94, 128.74, 128.60, 127.99, 127.88, 127.81, 127.69, 127.61, 127.54, 127.48, 127.45, 127.43, 126.59, 126.08, 124.17, 123.66, 123.57, 123.51, 122.78, 122.28, 41.86, 38.68, 30.80, 28.78, 24.12, 23.21, 14.26, 10.67. HRMS (ESI): Calculated for C₅₀H₃₉NO₂ ([M+]) 685.291, found 685.2967

6,8,11-tri([1,1'-biphenyl]-4-yl)-2-(2-ethylhexyl)-1H-perylene [1,12-efg]isoindole-1,3(2H)-dione

(6). The general procedure was followed exactly using 4-biphenylboronic acid (385 mg, 6.00 eq.). After recrystallization in DCM/Methanol the product was filtered and washed sparingly with methanol to give an orange solid (263 mg, 89% yield). ¹H NMR (400 MHz, Chloroform-*d*) δ = 9.19 (d, *J* = 9.3 Hz, 1H), 9.09 (d, *J* = 9.3 Hz, 1H), 8.44 (d, *J* = 8.4 Hz, 1H), 8.43 (d, *J* = 9.3 Hz, 1H), 8.38 (d, *J* = 9.3 Hz, 1H), 8.11 (s, 1H), 7.89-7.63 (m, 18H), 7.59 (d, *J* = 8.4 Hz, 1H), 7.55-7.46 (m, 6H), 7.46-7.37 (m, 3H), 3.70 (d, *J* = 7.3 Hz, 2H), 2.03-1.93 (m, 1H), 1.50-1.30 (m, 8H), 0.99 (t, *J* = 7.4 Hz, 3H), 0.90 (t, *J* = 7.1 Hz, 3H). ¹³C NMR (75 MHz, Chloroform-*d*) δ = 170.30, 170.24, 144.19, 140.81, 140.70, 140.57, 140.38, 139.24, 139.09, 138.88, 138.83, 133.77, 131.14, 131.08, 129.77, 129.25, 129.20, 129.10, 129.06, 128.92, 128.62, 128.30, 128.09, 127.78, 127.68, 127.50, 127.36, 127.34, 127.31, 127.18, 127.03, 126.49, 124.60, 124.13, 124.01, 123.15, 122.67, 42.04, 38.73, 30.81, 28.80, 24.14, 23.24, 14.28, 10.70. HRMS (ESI): Calculated for C₆₈H₅₁NO₂ ([M+]) 913.3920, found 913.3920

2-(2-ethylhexyl)-6,8,11-tris(4-methoxyphenyl)-1H-perylene[1,12-efg]isoindole-1,3(2H)-

dione (7). The general procedure was followed exactly using 4-methoxyphenylboronic acid (295 mg, 6.00 eq.). After recrystallization in DCM/Methanol the product was filtered and washed

sparingly with methanol to give a dark orange solid (224 mg, 89% yield). ^1H NMR (300 MHz, Chloroform-*d*) δ = 8.85 (d, J = 9.3 Hz, 1H), 8.73 (d, J = 9.3 Hz, 1H), 8.21 (d, J = 8.4 Hz, 1H), 8.18 (d, J = 9.3 Hz, 1H), 8.11 (d, J = 9.4 Hz, 1H), 7.90 (s, 1H), 7.56 (d, J = 8.6 Hz, 2H), 7.53-7.36 (m, 5H), 7.12 (d, J = 8.7 Hz, 2H), 7.09 (d, J = 8.6 Hz, 2H), 7.02 (d, J = 8.7 Hz, 2H), 3.98 (s, 3H), 3.96 (s, 3H), 3.91 (s, 3H), 3.53 (d, J = 7.2, 2H), 1.97-1.82 (m, 1H), 1.50-1.26 (m, 8H), 0.96 (t, J = 7.2 Hz, 3H), 0.91 (t, J = 6.8 Hz, 3H). ^{13}C NMR (75 MHz, Chloroform-*d*) δ = 169.92, 169.85, 159.44, 159.30, 159.21, 138.67, 138.64, 138.60, 133.91, 132.68, 132.54, 131.80, 131.72, 130.34, 129.03, 128.85, 128.80, 128.29, 127.97, 127.84, 127.64, 127.46, 127.22, 126.65, 126.11, 124.13, 123.55, 123.34, 123.30, 122.43, 122.03, 115.32, 114.19, 114.08, 55.56, 55.53, 55.53, 55.47, 41.81, 38.68, 30.80, 28.78, 24.12, 23.21, 14.25, 10.66. HRMS (ESI): Calculated for $\text{C}_{53}\text{H}_{45}\text{NO}_5$ ($[\text{M}^+]$) 775.3298, found 775.3287

References

- (1) (a) Demmig, S.; Langhals, H. *Chem. Ber.* **1988**, *121*, 225-230. (b) Boni, L.; Constantino, C.; Misoguti, L.; Aroca, R.; Zilio, S.; Mendonca, C. *Chemical Physics Letters* **2003**, *371*, 744-749.
- (2) Huang, C.; Barlow, S.; Marder, S. *J. Org. Chem.* **2011**, *76*, 2386-2407.
- (3) Sadrai, M.; Bird, G. *Opt. Commun.* **1983**, *51*, 62-64.
- (4) Ego, C.; Marsitzky, D.; Becker, S.; Zhang, J.; Grimsdale, A.; Mullen, K.; MacKenzie, J.; Silva, C.; Friend, R. *J. Am. Chem. Soc.* **2003**, *125*, 437-443.
- (5) Hagfeldt, A.; Boschloo, G.; Sun, L.; Kloo, L.; Pettersson, H. *Chem. Rev.* **2010**, *110*, 6595-6663.
- (6) (a) Benning, S.; Kitzerow, H.; *Liquid Crystals* **2000**, *27*, 7, 901-906. (b) Eccher, J.; Almeida, A.; Cazati, T.; Seggern, H.; Bock, H.; Bechtold, I. *Journal of Luminescence* **2016**, *180*, 31-37.
- (7) Klonis, N.; Wang, H.; Quazi, N.; Casey, J.; Neumann, G.; Hewish, D.; Hughes, A.; Deady, L.; Tilley, L. *Journal of Fluorescence* **2001**, *11* (1), 1-11.
- (8) (a) Wurthner, F. *Pure Appl. Chem.* **2006**, Vol 78, 12, 2341-2349. (b) Gavranovic, G.; Csihony, S.; Bowden, N.; Hawker, C.; Waymouth, R.; Moerner, W.; Fuller, G. *Macromolecules* **2006**, *39*, 8121-8127. (c) Kaiser, T.; Wang, H.; Stepanenko, V.; Wurthner, F. *Angew. Chem. Int. Ed.* **2007**, *46*, 5541-5544
- (9) (a) Ghosh, I.; Gosh, T.; Bardagi, J.; Konig, B. *Science* **2014**, *346*, 6210, 725-728. (b) Miyake, G.; Theriot, J. *Macromolecules* **2014**, *47*, 8255-8261. (c) Ramsey, B.; Pearson, R.; Beck, L. Miyake, G. *Macromolecules*, **2017**, *50* (7), 2668-2674. (d) Ryan, M.; Pearson, R.; French, T.; Miyake, G. *Macromolecules*, **2017**, *50* (12), 4616-4622

- (10) (a) Gorl, D.; Zhang, X.; Wurthner, F. *Angew. Chem. Int. Ed.* **2012**, *51*, 6328-6348. (b) Chen, S.; Slattum, P.; Wang, C.; Zang, L. *Chem. Rev.* **2015**, *115*, 11967-11998. (c) Wurthner, F.; Saha-Moller, C.; Fimmel, B.; Ogi, S.; Leowanawat, P.; Schmidt, D. *Chem. Rev.* **2016**, *116*, 962-1052.
- (11) Li, C.; Wonneberger, H. *Adv. Mater.* **2012**, *24*, 613-636.
- (12) Yang, Z.; Yuan, Y.; Jiang, R.; Fu, N.; Lu, X.; Tian, C.; Hu, W.; Fan, Q.; Huang, Wei. *Polym. Chem.* **2014**, *5*, 1372-1380.
- (13) (a) Pagoaga, B.; Mongin, O.; Caselli, M.; Vanossi, D.; Momicchoili, F.; Blachard-Desce, M.; Lemercier, G.; Hoffmann, N.; Ponterini, G.; *Phys. Chem. Chem. Phys.* **2016**, *18*, 4924-4941. (b) Goa, J.; Xiao, C.; Jiang, W.; Wang, Z. *Org. Lett.* **2014**, *16*, 394-397. (c) Dubey, R.; Efimov, A.; Lemmetyinen, H.; *Chem. Mater.* **2011**, *23*, 778-788. (d) Chao, C.; Leung, M.; Su, Y.; Chiu, K.; Lin, T.; Shieh, S.; Lin, S. *J. Org. Chem.* **2005**, *70*, 4323-4331. (e) Qiu, W.; Chen, S.; Sun, X.; Liu, Y.; Zhu, D. *Org. Lett.* **2006**, *8* (5), 867-870. (f) Chen, Z.; Debije, M.; Debaerdemeker, T.; Osswald, P.; Wurthner, F. *ChemPhysChem* **2004**, *5*, 137-140.
- (14) (a) Kelber, J.; Achard, M.; Bonneval, B.; Bock, H. *Chem. Eur. J.* **2011**, *17*, 8145-8155. (b) Alibert-Foout, S.; Dardel, S.; Bock, H.; Oukachmih, M.; Archambeau, S.; Seguy, I.; Jolinat, P.; Destruel, P. *Chem. Phys. Chem.* **2003**, *4*, 983-985. (c) Barentsen, H.; Dijk, M.; Kimkes, P.; Zuilhof, K.; Sudholter, E. *Macromolecules* **1999**, *32*, 1753-1762. (d) Manning, S.; Bogen, W.; Kelly, L. *J. Org. Chem.* **2011**, *76*, 6007-6013. (e) Bhowmick, D.; Linder, S.; Devaux, A.; Cola, D.; Zacharias, H. *Small*, **2012**, *8* (4), 592-601. (f) Manna, M.; Rasale, D.; Das, A. *RSC Adv.*, **2015**, *5*, 90158-90167. (g) Yang, M.; Chen, J.; Zhou, H.; Li, W.; Wang, Y.; Li, J.; Zhang, C.; Zhou, C.; Yu, C. *Biosensors and Bioelectronics*, **2016**, *75*, 404-410. (h) Sakai, H.; Ohkubo, K.; Fukuzumi, S.; Hasobe, T. *Chem. Asian. J.* **2016**, *11*, 613-624. (i) Yang, M.; Zhou, H.; Li, Y.; Zhang, Q.; Li, J.; Zhang, C.; Zhou, C.; Yu, C. *J. Mater. Chem. B*, **2017**, *5*, 6572. (j) Tokuo, K.; Sakai, H.; Sakanoue,

T.; Takenobu, T.; Araki, Y.; Wada, T.; Hasobe, T. *Mater. Chem. Front.*, **2017**, DOI: 10.1039/c7qm00301c

(15) Lin, Y.; Wang, Y.; Wang, J.; Hou, J.; LI, Y.; Zhu, D.; Zhan, X. *Adv. Mater.* **2014**, *26*, 5137-5142.

(16) (a) Benniston, A. C.; Harriman, A.; Li, P.; Rostron, J. P.; Ramesdonk, H. J. Van; Groeneveld, M. M.; Zhang, H.; Verhoeven, J. W. *J. Am. Chem. Soc.* **2005**, *127*, 16054–16064. (b) Tanaka, H.; Shizu, K.; Nakanotani, H.; Adachi, C. *Chem Mater.* **2013**, *25*, 3766–3771. (c) Fukuzumi, S.; Kotani, H.; Ohkubo, K.; Ogo, S.; Tkachenko, N. V.; Lemmetyinene, H. *J. Am. Chem. Soc.* **2004**, *126*, 1600-1601. (d) Lim, C.; Ryan, M.; McCarthy, B.; Theriot, J.; Sartor, S.; Damrauer, N.; Musgrave, C.; Miyake, G. *J. Am. Chem. Soc.* **2017**, *139*, 348-355. (e) Pearson, R.; Lim, C.; McCarthy, B.; Musgrave, C.; Miyake, G. *J. Am. Chem. Soc.* **2016**, *138* (35), 11399-11407.

(17) Ryan, M.; Theriot, J.; Lim, C.; Yang, H. Lockwood, A.; Garrison, N.; Lincoln, S; Musgrave, C.; Miyake, G. *Polymer Chem.* **2017**, *55* (18), 3017-3027.

(18) Hou, X.; Ke, C.; Bruns, C.; McGonigal, P.; Pettman, R.; Stoddart, J. *Nature Communications*, **2015**, *6*, 6884

(19) Williams, A.; Winfield, S.; Miller, J. *Analyst* **1983**, *108*, 1067-1071.

(20) Umberger, J.Q.; LaMer, V.K. *J. Am. Chem. Soc.*, **1945**, *67*, 1099-1109

Chapter 3 – Organocatalyzed Atom Transfer Radical Polymerization Using *N*-Aryl Phenoxazines as Photoredox Catalysts

Overview

N-Aryl phenoxazines have been synthesized and introduced as strongly reducing metal-free photoredox catalysts in organocatalyzed atom transfer radical polymerization for the synthesis of well-defined polymers. Experiments confirmed quantum chemical predictions that, like their dihydrophenazine analogs, the photoexcited states of phenoxazine photoredox catalysts are strongly reducing and achieve superior performance when they possess charge transfer character. We compare phenoxazines to previously reported dihydrophenazines and phenothiazines as photoredox catalysts to gain insight into the performance of these catalysts and establish principles for catalyst design. A key finding reveals that maintenance of a planar conformation of the phenoxazine catalyst during the catalytic cycle encourages the synthesis of well-defined macromolecules. Using these principles, we realized a core substituted phenoxazine as a visible light photoredox catalyst that performed superior to UV-absorbing phenoxazines as well as previously reported organic photocatalysts in organocatalyzed atom transfer radical polymerization. Using this catalyst and irradiating with white LEDs resulted in the production of polymers with targeted molecular weights through achieving quantitative initiator efficiencies, which possess dispersities ranging from 1.13 to 1.31.

Introduction

Atom transfer radical polymerization (ATRP) is the most used controlled radical polymerization (CRP) for the synthesis of polymers with controlled molecular weight (MW),

dispersity (\bar{D}), architecture, and composition.¹ Traditionally, metal catalysts have been employed to mediate the equilibrium between an alkyl halide and a carbon centered radical, produced by reduction of the halide, and deter bimolecular termination pathways.² Concerns about metal contamination of polymers intended for biomedical or electronic applications have motivated efforts to lower metal catalyst loadings and enhance purification methods.³ Although CRPs exist that are mediated by organic catalysts and which thus entirely circumvent the issue of metal contamination,⁴ organic catalysts capable of mediating an organocatalyzed ATRP (O-ATRP) are limited because of the required significant reducing power required to reduce alkyl bromides commonly used for ATRP (~ -0.6 to -0.8 V vs SCE).⁵

Photoredox catalysis presents a strategy to drive chemical transformations under mild conditions through the generation of reactive open-shell catalysts via photoexcitation.⁶ Recently, work in this field has heavily focused on polypyridal ruthenium and iridium complexes because such metal complexes efficiently absorb visible light, possess sufficiently long excited state lifetimes as a result of metal to ligand charge transfer (MLCT), and have tunable redox properties. However, most photoredox catalysts (PCs) do not possess the reducing power to directly reduce an alkyl bromide through an outer sphere electron transfer mechanism. Commonly, supplemental sacrificial electron donors are required for alkyl bromide reduction through a reductive quenching pathway. The addition of sacrificial electron donors, however, introduces potential side-reactions⁷ that impede the ability to synthesize polymers with low \bar{D} .⁸ Select strongly reducing iridium⁹ or copper¹⁰ PCs can directly reduce an alkyl bromide through an oxidative quenching pathway, and elimination of the sacrificial electron donor can facilitate the synthesis of well-defined polymers.¹¹ Light mediated CRPs further introduce spatial and temporal control as an attractive interactive feature for the incorporation of added synthetic complexity.¹² However, the concerns of metal con-

tamination and the sustainability of iridium or ruthenium metal PCs motivate the use of organic PCs.^{14,13}

In accord with transition metal PCs, few organic PCs are able to directly reduce an alkyl bromide without the addition of a sacrificial electron donor.¹⁴ Strongly reducing organic catalysts, including perylene,¹⁵ N-aryl phenothiazines,¹⁶ and N,N-diaryl dihydrophenazines¹⁷ have been demonstrated as organic PCs capable of mediating O-ATRP (Figure 3.1). Continued progress in this field is required to further understand the mechanism of this polymerization to realize even more efficient PCs.

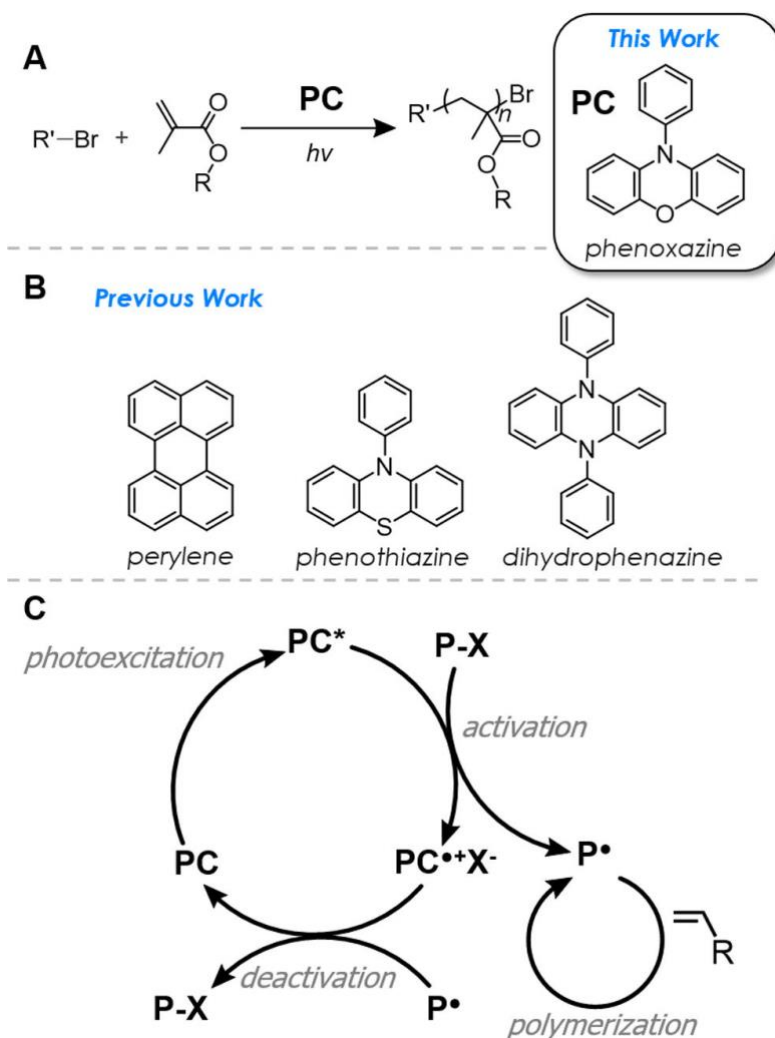


Figure 3.1. (A) O-ATRP mediated by organic PCs using alkyl bromide initiators and aryl phenoxazines studied in this work. (B) Organic PCs examined in previous work. (C) Proposed, general photoredox catalytic cycle of O-ATRP.

A proposed general photoredox O-ATRP mechanism involves photoexcitation of the PC to an excited state PC (PC^*) which is capable of reducing alkyl bromides via an oxidative quenching pathway to generate the active radical for polymerization propagation, while yielding the radical cation PC ($PC^{\bullet+}$) and Br^- ion pair complex, $PC^{\bullet+}Br^-$ (Figure 3.1C). Efficient deactivation is central to the production of well-defined polymers. Deactivation requires the $PC^{\bullet+}Br^-$ complex to be sufficiently oxidizing relative to the propagating radical to regenerate the alkyl bromide and ground state PC; subsequent photoexcitation of the PC reinitiates the catalytic cycle. Here, we report N-aryl phenoxazines as a new class of PCs for O-ATRP which produce well-defined polymers with low dispersities. Through following our maturing catalyst design principles, we report a visible light phenoxazine PC that produces polymers with \bar{D} ranging from 1.13 to 1.31 over a range of polymer MWs while achieving quantitative initiator efficiency (I^*).

To accelerate our progress in developing O-ATRP, we previously used quantum chemical calculations to guide the discovery and design of strongly reducing diaryl dihydrophenazines PCs for O-ATRP.¹⁷ We based our computationally directed strategy on the hypothesis that photoexcitation of the PC delivers, through intersystem crossing (ISC) from the singlet excited state PC ($^1PC^*$), a triplet excited state PC ($^3PC^*$) which is responsible for the alkyl bromide reduction. This hypothesis hinges on the necessity of the photoexcited species to possess a sufficiently long lifetime for photoredox catalysis.

Our continued work in this field has been piqued by the impressively strong excited state reduction potentials ($E^{0*} = E^0(2PC^{\bullet+}/PC^*)$) of N,N-diaryl dihydrophenazines and N-aryl phenothiazines (~ -2 V vs SCE), which are even more reducing than commonly used metal PCs, such as fac-Ir(ppy)³ (-1.73 V vs SCE).¹⁸ These strong E^{0*} s and the success of the diaryl dihydrophenazines in O-ATRP further drew our attention toward N-aryl phenoxazines as a potential class of organic PCs for O-ATRP. We hypothesized that phenoxazines possessed characteristic traits that would distinguish them as organic PCs and make them successful catalysts for O-ATRP. Interestingly, these N, S, and O containing heterocycles are found in biologically relevant molecules¹⁹ and organic electronic applications.²⁰

Results and Discussion

DFT calculations predict that N-aryl phenoxazines possess similarly strong E^{0*} s (~ -2 V vs SCE) in their lowest lying triplet excited state as dihydrophenazines and phenothiazines, which was corroborated experimentally.²¹ Although dihydrophenazines are stronger excited state reductants, the radical cations of phenoxazines and phenothiazines [$E^0(2PC^{\bullet+}/PC^*) = \sim 0.5$ V vs SCE] are more oxidizing than those of dihydrophenazines [$E^0(2PC^{\bullet+}/PC^*) = \sim 0.0$ V vs SCE]; all three classes of PCs possess an oxidation potential capable of deactivating the propagating radical (e.g., ~ -0.8 V vs SCE for methyl methacrylate), as required for a successful O-ATRP. Lastly, reports on the photophysical properties of phenoxazines suggested their promise as PCs; the phosphorescence quantum yield of 10-phenylphenoxazine (1) at 77 K was reported to be 94% with a lifetime as long as 2.3s.²² These properties highlight the efficient ISC to the triplet manifold and slow non-radiative decay attributed to small Franck–Condon vibrational overlap factors between $^3PC^*$ and the ground state.

Our analysis of exchanging the sulfur in phenothiazines with the oxygen in phenoxazines identified several distinct phenomena that alter the physical properties of these molecules and which we propose manifest in improvements in PC performance for O-ATRP, qualitatively assessed through analysis of the polymer product. The significant distinction between these two systems is the conformation of their heterocyclic rings. The smaller van der Waals radius of oxygen (1.52 Å) relative to sulfur (1.80 Å) permits the ground state phenoxazine (e.g., PC 1) to access a planar geometry similarly to dihydrophenazines (nitrogen, 1.55, Å). In contrast, phenothiazine adopts a bent boat conformation in its ground state, observable in crystal structures²³ and predicted by our computations (Figure 3.2). However, upon oxidation to the radical cation state ${}^2\text{PC}^{\bullet+}$, all three PCs adopt a planar conformation.

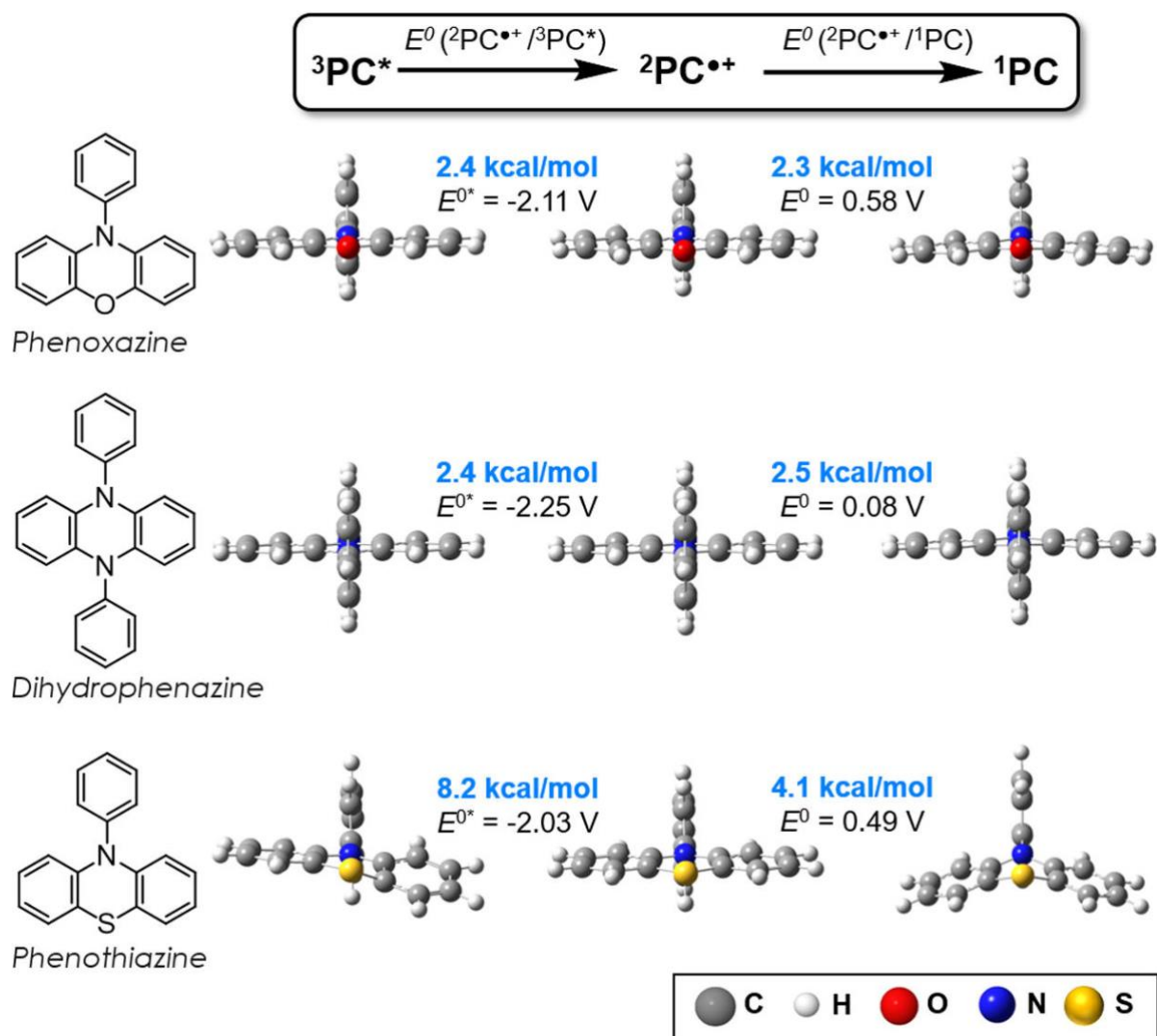


Figure 3.2. Geometric reorganization energies and reduction potentials (vs SCE) for 10-phenylphenoxazine, diphenyl dihydrophenazine, and 10-phenylphenothiazine (bottom) transitioning from the $^3PC^*$ to $^2PC^{\bullet+}$ to 1PC species involved in the proposed mechanism for photoredox O-ATRP. Reduction potentials were computed here with the improved 6-311+G** basis set compared to 6-31+G** used in the previous report.¹⁷

The consequences of phenothiazine adopting bent con- formations in the ground and triplet states, but a planar geometry in the radical cation state, introduce larger structural reorganizations during electron transfer (ET) as compared to the consistently planar phenoxazines and

dihydrophenazines. We calculated a structural reorganization penalty associated with oxidation of the bent 10-phenylphenothiazine triplet state to the planar radical cation of 8.2 kcal/mol. In contrast, the triplet and radical cation states of **1** are both planar, analogous to diaryl dihydrophenazines, which results in a lower reorganization energy of only 2.4 kcal/mol. As phenoxazine, dihydrophenazine, and phenothiazine derivatives, possess similar E^{0*} s (-2.11, -2.25, and -2.03 V, respectively), we expect a kinetically faster activation (reduction of the alkyl bromide) in O-ATRP by phenoxazines and dihydrophenazines because of their lower reorganization energies for ET.

Polymerization deactivation involves reduction of the planar phenylphenothiazine radical cation to regenerate the bent ground state. We calculate a reorganization energy for this ET of 4.1 kcal/mol. For **1** or diphenyl dihydrophenazine, the same reduction process requires lower reorganization energies of 2.3 or 2.5 kcal/mol, respectively consistent with the conservation of the planarity of the cation radical and ground states. Given the similar ground state oxidation potentials for the phenoxazine and phenothiazine (0.58 and 0.49 V), the radical cation of **1** is likely kinetically faster in deactivation, which imparts better control in O-ATRP (*vide infra*). How this concept pertains to the less oxidizing dihydrophenazine $PC^{\bullet+}$ requires further investigation, although previous results demonstrated that dihydrophenazines are efficient PCs for O-ATRP.¹⁷

Toward the goal of designing phenoxazines as PCs for O-ATRP we applied the concepts conceived from our previous study of diaryl dihydrophenazines, which revealed that PCs with spatially separated singly occupied molecular orbitals (SOMOs) in their $^3PC^*$ state yielded PCs with superior performance in O-ATRP in regards to achieving the highest I^* and producing polymers with the lowest \bar{D} . As such, we investigated strongly reducing N-aryl phenoxazines with spatially separated SOMOs (with the lower lying SOMO localized on the phenoxazine core and

the higher lying SOMO localized on the aryl substituent) and localized SOMOs (with both SOMOs localized on the phenoxazine core), to evaluate their performance as O-ATRP PCs and determine if this concept extends to phenoxazines (Figure 3.3).

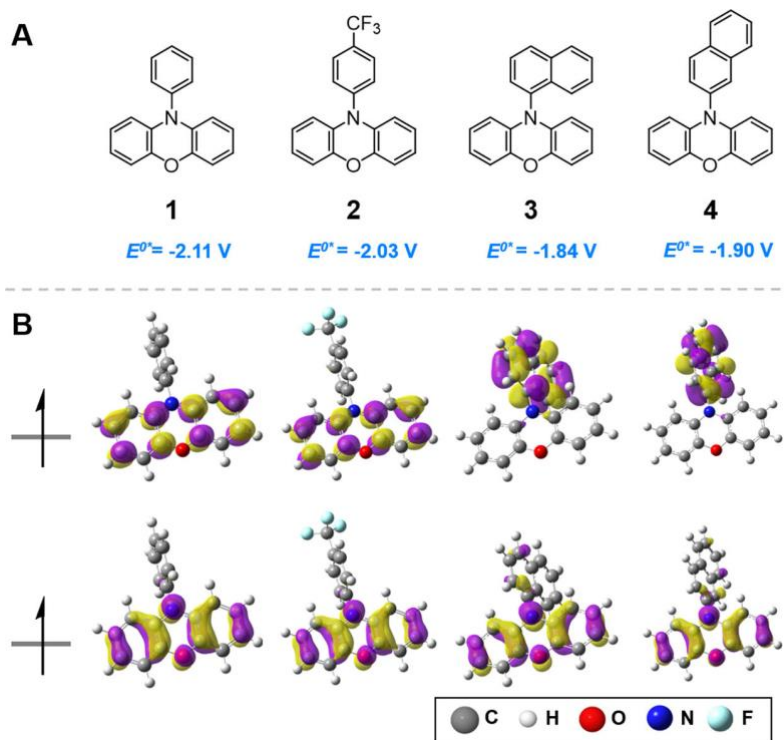


Figure 3.3. (A) *N*-Aryl phenoxazines studied in this work along with computed triplet state reduction potentials. (B) Computed triplet state SOMOs of phenoxazine derivatives.

In the cases of diphenyl dihydrophenazine and 1, we calculate that neither exhibits spatially separated SOMOs. In contrast, incorporation of electron withdrawing trifluoromethyl functionalization on the para position of the N-phenyl substituents of the dihydrophenazine yielded spatially separated SOMOs whereas this substitution on phenoxazine (2) results in both SOMOs localized on the phenoxazine core. However, for both dihydrophenazines and phenoxazines, *N*-aryl functionalization(s) with 1- or 2-naphthalene yielded molecules with spatially separated SOMOs and thus predicted intramolecular charge transfer from the heterocyclic ring to the

naphthalene substituent upon photoexcitation and subsequent intersystem crossing to the triplet state.

All four phenoxazine derivatives were synthesized through C–N cross-couplings from commercially available reagents and employed in the polymerization of MMA.²¹ A screen of common ATRP alkyl bromide initiators revealed that diethyl 2-bromo-2-methylmalonate (DBMM) served as the superior initiator to produce polymers with the lowest \bar{D} while achieving the highest I^* (Table 3.7). To evaluate the PCs, polymerizations using DBMM as the initiator were conducted in dimethylacetamide and irradiated with a 365 nm UV nail curing lamp (54 W) (Table 3.1). In accord with diaryl dihydrophenazines, N-aryl phenoxazines possessing localized SOMOs (PCs 1 and 2) did not perform as well as the PCs with separated SOMOs (PCs 3 and 4). Specifically, 1 and 2 produced poly(methyl methacrylate) (PMMA) with a relatively high \bar{D} of 1.48 and 1.45, respectively (runs 1 and 2). Polymerization results with PCs 3 and 4 were superior, and produced PMMA with lower dispersities (\bar{D} = 1.22 and 1.11, respectively) while achieving high I^* s of 92.6 and 77.3%, respectively (runs 3 and 4).

Table 3.1. Results of the O-ATRP of MMA Using PCs 1 through 4^a.

run no.	PC	conv (%)	M_w (kDa)	M_n (kDa)	dispersity (\bar{D})	I^* (%)
1	1	95.6	10.6	7.2	1.48	137
2	2	55.3	9.5	6.5	1.45	85.5
3	3	78.8	10.8	8.8	1.22	92.6
4	4	80.2	11.9	10.8	1.11	77.3

^a[MMA]:[DBMM]:[PC] = [1000]:[10]:[1]; 9.35 μ mol PC, 1.00 mL dimethylacetamide, and irradiated with a 54 W 365 nm light source for 8 h.

Further, molecular weight control could be obtained using either PC through modulation of the monomer (runs 5 to 9 for PC 3; runs 13-17 for PC 4) or initiator (runs 10-12 for PC 3; runs 18-20 for PC 4) ratios (Table 3.2). Overall, PC 3 produced PMMA through higher I^* (~80–100%) while PC 4 produced PMMA with lower \mathcal{D} (as low as 1.07). This 1-naphthalene versus 2-naphthalene substitution effect influencing high I^* or low \mathcal{D} , respectively was also observed with diaryl dihydrophenazines.

Table 3.2. Results of the O-ATRP of MMA Using PCs 3 and 4.^a

run no.	PC	[MMA]:[DBMM]:[PC]	conv (%)	M_w (kDa)	M_n (kDa)	dispersity (\mathcal{D})	I^* (%)
5	3	[500]:[10]:[1]	80.8	5.8	4.9	1.16	86.1
6	3	[1000]:[10]:[1]	78.8	10.8	8.8	1.22	92.6
7	3	[1500]:[10]:[1]	72.2	11.4	9.5	1.19	116
8	3	[2000]:[10]:[1]	76.5	18.4	14.6	1.26	107
9	3	[2500]:[10]:[1]	78.4	25.9	19.8	1.31	101
10	3	[1000]:[5]:[1]	74.6	26.4	19.1	1.38	79.6
11	3	[1000]:[15]:[1]	74.5	8.3	6.9	1.20	75.7
12	3	[1000]:[20]:[1]	80.7	5.5	4.6	1.19	92.9
13	4	[500]:[10]:[1]	85.1	5.9	5.4	1.09	84.1
14	4	[1000]:[10]:[1]	80.2	11.9	10.7	1.11	77.3
15	4	[1500]:[10]:[1]	68.9	12.2	9.8	1.25	109
16	4	[2000]:[10]:[1]	58.2	14.7	112.5	1.17	95.2
17	4	[2500]:[10]:[1]	65.9	21.2	17.3	1.23	96.6
18	4	[1000]:[5]:[1]	70.5	22.3	16.8	1.35	85.3
19	4	[1000]:[15]:[1]	70.9	9.3	8.3	1.12	60.6
20	4	[1000]:[20]:[1]	76.1	6.8	6.1	1.07	64.0

^aSee the Supporting Information for experimental details.

Our analysis of the polymerization of MMA by 3 and 4 showed that both PCs imparted control over the polymerization that is becoming expected from O-ATRP. Specifically, a linear growth in polymer molecular weight as well as a low dispersity during the course of polymerization was attained (Figure 3.4A and B). Additionally, temporal control was demonstrated using a pulsed irradiation sequence (Figure 3.4C–F). Monomer conversion was only observed during irradiation, which resulted in a linear increase in number-average MW (M_n) while producing PMMA with low \mathcal{D} .

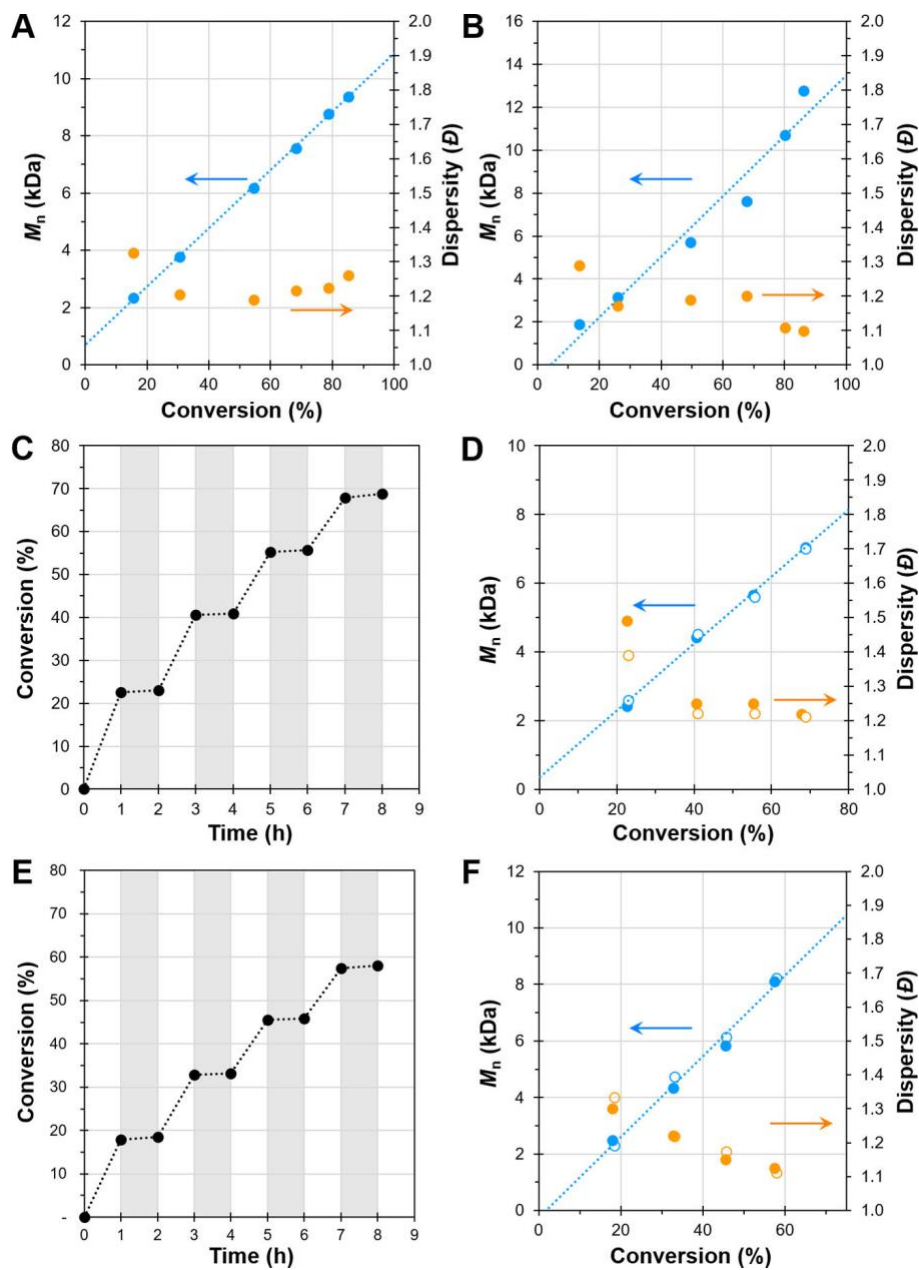


Figure 3.4. Plots of molecular weight (M_n , blue) and dispersity (D , orange) as a function of monomer conversion for the polymerization of MMA catalyzed by 3 (A) and 4 (B). Plots of conversion vs time using 3 (C) or 4 (E) (irradiation in white and dark periods in gray) and plots of molecular weight (M_n , blue) and dispersity (D , orange) as a function of MMA conversion using a pulsed-irradiation sequence and PC 3 (D) or 4 (F) (filled markers are data directly after

irradiation while open markers are data directly after the dark period) Conditions for all plots: $[MMA]:[DBMM]: [PC] = [1000]:[10]:[1]$; $9.35 \mu\text{mol PC}$, $1.00 \text{ mL dimethylacetamide}$, and irradiated with UV-light.

Both PCs also efficiently polymerized other methacrylates, including benzyl methacrylate (BnMA), isobutyl methacrylate (BMA), and isododecyl methacrylate (IDMA) (Table 3.5). As such, 3 was used to perform chain extension polymerizations from an isolated PMMA ($M_w = 9.9 \text{ kDa}$, $\bar{D} = 1.12$) macro- initiator because the ATRP mechanism inherently reinstalls the bromine chain end group onto the growing polymer chain (Figure 3.5). Chain extensions from this PMMA macroinitiator onto the growing polymer chain (Figure 3.5). Chain extensions from this PMMA macroinitiator with MMA, DMA, BnMA, and BMA were successful, both confirming high bromine chain end group fidelity and allowing the synthesis of block polymers.

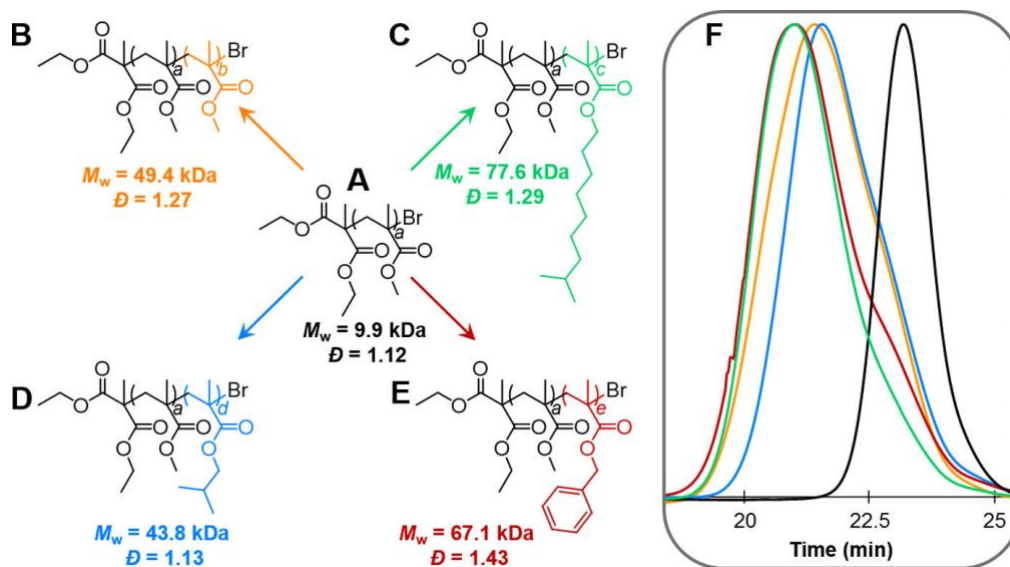


Figure 3.5. Chain extension polymerizations from a PMMA macroinitiator (A) with MMA (B), IDMA (C), BMA (D), and BnMA (E). Gel permeation chromatography traces of the polymers depicted by the chemical structures with corresponding color schemes (F).

To further establish these naphthalene phenoxazines as efficient PCs, we next directly compared 3 and 1-naphthalene-10-phenothiazine as PCs for O-ATRP under our polymerization conditions (Figure 3.16). Both catalysts exhibited nearly identical rates of polymerization, achieving 85.1% and 88.4% monomer conversion after 10 h for 3 and the phenothiazine, respectively. Additionally, both PCs achieved high I*s of 93.5% and 95.6%, respectively. However, a significant difference in polymerization performance was observed when comparing the \bar{D} of the resulting PMMA. When using 3, PMMA was produced with $\bar{D} = 1.26$, while the phenothiazine produced PMMA with comparatively higher $\bar{D} = 1.66$, consistent with previous reports^{16a,b} using this PC.

As inferred above, the higher \bar{D} of the PMMA produced by the phenothiazine is attributed to the larger reorganization energies of the phenothiazines. Incorporation of O versus S in the core of phenoxazines versus the core of phenothiazines imparts distinct quantitative differences in the electronic and geometric structures of these molecules that affect their performance as PCs for O-ATRP. As such, the planarity of phenoxazines throughout the photoexcitation and ET processes causes them to perform more closely to diaryl dihydrophenazines as PCs for O-ATRP. We hypothesize that the differences between these PCs specifically manifest in each of their abilities to balance the rates of activation and deactivation which results in the differences observed in the \bar{D} of the resulting PMMA produced by each PC.

An additional consideration when comparing phenoxazines, dihydrophenazines, and phenothiazines is that the planar core of phenoxazines and dihydrophenazines promotes intramolecular charge transfer to charge separated SOMOs while the bent phenothiazine core limits electronic coupling between the heterocyclic ring and the N-aryl substituent and consequently the ability to form an intramolecular charge transfer complex.²⁴ The planar phenoxazine core versus

the bent phenothiazine core can be visualized in the X-ray crystal structures of the PCs (Figure 3.6). The electrostatic potential (ESP) mapped electron density of the $^3\text{PC}^*$ state of these compounds reveal that electron density is transferred to the naphthalene substituent (red region) in phenoxazine upon photoexcitation and ISC from ^1PC , even more so with dihydrophenazines, while electron density remains localized on the phenothiazine core (Figure 3.7).

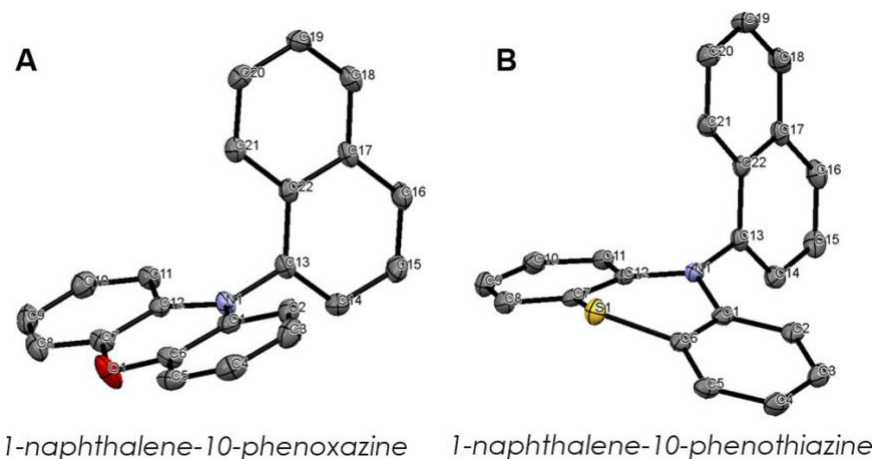


Figure 3.6. X-ray crystal structures of 1-naphthalene substituted planar phenoxazine (A) and bent phenothiazine (B).

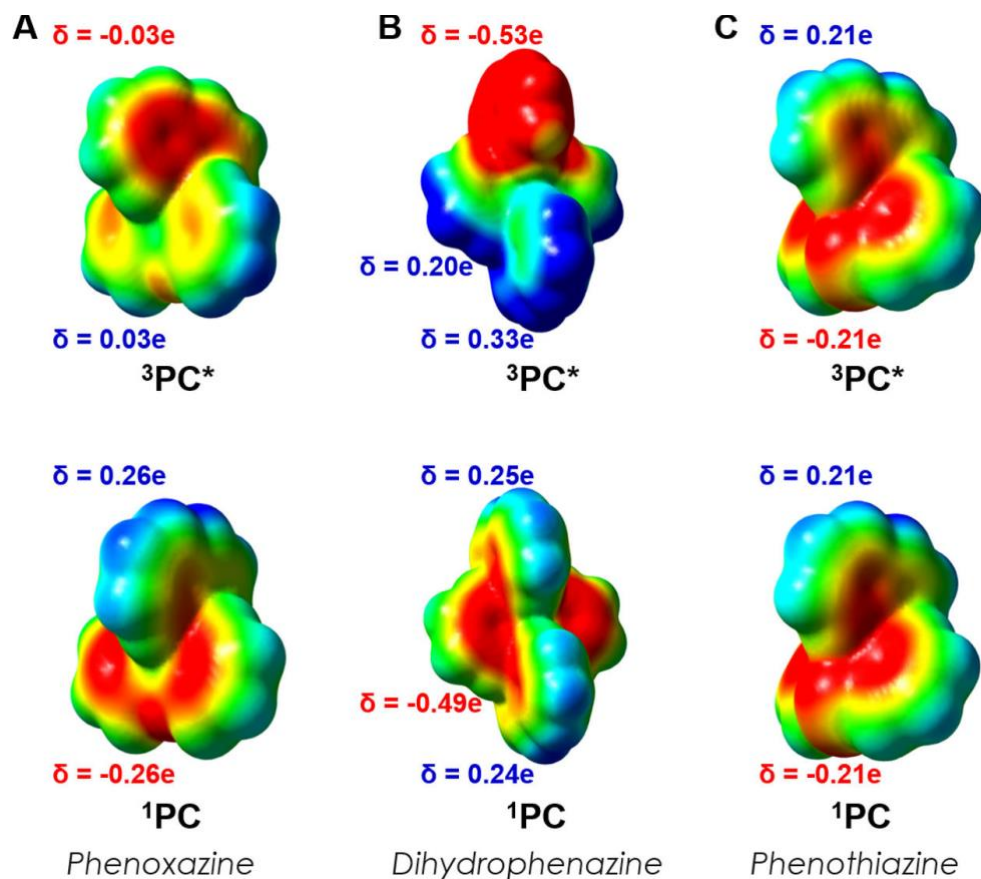


Figure 3.7. ESP mapped electron density of 1PC and $^3PC^*$ of 1-naphthalene substituted phenoxazine (A), dihydrophenazine (B), and phenothiazine (C).

We further envisaged that a visible light absorbing phenoxazine derivative would provide an even more efficient polymerization catalyst, as irradiation of the reaction with high energy UV-light can initiate non-desirable reaction pathways, which may increase the \bar{M}_n of the produced polymer and lower I^* .²⁵ To realize a visible light absorbing PC we explored a core substituted phenoxazine derivative. Computations predicted that PC 5, possessing 4-biphenyl core substitutions, would be an excellent target PC with $^3PC^*$ possessing a strong reduction potential and spatially separated SOMOs, while 1PC would exhibit an absorbance profile in the visible spectrum. The visible light absorbing PC 5 was synthesized in high yield from PC 3 through selective bromination at the 3- and 7-positions on the phenoxazine core using N-bromosuccinimide

followed by Suzuki cross-coupling.²¹ A similar synthetic strategy was recently reported to synthesize thiophene core substituted phenothiazines for use as visible light absorbing catalysts for cationic polymerization.²⁶ The absorbance profile of PC 5 was not only red-shifted ($\Delta\lambda_{\text{max}} = 65$ nm versus noncore substituted PC 3) into the visible spectrum ($\lambda_{\text{max}} = 388$ nm), but also exhibited an extremely enhanced molar extinction coefficient ($\epsilon = 26635 \text{ M}^{-1}\text{cm}^{-1}$ at $\lambda_{\text{max}} = 388$ nm), making it significantly more efficient at absorbing visible light than the noncore substituted 1-naphthalene functionalized phenoxazine, dihydro-phenazine, or phenothiazine (Figure 3.8).

The polymerization performance of PC 5 confirmed our predictions that it would be an excellent PC for O-ATRP, demonstrating superior control over the polymerization than the UV-absorbing phenoxazines or even previously reported dihydrophenazines. The polymerization of MMA using PC 5 irradiated by white LEDs was efficient and showcased characteristics of a controlled polymerization with a linear increase in polymer M_n and a low polymer \bar{D} during the course of polymerization (Figure 3.8C). Furthermore, the molecular weight of the polymer could be tailored through manipulation of either the monomer or initiator loading, while keeping the polymerization otherwise constant, to produce polymers with \bar{D} of 1.13–1.31 while achieving quantitative I^* (Table 3.3).

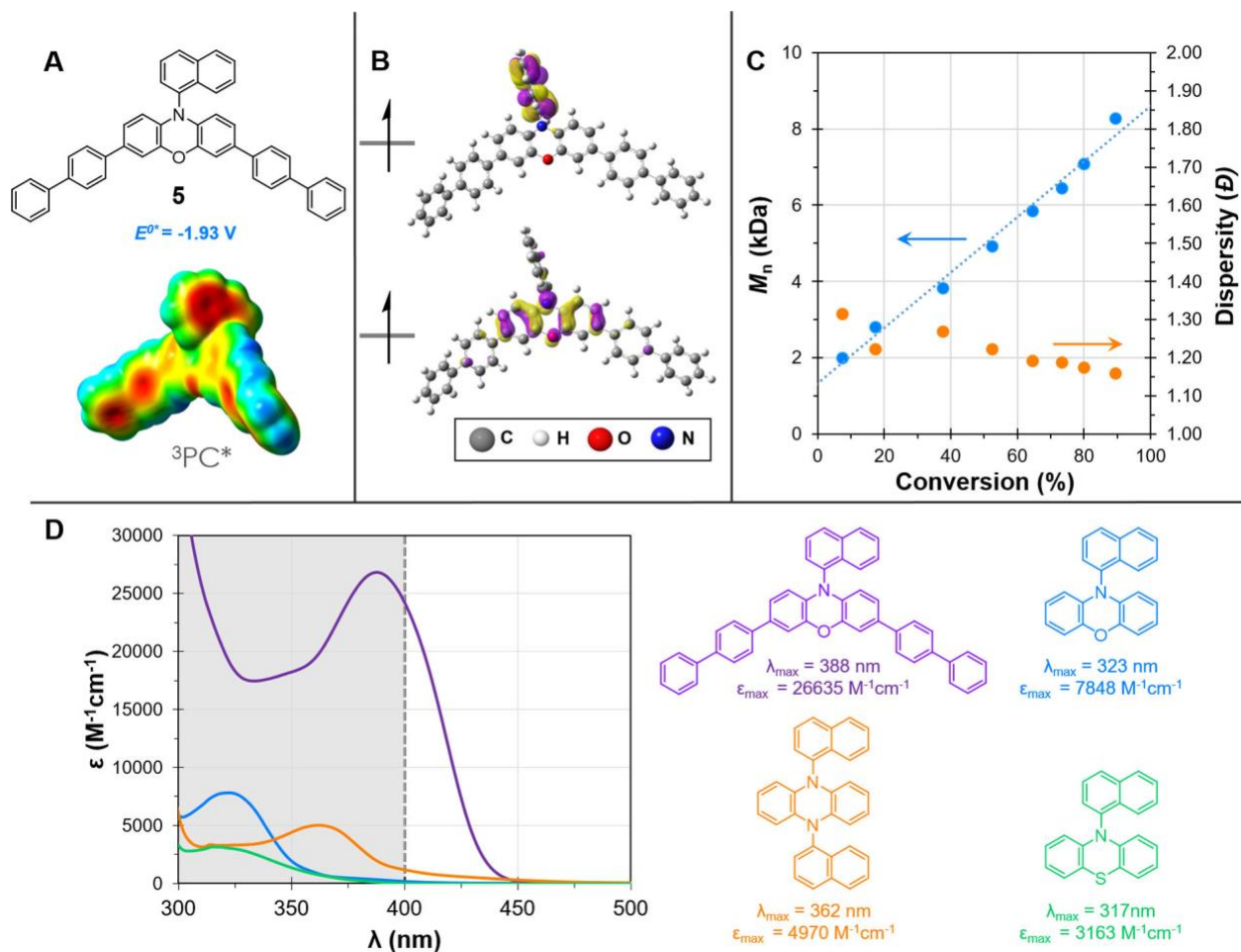


Figure 3.8. Properties of PC 5. (A) Structure, computed triplet excited state reduction potential, and ESP mapped electron density of $^3PC^*$ 5. (B) Computed triplet state SOMOs of PC 5. (C) Plot of M_n and \bar{D} as a function of monomer conversion for the polymerization of MMA by PC 5; $[MMA]:[DBMM]:[5] = [1000]:[10]:[1]$; 9.35 μmol PC, 1.00 mL dimethylacetamide, and irradiated with white LEDs. (D) UV-vis spectrum of PC 5 and 1-naphthalene functionalized phenoxazine, dihydrophenazine, and phenothiazine, with color coded structures, and extinction coefficients at their respective λ_{max} with the visible absorbance spectrum highlighted in white.

Table 3.3. Results of the O-ATRP of MMA Using PC 5^a

run no.	[MMA]:[DBMM]:[5]	conv (%)	M_w (kDa)	M_n (kDa)	Dispersity (\mathcal{D})	I^* (%)
21	[500]:[10]:[1]	67.2	4.07	3.64	1.13	99.4
22	[1500]:[10]:[1]	75.2	13.7	11.8	1.16	98.0
23	[2000]:[10]:[1]	90.9	22.9	17.5	1.31	105
24	[2500]:[10]:[1]	87.5	27.5	21.3	1.29	104
25	[1000]:[5]:[1]	89.9	23.0	18.1	1.27	101
26	[1000]:[15]:[1]	73.8	6.17	5.31	1.16	97.5
27	[1000]:[20]:[1]	72.1	4.52	3.76	1.20	103

^aSee the Supporting Information for experimental details.

Conclusion

N-Aryl phenoxazines have proven to be efficient PCs for O- ATRP that produce polymers with controlled molecular weights and low dispersity. Through the culmination of computational and experimental results, we report a visible light absorbing phenoxazine photoredox catalyst that produces polymers with controlled molecular weights and low dispersities, achieving quantitative initiator efficiencies that out- compete previously reported organic PCs for O-ATRP. The continued establishment of design principles for PCs capable of mediating O-ATRP will further expand the scope and impact of this polymerization methodology, which we foresee will translate to an additional means for selective small molecule transformations. Our future work will investigate the intricacies of the charge transfer state that is responsible for efficient photoredox catalysis, which we hypothesize provides extended excited state lifetimes and minimizes undesirable back electron transfer.

Experimental

1. Materials and Methods

Phenoxazine was purchased from Beantown Chemical. 4-biphenyl boronic acid was purchased from TCI America. Glacial acetic acid was purchased from VWR. All other reagents were purchased from Sigma-Aldrich. Chemicals used in polymerizations, including isobutyl

methacrylate (BMA), benzyl methacrylate (BnMA), isodecyl methacrylate (IDMA), methyl methacrylate (MMA), diethyl 2-bromo-2-methyl malonate (DBMM), dimethylacetamide (DMA) were purified by vacuum distillation followed by three freeze-pump-thaw cycles and stored under nitrogen atmosphere. Dioxane was purified using an mBraun MB-SPS-800 solvent purification system and kept under nitrogen atmosphere. Dicyclohexylphosphino-2,6-diisopropoxybiphenyl (RuPhos) and chloro-(2-dicyclohexylphosphino-2,6-diisopropoxy-1,1-biphenyl) [2-(2-aminoethyl)phenyl] palladium(II) - methyl-t-butyl ether adduct (RuPhos precatalyst) were stored under nitrogen atmosphere and used as received. Aryl halides used in the catalyst synthesis were degassed and stored under nitrogen. A Vogue Professional Powerful & Double Wide 54 watt UV lamp Light Nail Dryer was used as the UV light source. One sixteen inch strip of double-density white LEDs, purchased from Creative Lighting Solutions (item no. CL-FRS1210-5M-12V-WH), was wrapped inside a 400 mL beaker and used as a visible light source.

Nuclear magnetic resonance spectra were recorded on a Varian 300 MHz NMR Spectrometer for polymerization conversions and using a Varian 400 MHz or Varian 500 MHz NMR Spectrometer for all other characterizations. All ^1H NMR experiments are reported in δ units, parts per million (ppm), and were measured relative to the signals for residual chloroform (7.26 ppm) or benzene (7.15 ppm) in the deuterated solvent. All ^{13}C NMR spectra are reported in ppm relative to CDCl_3 (77.23 ppm) or C_6D_6 (128.62 ppm). Analysis of polymer molecular weights was performed via gel permeation chromatography (GPC) coupled with multi-angle light scattering (MALS), using an Agilent HPLC fitted with one guard column, three PLgel 5 μm MIXED-C gel permeation columns, a Wyatt Technology TrEX differential refractometer, and a Wyatt Technology miniDAWN TREOS light scattering detector, using THF as the eluent at a flow rate of 1.0 mL/min. Ultraviolet-visible spectroscopy was performed on an Cary 5000

spectrophotometer using DMA as the solvent. Emission spectroscopy was performed on a SLM 8000C spectrofluorimeter using DMA as the solvent. Cyclic voltammetry was performed with a CH Instruments electrochemical analyzer with a Ag/AgNO₃ (0.01 M in MeCN) reference electrode using DMA as the solvent for the working electrode. Samples were sparged with argon for 5 minutes prior to both emission and electrochemical measurements.

2. Procedures

Synthesis of N-aryl phenoxazine catalysts:

10-Phenylphenoxazine (1) A 50 mL storage flask was charged with a stir bar, flame dried under vacuum and back filled with nitrogen three times. The flask was then charged with phenoxazine (183 mg, 1.0 mmol, 1.00 eq.), NaO^tBu (192.2 mg, 2.0 mmol, 2.00 eq.), and RuPhos (12 mg, 0.03 mmol, 0.03 eq.). The flask was taken into a nitrogen filled glovebox where RuPhos Precat (21mg, 0.03 mmol, 0.03 eq.), 1 mL dry dioxane and bromobenzene (0.11 mL, 2.0 mmol 2.00 eq.) were added. The flask was placed in an oil bath at 130° C while stirring for 48 hours. The flask was then cooled to room temperature, diluted with CH₂Cl₂, and the solution was washed with water three times, brine once, dried over MgSO₄ and purified by recrystallization from CH₂Cl₂ layered with hexanes at - 25° C to give 60 mg of yellow crystals, 23% yield. NMR matched that reported previously.²⁷

4-Trifluoromethylphenyl -10-phenoxazine (2) A 100 mL storage flask was charged with a stir bar, flame dried under vacuum and back filled with nitrogen three times. The flask was then charged with phenoxazine (800 mg, 4.37 mmol, 1.00 eq.), NaO^tBu (840 mg, 8.74 mmol, 2.00 eq.), and RuPhos (52.4 mg, 0.13 mmol, 0.03 eq.). The flask was placed into a nitrogen filled glovebox

where RuPhos Precat (91.77 mg, 0.13 mmol, 0.03 eq.), and 4 mL dry dioxane and 4-bromobenzotrifluoride (1.22 mL, 8.74 mmol, 2.00 eq.) were added. The flask was placed in an oil bath at 130° C while stirring for 48 hours. The flask was then cooled to room temperature, diluted with CH₂Cl₂, and the solution was washed with water three times, brine once, dried over MgSO₄ and purified by recrystallization from CH₂Cl₂ layered with hexanes on top at -25° C to yield 987 mg of yellow crystals, 69% yield. Final purification was conducted via sublimation at 100 mTorr at 175° C. ¹H NMR (CDCl₃, 500 MHz) δ 7.87 (d, J = 8.20 Hz, 2H), 7.51 (d, J = 8.15 Hz, 2H), 6.73 (dd, J = 7.85, 1.75 Hz, 2H), 6.68 (m, 2H), 6.62 (td, J = 7.85, 1.75 Hz, 2H), 5.90 (d, J = 8.20 Hz, 2H). ¹³C NMR (CDCl₃, 400MHz) δ 144.10, 142.73, 133.89, 131.76, 130.97, 130.64, 128.44, 123.52, 122.09, 115.93, 113.39. ¹⁹F NMR (CDCl₃, 300MHz) δ 62.55. HRMS (ESI): calculated for M+ C₁₉H₁₂F₃NO, 327.0871; observed 327.0869.

1-Naphthalene-10-phenoxazine (3) A stir bar was placed into a 100 mL storage flask, flame dried under vacuum and then back filled with nitrogen three times. The flask was then charged with phenoxazine (1.00 g, 5.46 mmol, 1.00 eq.), NaO^tBu (1.054 g, 10.92 mmol, 2.00 eq.), and RuPhos (65.6 mg, 0.16 mmol, 0.03 eq.). The flask was taken into a nitrogen filled glovebox where RuPhos Precat (114.75 mg, 0.16 mmol, 0.03 eq.), 6 mL dry dioxane and 1-bromonaphthalene (1.53 mL, 10.92 mmol, 2.00 eq.) were added. The flask was placed in an oil bath at 130° C while stirring for 48 hours. The flask was then cooled to room temperature, diluted with CH₂Cl₂, and the solution was washed with water three times, brine once, dried over MgSO₄ and purified by recrystallization from CH₂Cl₂ layered with hexanes on top at -25° C to yield 790 mg of yellow crystals, 47% yield. Final purification was conducted via sublimation at 100 mTorr at 190° C. ¹H NMR (CDCl₃, 500 MHz) δ 8.08 (d, J = 8.35 Hz, 1H), 7.99 (dd, J = 8.20, 3.95 Hz, 2H), 7.66 (t, J = 7.25 Hz, 1H), 7.56

(m, 2H), 7.48 (m, 1H), 6.74 (dd, $J = 7.90, 1.45$ Hz, 2H), 6.63 (t, $J = 7.85$ Hz, 2H), 6.49 (td, $J = 7.85, 1.45$ Hz, 2H), 5.71 (dd, $J = 7.90, 1.45$ Hz, 2H). ^{13}C NMR (CDCl_3 , 400MHz) δ 144.09, 135.77, 135.24, 134.48, 131.56, 129.35, 129.14, 128.95, 127.50, 127.07, 127.04, 123.57, 123.53, 121.47, 115.58, 113.57. HRMS (ESI): calculated for M^+ $\text{C}_{22}\text{H}_{15}\text{NO}$, 309.1154; observed 309.1152.

2-Naphthalene-10-phenoxazine (4) A 100 mL storage flask was charged with a stir bar, flame dried under vacuum then back filled with nitrogen three times. The flask was then charged with phenoxazine (1.00 g, 5.46 mmol, 1.00 eq.), NaO^tBu (1.054 g, 10.92 mmol, 2.00 eq.), and RuPhos (65.6 mg, 0.16 mmol, 0.03 eq.). The flask was taken into a nitrogen filled glovebox where RuPhos Precat (114.75 mg, 0.16 mmol, 0.03 eq.), 6mL dry dioxane and 2-bromonaphthalene (2.26 mg, 10.92 mmol, 2.00 eq.) were added. The flask was placed in an oil bath at 130°C while stirring for 48 hours. The flask was then cooled to room temperature, diluted with CH_2Cl_2 , and the solution was washed with water three times, brine, dried over MgSO_4 and purified by recrystallization from CH_2Cl_2 at -25°C to yield 890 mg of light yellow, flakey crystals, 53% yield. Final purification was conducted via sublimation at 100 mTorr at 195°C . ^1H NMR (CDCl_3 , 400 MHz) δ 8.08 (d, $J = 8.60$ Hz, 1H), 7.95 (d, $J = 7.00$ Hz, 1H), 7.88 (m, 2H), 7.57 (m, 2H), 7.42 (dd, $J = 8.64, 2.04$ Hz, 1H), 6.73 (dd, $J = 7.84, 1.56$ Hz, 2H), 6.66 (t, $J = 7.52$ Hz, 2H), 6.57 (td, $J = 8.12, 1.60$ Hz, 2H), 5.99 (d, $J = 7.96$ Hz, 2H). ^{13}C NMR (CDCl_3 , 400 MHz) δ 144.42, 136.74, 135.06, 134.78, 133.28, 131.55, 130.29, 128.23, 128.15, 127.12, 126.78, 123.49, 121.66, 115.74, 113.78. HRMS (ESI): calculated for M^+ $\text{C}_{22}\text{H}_{15}\text{NO}$, 309.1154; observed 309.1151.

1-Naphthalene-10-phenothiazine A stir bar was placed in a 50 mL storage flask, flame dried under vacuum and then back filled with nitrogen three times. The flask was then charged with

phenothiazine (0.600 g, 3.01 mmol, 1.00 eq.), NaO^tBu (0.578 g, 6.02 mmol, 2.00 eq.), and RuPhos (42.2 mg, 0.09 mmol, 0.03 eq.). The flask was taken into a nitrogen filled glovebox where RuPhos Precat (73.8 mg, 0.09 mmol, 0.03 eq.), 3 mL dry Dioxane and 1-bromonaphthalene (0.84 mg, 6.02 mmol, 2.00 eq.) were added. The flask was placed in an oil bath at 130° C while stirring for 48 hours. The flask was then cooled to room temperature, diluted with CH₂Cl₂, and the solution was washed with water three times, brine once, dried over MgSO₄ and purified by recrystallization from CH₂Cl₂ layered with hexanes on top at -25° C to yield 253 mg of a yellowish solid, 26% yield. Final purification was conducted via sublimation at 100 mTorr at 155° C. NMR matched that reported previously.²⁸

3,7-Dibromo 1-Naphthalene-10-phenoxazine A literature procedure was adapted for this synthesis.²⁹ 1-Naphthalene-10-phenoxazine (800 mg, 2.58 mmol, 1eq.) was dissolved in 80mL of chloroform. 80mL of glacial acetic acid was then added to the stirring mixture. Aluminum foil was thoroughly wrapped around to cover the reaction vial, blocking out light. In the dark, powdered N-Bromosuccinimide (944 mg, 5.30 mmol, 2.05 eq.) was added in small portions over a 20 minute period. After 2 hours at room temperature the reaction mixture was concentrated under vacuum. The resulting solid was washed three times with water, brine, then dried with MgSO₄. A light tan powder (1.0 g, 2.14 mmol, 82.8% yield) was collected. This was used for the Suzuki coupling without further purification. ¹H NMR (C₆D₆, 500 MHz) δ 7.82 (d, J = 8.48 Hz, 1H), 7.57 (dd, J = 25.02, 8.3 Hz, 2H), 7.19 (m, 1H), 7.12 (t, J = 8.03 Hz, 2H), 6.88 (dd, J = 7.32, 0.57 Hz, 3H), 6.84 (d, J = 2.19 Hz, 2H), 6.36 (dd, J = 8.54, 2.21 Hz, 2H). ¹³C NMR (CDCl₃, 400MHz) δ 144.27, 135.82, 134.22, 133.32, 130.91, 129.88, 129.15, 128.87, 127.83, 127.29, 127.06, 126.62, 123.02, 118.86, 114.74, 113.06.

3,7-Di(4-biphenyl) 1-Naphthalene-10-Phenoxazine (5) A 200mL schlenk flask was flame dried, filled with nitrogen, and equipped with a stir bar and reflux condenser before 3,7-Dibromo 1-Naphthalene-10-phenoxazine (225 mg, 0.48 mmol, 1 eq.), 4-biphenylboronic acid (381.8 mg, 1.9 mmol, 4 eq.) was added, then dissolved in 20 mL of THF. 6 mL of K₂CO₃ (2M) was syringed into the solution and then heated to 80°C and stirred for 20 minutes. After which, Palladium tetrakis(triphenylphosphine) (93 mg, 15% mol) in a 20mL solution of THF was added then heated to 100°C and left to run for 24 hours. Once complete, the reaction was concentrated under vacuum, dissolved in DCM, and washed with water two times, brine, then dried with MgSO₄. A bright yellow powder was collected (270 mg, 0.44 mmol, 91.6% yield) after recrystallization in DCM/Methanol. ¹H NMR (C₆D₆, 500 MHz) δ 8.18 (d, J = 8.35 Hz, 1H), 7.69 (d, J = 8.09 Hz, 2H), 7.66 (dd, J = 7.21, 2.22 Hz, 2H), 7.51 (d, J = 7.21 Hz, 4H), 7.46 (m, 8H), 7.37 (d, J = 2.0 Hz, 2H), 7.25 (m, 8H), 6.73 (dd, J = 2.03 Hz, 2H), 5.88 (d, J = 8.28 Hz, 2H). ¹³C NMR (C₆D₆, 300 MHz) δ 144.49, 140.93, 139.74, 139.02, 135.69, 135.17, 134.49, 133.60, 131.47, 129.06, 128.82, 128.72, 127.52, 127.08, 126.95, 126.86, 126.76, 126.56, 123.38, 122.05, 114.23, 113.98.

Control experiments

Control polymerizations revealed negligible or no polymerization in the absence of any of the components pertinent to the O-ATRP system (light, PC, or initiator) or in the presence of oxygen.

General procedure for O-ATRP of MMA using a UV light source

A 20 mL scintillation vial equipped with a small stirbar was transferred into a nitrogen-atmosphere glove box. To this vial DMA, methyl methacrylate (MMA), photocatalyst from a stock solution in DMA and initiator were added in that order via pipette. The vial was tightly sealed and wrapped in aluminum foil. The vial was transferred out of the glove box, the aluminum foil was removed, then placed under UV irradiation while stirring (Figure 3.9). Timing of the polymerization started once the vial was placed under irradiation. To analyze the progress of the polymerization at a given time point, aluminum foil was wrapped around the vial, the timer was stopped and the sample was taken back into the glove box where a 0.1 mL aliquot of the reaction was removed via syringe and injected into a vial containing 0.7 mL CDCl_3 with 250 ppm butylated hydroxytoluene (BHT) to quench the reaction. The reaction vessel was then transferred back under UV irradiation where the timer was once again started. This aliquot was then analyzed via NMR for conversion. After NMR, the volatiles were removed from the sample, re-dissolved in THF and passed through a syringe filter for analysis by gel permeation chromatography coupled with multi-angle light scattering.



Figure 3.9. Photograph of the reaction setup for O-ATRP using UV irradiation.

Monomer scope

The polymerization of different monomers - BMA, BnMA and DMA - were carried out using the general polymerization conditions described above. A ratio of [1000]:[10]:[1], [monomer]:[initiator]:[catalyst] was used with 9.35 mmol of monomer used in each trial. An equal volume of DMA to monomer was used. After the polymerization was allowed to run for 8 hours an aliquot was taken for analysis of monomer conversion by ^1H NMR, after which, methanol was immediately added to the reaction mixture to precipitate out the polymer. The resulting solid polymer was filtered then dried and used for analysis by gel permeation chromatography coupled with multi-angle light scattering. The results from these polymerizations are given in Table 3.5.

General procedure for chain extension of poly methyl methacrylate with various monomers by photocatalyzed O-ATRP

Synthesis of PMMA Macroinitiator

Catalyst 3 (23.2 mg, .0748 mmol, 8 eq.) was dissolved in 8.00 mL DMA and stirred with MMA (8.00 mL, 74.8 mmol, 1000 eq.), and DBMM (143 μL , 0.748 mmol, 10 eq.) in a 20 mL scintillation vial in a nitrogen-filled glove box. The reaction mixture was then wrapped in aluminum foil, removed from the glove box and placed into the aforementioned UV apparatus. The reaction ran for 4 hours before the reaction media was poured into 800 mL of stirring room temperature methanol. The resulting polymer was stirred for an hour before being dissolved in a minimal amount of dichloromethane. The polymer was dissolved with dichloromethane and re-precipitated into stirring methanol a total of three times to remove unreacted monomer, initiator or catalyst ($M_n = 8.83$ kDa, $M_w = 9.85$ kDa, $\text{Đ} = 1.12$).

Synthesis of Block Copolymers from isolated macroinitiator

Block copolymers were synthesized using a ratio of [1500]:[10]:[1], [monomer]:[initiator]:[catalyst] using 0.100 g of macroinitiator in each trial, and catalyst 3. Each reaction was set up using the same method as the general polymerization procedure described above. The polymerizations were all run for 10 hours before the reaction media was poured into 100 mL of stirring, room temperature methanol. The resulting polymers were collected via vacuum filtration and dried under vacuum. The results from these polymerizations are given in Table 3.6.

General procedure for O-ATRP of MMA using a visible light source

A 20 mL scintillation vial equipped with a small stirbar was transferred into a nitrogen-atmosphere glove box. To this vial DMA, methyl methacrylate (MMA), photocatalyst from a stock solution in DMA and initiator were added in that order via pipette. Timing of the polymerization started once the vial was placed into an LED-lined beaker (Figure 3.10). To analyze the progress of the polymerization at a given time point, a 0.1 mL aliquot of the reaction was removed via syringe and injected into a vial containing 0.7 mL CDCl_3 with 250 ppm butylated hydroxytoluene (BHT) to quench the reaction. This aliquot was then analyzed via NMR for conversion. After NMR, the volatiles were removed from the sample, re-dissolved in THF and passed through a syringe filter for analysis by gel permeation chromatography coupled with multi-angle light scattering.

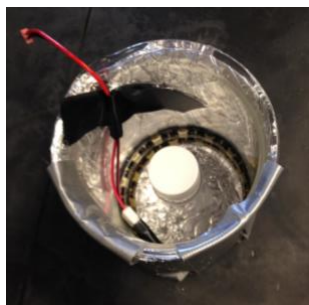


Figure 3.10. Photograph of the reaction setup for O-ATRP using visible light LED beakers.

3. Characterization of Catalysts' Photoredox Properties

UV-vis absorption spectroscopy

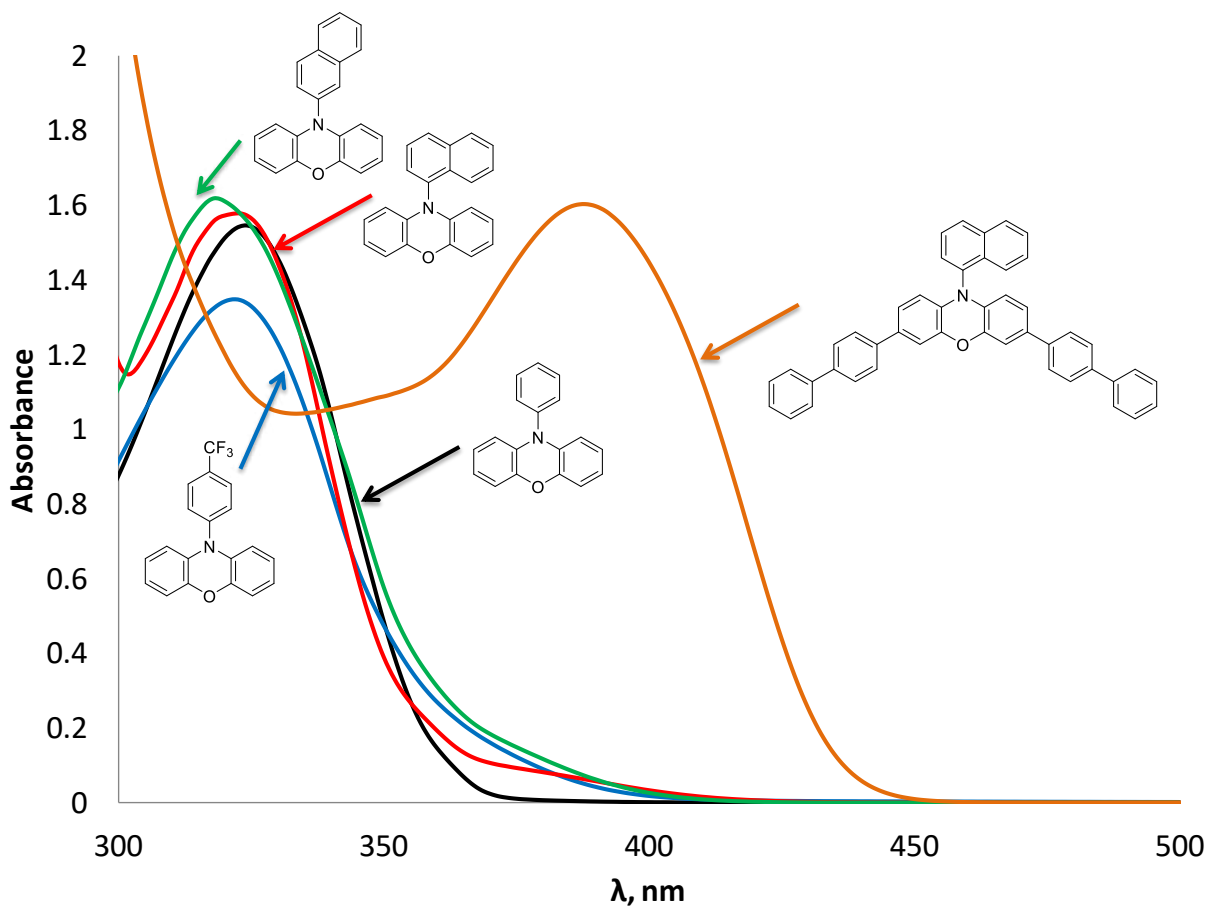


Figure 3.11. UV-vis absorption spectrums of the phenoxazine photocatalysts. PC 1-4 were taken at 0.20 mM and PC 5 was taken at 0.06mM. Solvent = DMA. Path length = 1cm.

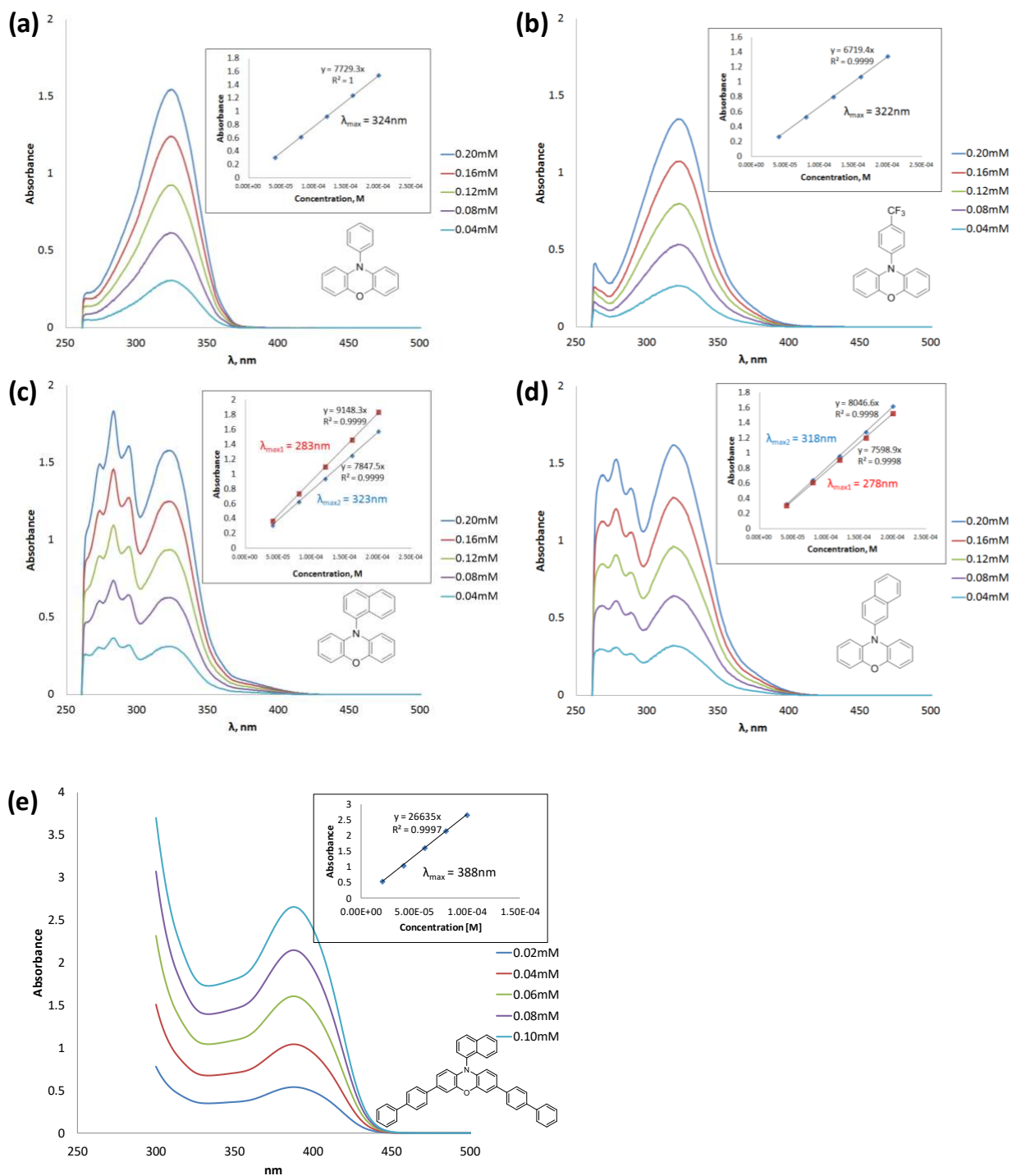


Figure 3.12. UV-vis absorption of the phenoxazine catalysts taken at different concentrations in DMA. Path length = 1cm.

Fluorescence spectroscopy

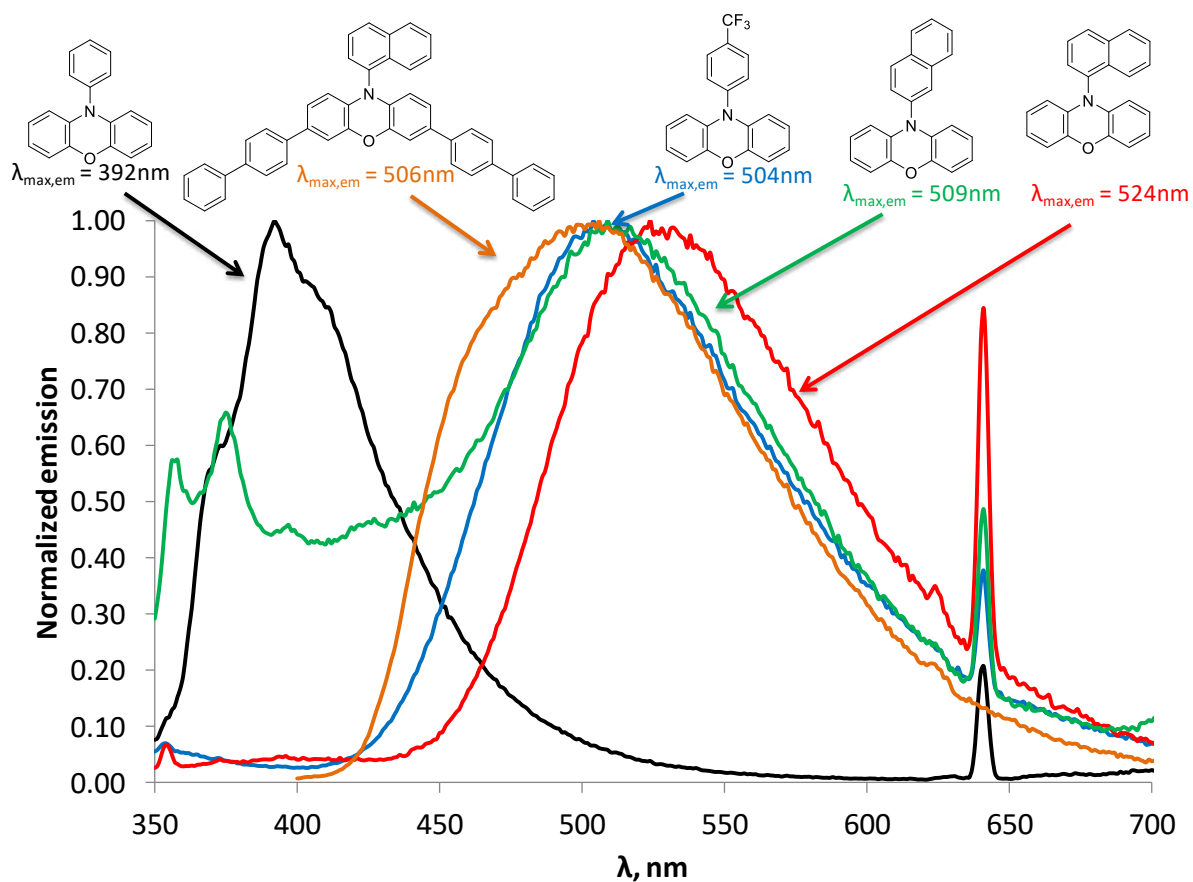


Figure 3.13. Plot of the normalized emission spectrums of the phenoxazine photocatalysts in DMA.

PC 1-4 were irradiated with 320 nm light while PC 5 was irradiated with 380nm light.

Cyclic voltammetry

Work performed by co-author Chern-Hooi Lim

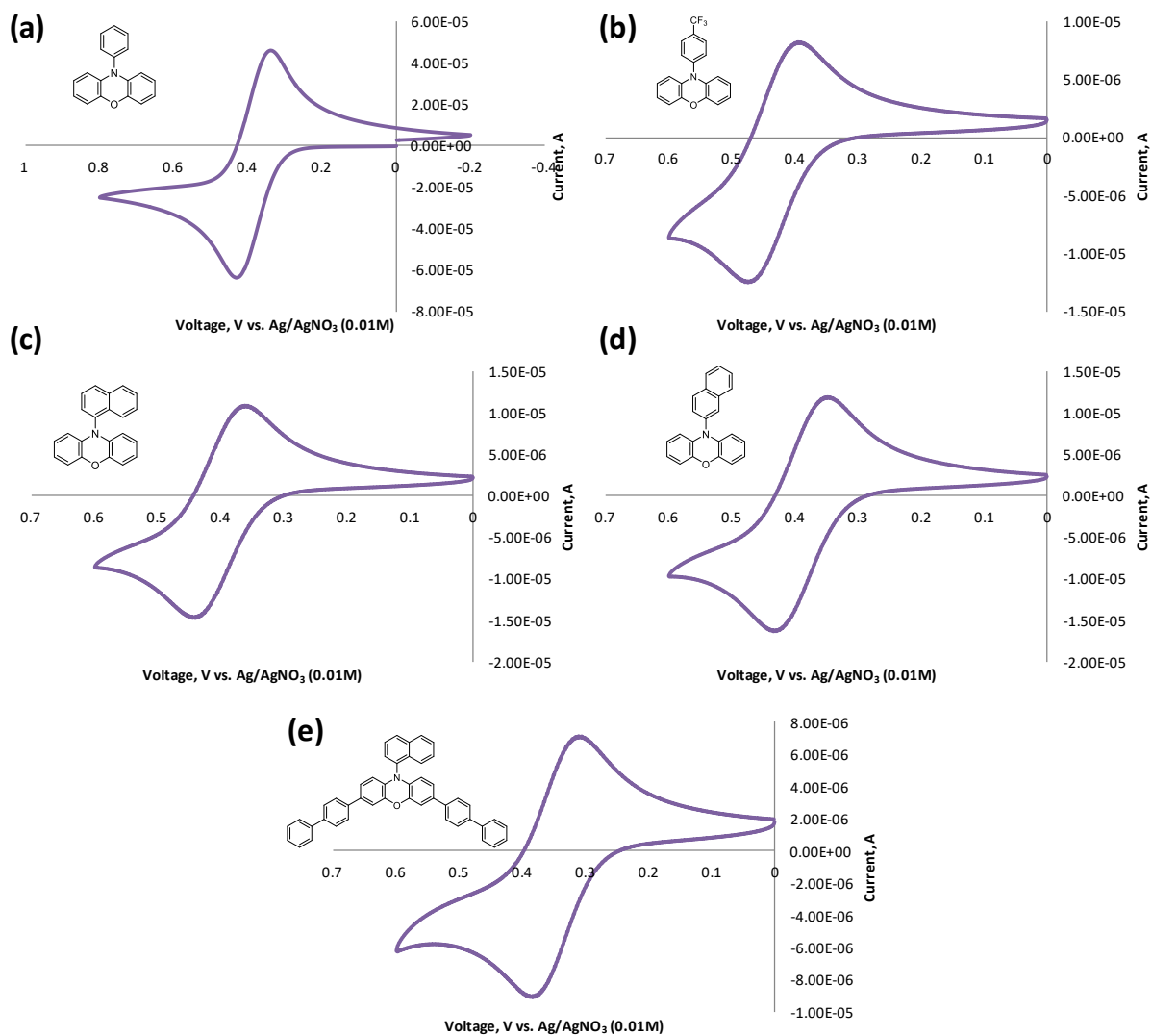


Figure 3.14. Cyclic voltammograms of the phenoxazine photocatalysts performed in a 3-compartment electrochemical cell. Reference electrode: Ag/AgNO₃ (0.01M) in MeCN; electrolyte: 0.1 M NBu₄PF₆; scan rate: 0.10 V/s. DMA is used as the solvent in the working electrode compartment for (b)-(e) while MeCN is used as the solvent in (a). Platinum is used as both the working and counter electrodes.

Experimental and theoretical determination of excited state reduction potentials

Work performed by co-author Chern-Hooi Lim

Table 3.4. Calculation of excited state reduction potentials of photocatalysts 1-5.

PC	abs λ_{\max} (nm) ^a	$\epsilon \lambda_{\max}$ (M ⁻¹ cm ⁻¹) ^b	em λ_{\max} (nm) ^c	E(em λ_{\max}) (V vs. SCE) ^d	E(triplet), theo (V vs. SCE) ^e
1	324	7729	392	3.16	2.69
2	322	6719	504	2.46	2.63
3	323	7848	524	2.37	2.39
4	318	8047	509	2.44	2.45
5	388	26635	506	2.45	2.41

PC	E _{1/2} (PC ^{•+} /PC) (V vs. SCE) ^f	E ⁰ (PC ^{•+} /PC), theo (V vs. SCE) ^e	E ^{0*} (PC ^{•+} /PC [*]) (V vs. SCE)	E ^{0*} (PC ^{•+} / ³ PC [*]), theo (V vs. SCE) ^e
1	0.68	0.58	-2.48 ^g	-2.11
2	0.73	0.59	-1.73	-2.03
3	0.70	0.55	-1.67	-1.84
4	0.69	0.55	-1.75	-1.90
5	0.65	0.48	-1.80	-1.93

^aMaximum absorption wavelength; PC 3 and 4 exhibit another λ_{\max} at higher energy wavelengths of 283 nm and 278 nm, respectively. ^bMolar absorptivity at the reported λ_{\max} . ^cMaximum emission wavelength when irradiated with 320 nm light (PC 1-4) and 380 nm light (PC 5). ^dEnergy of emitted photons. ^eTheoretical predictions from DFT calculations at uM06/6-311+Gdp/CPCM-

H₂O//uM06/6-31+Gdp/CPCM-H₂O level of theory. ^fObtained from cyclic voltammetry. ^gThe E^{0} of PC 1 is significantly more negative than PC 2-5 and deviates from the predicted trend. In the DFT calculations, the triplet excited state was explicitly assumed while the observed emission is likely fluorescence from the relaxed singlet excited state.*

4. Computational Details

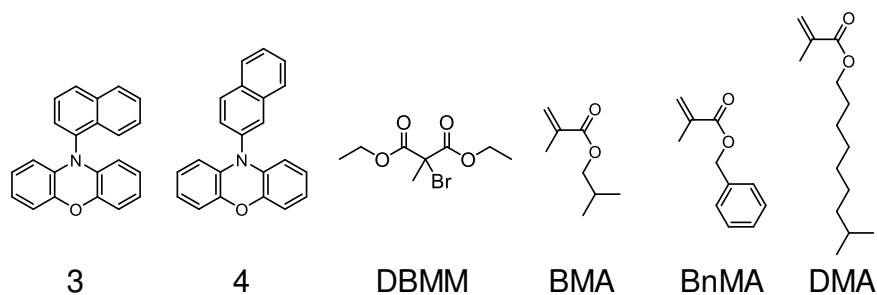
Work performed by co-author Chern-Hooi Lim

Standard reduction potentials (E⁰) were calculated following previously reported procedures.^{30,31,32,33} A value of -100.5 kcal/mol was assumed for the reduction free energy of the standard hydrogen electrode (SHE) as described in Ref. 4. Thus, E⁰ = (-100.5 - ΔG_{red})/23.06 (V vs. SHE); for E⁰ (PC^{•+}/³PC*), ΔG_{red} = G(³PC*) - G(PC^{•+}) while for E⁰ (PC^{•+}/PC), ΔG_{red} = G(PC) - G(PC^{•+}). The Gibbs free energies of ³PC*, PC^{•+}, and PC (for PC 1-4) were calculated at the unrestricted M06/6-311+G** level of theory in CPCM-H₂O solvent (single point energy) using geometries optimized at unrestricted M06/6-31+G** level of theory in CPCM-H₂O solvent. The triple zeta basis set (6-311+G**) generally improves the E⁰ (PC^{•+}/PC) by ~0.1V relative to 6-31+G**, while the triplet energy is invariant for these two basis sets. To reference to the Saturated Calomel Electrode (SCE), E⁰ (vs. SHE) is converted to E⁰ (vs. SCE) using E⁰ (vs. SCE) = E⁰ (vs. SHE) - 0.24 V. Triplet energies (in eV) of PCs were obtained by [G(³PC*) - G(PC)], in kcal/mol]/23.06. Population analysis was performed using electrostatic potential-derived charges with the CHELPG method³⁴ performed at the unrestricted M06/6-31G** level of theory in CPCM-H₂O solvent.

Geometry optimization of PC 5 (3,7-Di(4-biphenyl) 1-Naphthalene- 10-Phenoxazine) was performed at the unrestricted M06/Lanl2dz level of theory in CPCM-H₂O solvent; the smaller Lanl2dz basis sets was employed for computational efficiency due to its extensive structure. Singlet point calculation at the converged M06/Lanl2dz geometry was then performed at the unrestricted M06/6-311+G** level of theory in CPCM-H₂O solvent.

5. Supplemental Polymerization Data

Table 3.5. Polymerization Results of O-ATRP of Methacrylates.^a



PC	Monomer	Time (h)	Conv (%)	M _n (kDa)	M _w (kDa)	Đ (M _w /M _n)	I* (%)
3	BMA	8	62.0	13.5	16.4	1.22	67.4
3	BnMA	8	46.1	8.2	11.6	1.41	102
3	DMA	8	87.5	20.9	28.3	1.35	42.9
4	BMA	8	62	15.2	17.3	1.14	59.7
4	BnMA	8	77.1	12.5	16.0	1.28	110
4	IDMA	8	83.2	21.7	28.4	1.31	39.6

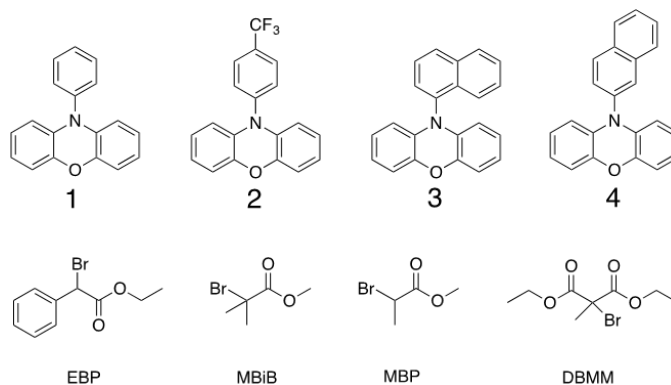
^aPolymerizations of vinyl monomers were performed at [1000]:[10]:[1] using DBMM as the initiator and the same volume of solvent as that of the monomer added.

Table 3.6. Polymerization Results of O-ATRP PMMA chain extensions.^a

PC	Monomer A	Monomer B	Time (h)	M _n (kDa)	M _w (kDa)	Đ (M _w /M _n)
3	MMA	MMA	10	38.8	49.4	1.27
3	MMA	BMA	10	38.8	43.8	1.13
3	MMA	IDMA	10	59.8	77.6	1.29
3	MMA	BnMA	10	46.8	67.1	1.43

^aPolymerization chain extensions were performed at [1500]:[10]:[1] using a PMMA macroinitiator and the same volume of solvent as that of the monomer added.

Table 3.7. Polymerization Results of O-ATRP initiator screen for PC 1-4.^a



PC	Initiator	Time (h)	Conv (%)	M _n (kDa)	M _w (kDa)	Đ (M _w /M _n)	I* (%)
1	EBP	8	92.2	8.01	14.3	1.79	119
1	DBMM	8	95.6	7.16	10.6	1.48	137
2	EBP	8	61.2	15.4	20.7	1.34	41.2
2	DBMM	8	55.3	6.54	9.48	1.45	85.5
3	EBP	8	66.4	9.29	12.6	1.36	74.2
3	MBiB	8	76.5	9.58	11.8	1.23	81.8
3	MBP	8	70.7	10.9	14.1	1.29	66.4
3	DBMM	8	78.8	8.79	10.8	1.22	92.6
4	EBP	8	59.0	11.3	13.6	1.21	54.7
4	MBiB	8	69.2	11.3	15.0	1.34	63.3
4	MBP	8	31.7	5.80	6.87	1.19	57.6
4	DBMM	8	80.2	10.7	11.9	1.11	77.3

^aPolymerizations were performed at [1000]:[10]:[1] for [MMA]:[Initiator]:[PC] using the same volume of DMA as that of the monomer added.

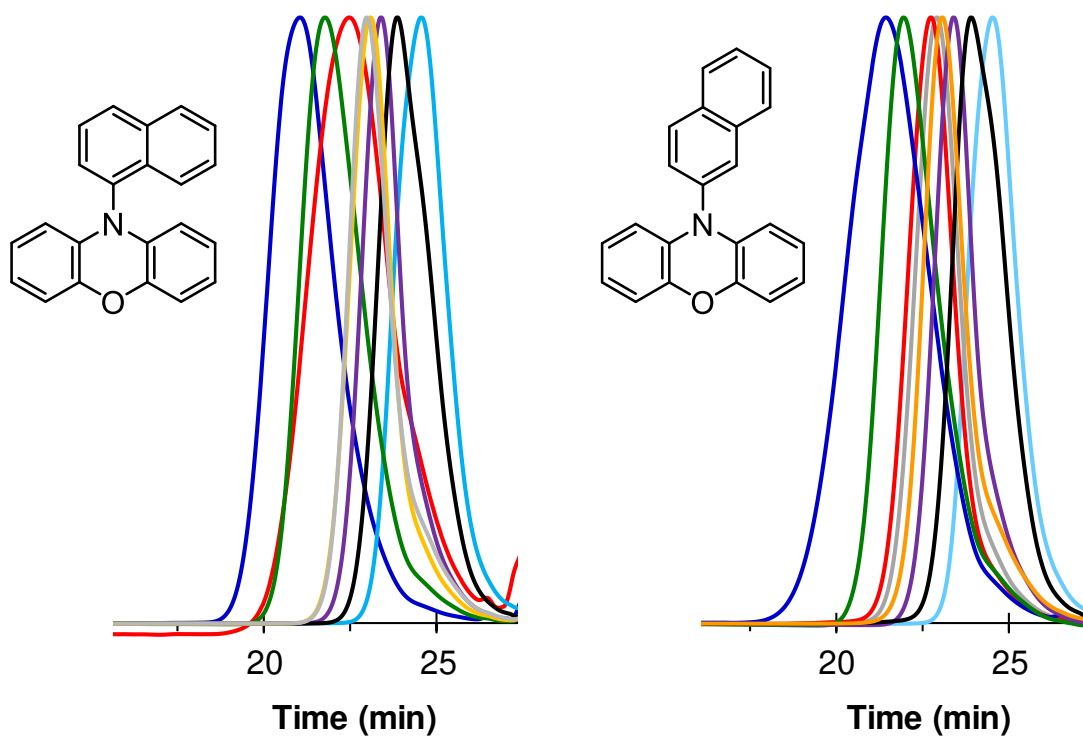


Figure 3.15. Gel permeation traces of PMMA produced using 3 (left) and 4 (right) reported in Table 3.2 of the Main Text. Color scheme corresponds to: (left plot) run 5 (light blue), run 6 (gray), run 7 (orange), run 8 (red), run 9 (green), run 10 (blue), run 11 (purple), run 12 (black); (right plot) run 13 (light blue), run 14 (orange), run 15 (gray), run 16 (red), run 17 (green), run 18 (blue), run 19 (purple), run 20 (black).

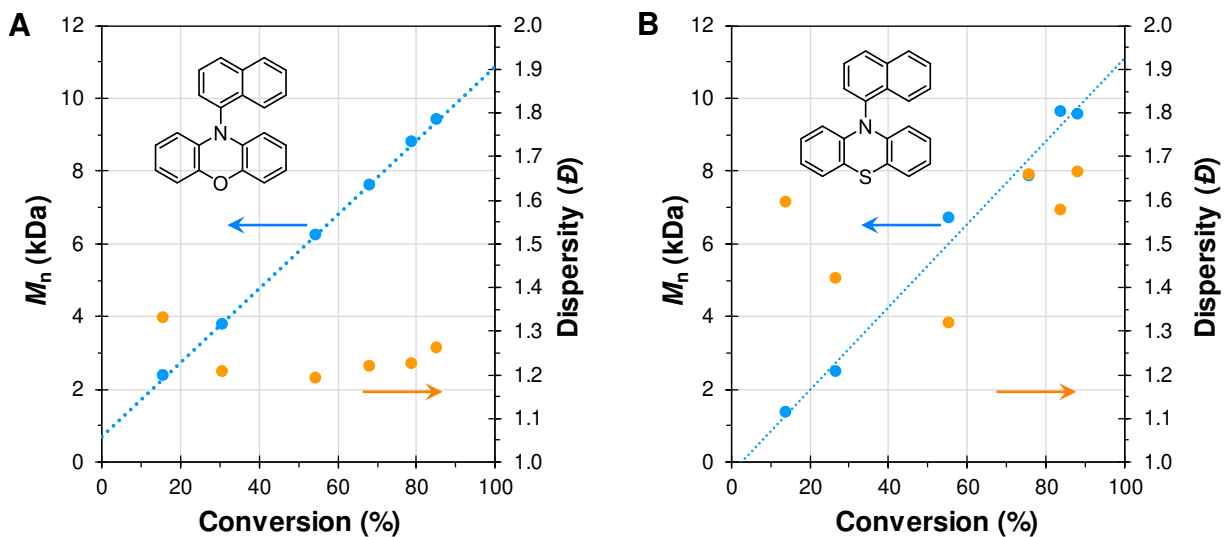


Figure 3.16. Plots of number average molecular weight (blue) and dispersity (orange) as a function of monomer conversion in the polymerization of methyl methacrylate catalyzed by 1-naphthylene-10-phenoxazine (A) and 1-naphthylene-10-phenthiazine (B). Conditions: $[MMA]:[DBMM]:[PC] = [1000]:[10]:[1]$; 9.35 μ moles PC, 1.00 mL dimethylacetamide, and irradiated with 365 nm light.

6. X-ray Crystallography Data

Work performed by co-author Chern-Hooi Lim and Brian Newell

Structures were determined for the compounds listed in Table 3.1. Single crystals were coated with Paratone-N oil and mounted under a cold stream of dinitrogen gas. Single crystal X-ray diffraction data were acquired on a Bruker Kappa APEX II CCD diffractometer with Mo K α radiation ($\lambda = 0.71073 \text{ \AA}$) and a graphite monochromator. Initial lattice parameters were obtained from a least-squares analysis of more than 100 reflections; these parameters were later refined against all data. None of the crystals showed significant decay during data collection. Data were integrated and corrected for Lorentz and polarization effects using Bruker APEX3 software, and semiempirical absorption corrections were applied using SCALE (Sheldrick, G. M. SADABS – a program for area detector absorption corrections). Space group assignments were based on systematic absences, E statistics, and successful refinement of the structures. Structures were solved using Direct Methods and were refined with the aid of successive Fourier difference maps against all data using the SHELXTL 6.14 software package (Sheldrick, G. M. SHELXTL, v. 6.12; Bruker AXS: Madison, WI, 1999). Thermal parameters for all non-hydrogen atoms were refined anisotropically. All hydrogen atoms were assigned to ideal positions and refined using a riding model with an isotropic thermal parameter 1.2 times that of the attached carbon atom (1.5 times for methyl hydrogens).

In the structure of 'gm01', there is a disordered solvate molecule that was found in Fourier difference maps. After numerous attempts to model the disorder failed, SQUEEZE (Spek, A. L. J. Appl. Crystallogr. 2003, 36, 7) was used to remove the remaining disordered components. According to the SQUEEZE output, approximately 4 dichloromethane solvent molecules are

present in the void space and were removed. The chemical data presented for 'gm01' do not include the components removed by SQUEEZE.

1-Naphthalene-10-phenoxazine

Table 3.8. *Crystal data and structure refinement for gm01.*

Identification code	gm01
Empirical formula	C ₂₂ H ₁₅ N O
Formula weight	309.35
Temperature	117(2) K
Wavelength	0.71073 Å
Crystal system	Triclinic
Space group	P-1
Unit cell dimensions	a = 8.8713(6) Å a = 83.142(4)°. b = 9.1631(6) Å b = 78.687(4)°. c = 11.2812(9) Å g = 71.594(4)°.
Volume	851.59(11) Å ³
Z	2
Density (calculated)	1.206 Mg/m ³
Absorption coefficient	0.074 mm ⁻¹
F(000)	324
Crystal size	0.374 x 0.132 x 0.097 mm ³
Theta range for data collection	1.844 to 27.480°.
Index ranges	-11 ≤ h ≤ 11, -11 ≤ k ≤ 11, -14 ≤ l ≤ 12
Reflections collected	13754
Independent reflections	3908 [R(int) = 0.0632]
Completeness to theta = 25.242°	99.9 %

Absorption correction Semi-empirical from equivalents

Max. and min. transmission 0.7466 and 0.6543

Refinement method Full-matrix least-squares on F^2

Data / restraints / parameters 3908 / 0 / 217

Goodness-of-fit on F^2 1.030

Final R indices [$I > 2\sigma(I)$] R1 = 0.0569, wR2 = 0.1236

R indices (all data) R1 = 0.0976, wR2 = 0.1452

Extinction coefficient n/a

Largest diff. peak and hole 0.714 and -0.316 e. \AA^{-3}

Table 3.9. Atomic coordinates ($\times 10^4$) and equivalent isotropic displacement parameters ($\text{\AA}^2 \times 10^3$)

for gm01. $U(\text{eq})$ is defined as one third of the trace of the orthogonalized U^{ij} tensor.

	x	y	z	$U(\text{eq})$
N(1)	6593(2)		5936(2)	2786(2) 20(1)
O(1)	4626(2)		8354(2)	1482(2) 32(1)
C(1)	7016(3)		7296(2)	2431(2) 18(1)
C(2)	8383(3)		7524(3)	2705(2) 22(1)
C(3)	8730(3)		8902(3)	2356(2) 27(1)
C(4)	7728(3)		10074(3)	1732(2) 27(1)
C(5)	6359(3)		9864(2)	1445(2) 24(1)
C(6)	6018(3)		8490(2)	1783(2) 21(1)

C(7)	4389(3)	6910(2)	1653(2)	21(1)
C(8)	3127(3)	6743(3)	1192(2)	26(1)
C(9)	2788(3)	5348(3)	1372(2)	28(1)
C(10)	3740(3)	4122(3)	1995(2)	25(1)
C(11)	5026(3)	4285(2)	2450(2)	21(1)
C(12)	5354(3)	5691(2)	2301(2)	18(1)
C(13)	7645(3)	4684(2)	3414(2)	18(1)
C(14)	7385(3)	4571(2)	4651(2)	22(1)
C(15)	8427(3)	3356(3)	5281(2)	26(1)
C(16)	9680(3)	2286(3)	4653(2)	24(1)
C(17)	9978(3)	2366(2)	3362(2)	19(1)
C(18)	11261(3)	1279(2)	2679(2)	22(1)
C(19)	11520(3)	1396(2)	1442(2)	23(1)
C(20)	10497(3)	2618(2)	816(2)	22(1)
C(21)	9246(3)	3692(2)	1437(2)	19(1)
C(22)	8944(3)	3600(2)	2728(2)	17(1)

Table 3.10. Bond lengths [Å] and angles [°] for gm01.

N(1)-C(1)	1.404(3)
N(1)-C(12)	1.407(3)
N(1)-C(13)	1.442(3)
O(1)-C(6)	1.389(3)

O(1)-C(7)	1.390(3)
C(1)-C(2)	1.390(3)
C(1)-C(6)	1.403(3)
C(2)-C(3)	1.387(3)
C(3)-C(4)	1.379(3)
C(4)-C(5)	1.390(3)
C(5)-C(6)	1.379(3)
C(7)-C(8)	1.379(3)
C(7)-C(12)	1.400(3)
C(8)-C(9)	1.386(3)
C(9)-C(10)	1.383(3)
C(10)-C(11)	1.394(3)
C(11)-C(12)	1.392(3)
C(13)-C(14)	1.365(3)
C(13)-C(22)	1.422(3)
C(14)-C(15)	1.421(3)
C(15)-C(16)	1.366(3)
C(16)-C(17)	1.425(3)
C(17)-C(18)	1.416(3)
C(17)-C(22)	1.429(3)
C(18)-C(19)	1.366(3)
C(19)-C(20)	1.413(3)
C(20)-C(21)	1.365(3)

C(21)-C(22) 1.425(3)

C(1)-N(1)-C(12) 118.99(17)

C(1)-N(1)-C(13) 119.37(17)

C(12)-N(1)-C(13) 120.20(16)

C(6)-O(1)-C(7) 117.86(16)

C(2)-C(1)-C(6) 118.03(19)

C(2)-C(1)-N(1) 122.80(19)

C(6)-C(1)-N(1) 119.17(19)

C(3)-C(2)-C(1) 120.6(2)

C(4)-C(3)-C(2) 120.8(2)

C(3)-C(4)-C(5) 119.4(2)

C(6)-C(5)-C(4) 119.9(2)

C(5)-C(6)-O(1) 117.30(19)

C(5)-C(6)-C(1) 121.2(2)

O(1)-C(6)-C(1) 121.44(19)

C(8)-C(7)-O(1) 117.07(19)

C(8)-C(7)-C(12) 121.4(2)

O(1)-C(7)-C(12) 121.50(19)

C(7)-C(8)-C(9) 119.9(2)

C(10)-C(9)-C(8) 119.6(2)

C(9)-C(10)-C(11) 120.4(2)

C(12)-C(11)-C(10) 120.5(2)

C(11)-C(12)-C(7)	118.12(19)
C(11)-C(12)-N(1)	122.76(18)
C(7)-C(12)-N(1)	119.12(18)
C(14)-C(13)-C(22)	121.46(19)
C(14)-C(13)-N(1)	119.5(2)
C(22)-C(13)-N(1)	119.06(19)
C(13)-C(14)-C(15)	120.0(2)
C(16)-C(15)-C(14)	120.2(2)
C(15)-C(16)-C(17)	121.2(2)
C(18)-C(17)-C(16)	122.86(19)
C(18)-C(17)-C(22)	118.5(2)
C(16)-C(17)-C(22)	118.7(2)
C(19)-C(18)-C(17)	121.4(2)
C(18)-C(19)-C(20)	120.1(2)
C(21)-C(20)-C(19)	120.5(2)
C(20)-C(21)-C(22)	120.7(2)
C(13)-C(22)-C(21)	122.67(19)
C(13)-C(22)-C(17)	118.47(19)
C(21)-C(22)-C(17)	118.9(2)

Table 3.11. Anisotropic displacement parameters ($\text{\AA}^2 \times 10^3$) for gm01. The anisotropic displacement factor exponent takes the form: $-2p^2[h^2 a^{*2}U^{11} + \dots + 2 h k a^* b^* U^{12}]$

U11 U22 U33 U23 U13 U12

N(1)	17(1)	17(1)	24(1)	2(1)	-8(1)	-3(1)
O(1)	22(1)	21(1)	53(1)	11(1)	-17(1)	-4(1)
C(1)	19(1)	19(1)	14(1)	-3(1)	1(1)	-4(1)
C(2)	24(1)	27(1)	17(1)	-1(1)	-6(1)	-8(1)
C(3)	30(2)	33(1)	23(1)	-2(1)	-5(1)	-16(1)
C(4)	35(2)	22(1)	25(1)	-3(1)	1(1)	-13(1)
C(5)	25(1)	18(1)	21(1)	0(1)	2(1)	0(1)
C(6)	16(1)	21(1)	23(1)	-3(1)	-1(1)	-3(1)
C(7)	19(1)	21(1)	22(1)	1(1)	-2(1)	-4(1)
C(8)	19(1)	32(1)	23(1)	6(1)	-8(1)	-5(1)
C(9)	22(1)	44(1)	23(1)	-2(1)	-8(1)	-13(1)
C(10)	27(1)	27(1)	25(1)	-3(1)	-3(1)	-11(1)
C(11)	20(1)	19(1)	21(1)	-1(1)	-5(1)	-3(1)
C(12)	15(1)	22(1)	15(1)	-2(1)	-2(1)	-3(1)
C(13)	16(1)	18(1)	22(1)	2(1)	-7(1)	-4(1)
C(14)	20(1)	24(1)	20(1)	-4(1)	-3(1)	-3(1)
C(15)	26(1)	35(1)	17(1)	1(1)	-6(1)	-8(1)
C(16)	22(1)	29(1)	21(1)	3(1)	-9(1)	-5(1)
C(17)	16(1)	20(1)	24(1)	2(1)	-8(1)	-6(1)
C(18)	19(1)	19(1)	28(1)	2(1)	-8(1)	-4(1)
C(19)	17(1)	23(1)	28(1)	-7(1)	-3(1)	-3(1)

C(20)	25(1)	24(1)	17(1)	-4(1)	-2(1)	-8(1)
C(21)	20(1)	20(1)	20(1)	2(1)	-7(1)	-6(1)
C(22)	16(1)	17(1)	21(1)	0(1)	-6(1)	-7(1)

Table 3.12. Hydrogen coordinates ($\times 10^4$) and isotropic displacement parameters ($\text{\AA}^2 \times 10^3$) for gm01.

	x	y	z	U(eq)
H(2)	9085	6729	3135	27
H(3)	9669	9040	2550	33
H(4)	7971	11017	1499	32
H(5)	5660	10666	1017	28
H(8)	2490	7584	752	31
H(9)	1907	5235	1069	34
H(10)	3515	3162	2113	30
H(11)	5682	3431	2865	25
H(14)	6506	5305	5090	26
H(15)	8253	3287	6141	31
H(16)	10363	1474	5084	29
H(18)	11955	450	3089	27
H(19)	12390	655	1001	28

H(20) 10682 2692 -45 26

H(21) 8569 4509 1005 23

1-Naphthalene-10-phenothiazine

Table 3.13. *Crystal data and structure refinement for gm03.*

Identification code gm03

Empirical formula C₂₂H₁₅N S

Formula weight 325.41

Temperature 100(2) K

Wavelength 0.71073 Å

Crystal system Monoclinic

Space group P2₁/n

Unit cell dimensions a = 14.790(5) Å a = 90°.

b = 6.904(2) Å b = 113.094(15)°.

c = 17.265(6) Å g = 90°.

Volume 1621.5(10) Å³

Z 4

Density (calculated) 1.333 Mg/m³

Absorption coefficient 0.201 mm⁻¹

F(000) 680

Crystal size 0.202 x 0.200 x 0.063 mm³

Theta range for data collection 1.542 to 24.710°.

Index ranges -13 ≤ h ≤ 17, -8 ≤ k ≤ 8, -20 ≤ l ≤ 20

Reflections collected 28247

Independent reflections 2763 [R(int) = 0.1046]

Completeness to theta = 24.710° 99.8 %

Absorption correction Semi-empirical from equivalents

Max. and min. transmission 0.7457 and 0.6585

Refinement method Full-matrix least-squares on F²

Data / restraints / parameters 2763 / 0 / 217

Goodness-of-fit on F² 1.045

Final R indices [I>2sigma(I)] R1 = 0.0422, wR2 = 0.1143

R indices (all data) R1 = 0.0633, wR2 = 0.1254

Extinction coefficient n/a

Largest diff. peak and hole 0.284 and -0.311 e.Å⁻³

Table 3.14. Atomic coordinates ($\times 10^4$) and equivalent isotropic displacement parameters ($\text{\AA}^2 \times 10^3$) for gm03. $U(\text{eq})$ is defined as one third of the trace of the orthogonalized U^{ij} tensor.

	x	y	z	U(eq)
C(1)	-215(2)	10115(3)	3208(1)	17(1)
C(2)	-763(2)	9721(4)	3691(2)	20(1)
C(3)	-1586(2)	10817(4)	3604(2)	24(1)
C(4)	-1904(2)	12296(4)	3015(2)	25(1)
C(5)	-1365(2)	12699(3)	2535(2)	21(1)
C(6)	-508(2)	11693(3)	2648(1)	18(1)

C(7)	781(2)	10373(3)	2016(2)	18(1)
C(8)	1081(2)	10194(4)	1349(2)	21(1)
C(9)	1590(2)	8574(4)	1279(2)	23(1)
C(10)	1776(2)	7097(4)	1864(2)	23(1)
C(11)	1450(2)	7249(3)	2517(2)	19(1)
C(12)	948(2)	8881(3)	2608(1)	15(1)
C(13)	990(2)	7543(3)	3922(1)	17(1)
C(14)	459(2)	5917(3)	3893(2)	21(1)
C(15)	852(2)	4420(4)	4489(2)	24(1)
C(16)	1780(2)	4569(4)	5092(2)	24(1)
C(17)	2362(2)	6237(3)	5140(2)	20(1)
C(18)	3335(2)	6436(4)	5746(2)	25(1)
C(19)	3872(2)	8066(4)	5792(2)	27(1)
C(20)	3462(2)	9618(4)	5232(2)	24(1)
C(21)	2528(2)	9473(4)	4630(1)	20(1)
C(22)	1957(2)	7781(3)	4558(1)	16(1)
N(1)	634(1)	9030(3)	3287(1)	17(1)
S(1)	256(1)	12566(1)	2155(1)	21(1)

Table 3.15. Bond lengths [\AA] and angles [$^\circ$] for gm03.

C(1)-C(2)	1.398(3)
C(1)-C(6)	1.407(3)

C(1)-N(1)	1.422(3)
C(2)-C(3)	1.390(3)
C(3)-C(4)	1.386(4)
C(4)-C(5)	1.385(3)
C(5)-C(6)	1.391(3)
C(6)-S(1)	1.766(2)
C(7)-C(8)	1.391(3)
C(7)-C(12)	1.403(3)
C(7)-S(1)	1.761(2)
C(8)-C(9)	1.380(3)
C(9)-C(10)	1.385(4)
C(10)-C(11)	1.393(3)
C(11)-C(12)	1.392(3)
C(12)-N(1)	1.425(3)
C(13)-C(14)	1.359(3)
C(13)-C(22)	1.430(3)
C(13)-N(1)	1.443(3)
C(14)-C(15)	1.413(3)
C(15)-C(16)	1.362(4)
C(16)-C(17)	1.421(3)
C(17)-C(18)	1.415(3)
C(17)-C(22)	1.425(3)
C(18)-C(19)	1.362(4)

C(19)-C(20) 1.410(4)

C(20)-C(21) 1.368(3)

C(21)-C(22) 1.418(3)

C(2)-C(1)-C(6) 117.8(2)

C(2)-C(1)-N(1) 122.5(2)

C(6)-C(1)-N(1) 119.7(2)

C(3)-C(2)-C(1) 121.1(2)

C(4)-C(3)-C(2) 120.7(2)

C(5)-C(4)-C(3) 118.5(2)

C(4)-C(5)-C(6) 121.5(2)

C(5)-C(6)-C(1) 120.1(2)

C(5)-C(6)-S(1) 118.82(19)

C(1)-C(6)-S(1) 120.86(18)

C(8)-C(7)-C(12) 121.0(2)

C(8)-C(7)-S(1) 119.34(18)

C(12)-C(7)-S(1) 119.50(18)

C(9)-C(8)-C(7) 120.4(2)

C(8)-C(9)-C(10) 119.4(2)

C(9)-C(10)-C(11) 120.2(2)

C(12)-C(11)-C(10) 121.4(2)

C(11)-C(12)-C(7) 117.5(2)

C(11)-C(12)-N(1) 120.8(2)

C(7)-C(12)-N(1)	121.7(2)
C(14)-C(13)-C(22)	120.8(2)
C(14)-C(13)-N(1)	121.8(2)
C(22)-C(13)-N(1)	117.3(2)
C(13)-C(14)-C(15)	120.7(2)
C(16)-C(15)-C(14)	120.3(2)
C(15)-C(16)-C(17)	120.8(2)
C(18)-C(17)-C(16)	122.6(2)
C(18)-C(17)-C(22)	118.2(2)
C(16)-C(17)-C(22)	119.1(2)
C(19)-C(18)-C(17)	121.6(2)
C(18)-C(19)-C(20)	120.2(2)
C(21)-C(20)-C(19)	120.0(2)
C(20)-C(21)-C(22)	121.1(2)
C(21)-C(22)-C(17)	118.9(2)
C(21)-C(22)-C(13)	122.9(2)
C(17)-C(22)-C(13)	118.2(2)
C(1)-N(1)-C(12)	121.29(18)
C(1)-N(1)-C(13)	119.55(18)
C(12)-N(1)-C(13)	115.79(18)
C(7)-S(1)-C(6)	99.90(11)

Table 3.16. Anisotropic displacement parameters ($\text{\AA}^2 \times 10^3$) for gm03. The anisotropic

displacement factor exponent takes the form: $-2p^2[h^2 a^{*2}U^{11} + \dots + 2 h k a^* b^* U^{12}]$

	U11	U22	U33	U23	U13	U12
C(1)	15(1)	18(1)	16(1)	-5(1)	5(1)	-2(1)
C(2)	20(1)	21(1)	19(1)	-4(1)	7(1)	-5(1)
C(3)	21(1)	29(2)	25(1)	-9(1)	12(1)	-4(1)
C(4)	19(1)	30(2)	26(1)	-5(1)	9(1)	3(1)
C(5)	19(1)	20(1)	21(1)	-3(1)	5(1)	2(1)
C(6)	18(1)	19(1)	15(1)	-5(1)	6(1)	-3(1)
C(7)	12(1)	19(1)	20(1)	-2(1)	4(1)	-3(1)
C(8)	20(1)	24(1)	18(1)	2(1)	7(1)	-2(1)
C(9)	22(1)	29(2)	22(1)	-2(1)	13(1)	-1(1)
C(10)	17(1)	28(2)	23(1)	-3(1)	8(1)	2(1)
C(11)	15(1)	22(1)	19(1)	2(1)	5(1)	-1(1)
C(12)	11(1)	19(1)	13(1)	-3(1)	3(1)	-4(1)
C(13)	19(1)	18(1)	15(1)	0(1)	10(1)	3(1)
C(14)	22(1)	23(1)	19(1)	-4(1)	10(1)	-3(1)
C(15)	33(2)	20(1)	24(1)	-4(1)	16(1)	-5(1)
C(16)	34(2)	19(1)	22(1)	4(1)	14(1)	3(1)
C(17)	23(1)	22(1)	17(1)	1(1)	12(1)	6(1)
C(18)	26(1)	28(2)	20(1)	6(1)	9(1)	9(1)
C(19)	17(1)	36(2)	22(1)	2(1)	3(1)	2(1)

C(20) 21(1) 25(1) 24(1) 1(1) 7(1) -3(1)

C(21) 21(1) 22(1) 16(1) 4(1) 8(1) 3(1)

C(22) 17(1) 19(1) 14(1) -2(1) 9(1) 2(1)

N(1) 14(1) 21(1) 15(1) 1(1) 6(1) 2(1)

S(1) 24(1) 18(1) 24(1) 2(1) 12(1) 1(1)

Table 3.17. Hydrogen coordinates ($\times 10^4$) and isotropic displacement parameters ($\text{\AA}^2 \times 10^3$) for gm03.

	x	y	z	U(eq)
H(2)	-569	8688	4085	24
H(3)	-1934	10549	3951	29
H(4)	-2479	13016	2942	30
H(5)	-1586	13686	2119	25
H(8)	934	11193	940	25
H(9)	1812	8474	833	27
H(10)	2125	5977	1819	27
H(11)	1574	6216	2909	23
H(14)	-182	5786	3467	25
H(15)	468	3304	4470	29
H(16)	2040	3546	5485	29
H(18)	3620	5408	6130	30
H(19)	4526	8159	6202	32
H(20)	3833	10763	5274	28
H(21)	2258	10522	4254	23

References

- (1) (a) Matyjaszewski, K.; Tsarevsky, N. V. *J. Am. Chem. Soc.* 2014, 136, 6513–6533. (b) Matyjaszewski, K.; Tsarevsky, N. V. *Nat. Chem.* 2009, 1, 276–288. (c) Kamigaito, M.; Ando, T.; Sawamoto, M. *Chem. Rev.* 2001, 101, 3689–3745.
- (2) (a) Boyer, C.; Corrigan, N. A.; Jung, K.; Nguyen, D.; Nguyen, T.-K.; Adnan, N. N. M.; Oliver, S.; Shanmugam, S.; Yeow, J. *Chem. Rev.* 2016, 116, 1803–1949. (b) Ouchi, M.; Terashima; Sawamoto, M. *Chem. Rev.* 2009, 109, 4963–5050. (c) Rosen, B. M.; Percec, V. *Chem. Rev.* 2009, 109, 5069–5119.
- (3) (a) Tsarevsky, N. V.; Matyjaszewski, K. *Chem. Rev.* 2007, 107, 2270–2299. (b) Ding, M.; Jiang, X.; Zhang, L.; Cheng, Z.; Zhu, X. *Macromol. Rapid Commun.* 2015, 36, 1702–1721. (c) Matyjaszewski, K.; Jakubowski, W.; Min, K.; Tang, W.; Huang, J.; Braunecker, W. A.; Tsarevsky, N. V. *Proc. Natl. Acad. Sci. U. S. A.* 2006, 103, 15309–15314.
- (4) (a) Shanmugam, S.; Boyer, C. *J. Am. Chem. Soc.* 2015, 137, 9988–9999. (b) Xu, J.; Shanmugam, S.; Boyer, C. *ACS Macro Lett.* 2015, 4, 926–932. (c) Xu, J.; Shanmugam, S.; Duong, H. T.; Boyer, C. *Polym. Chem.* 2015, 6, 5615–5624. (d) Chen, M.; MacLeod, M. J.; Johnson, J. A. *ACS Macro Lett.* 2015, 4, 566–569. (e) Ohtsuki, A.; Lei, L.; Tanishima, M.; Goto, A.; Kaji, H. *J. Am. Chem. Soc.* 2015, 137, 5610–5617. (f) Goto, A.; Zushi, H.; Hirai, N.; Wakada, T.; Tsujii, Y.; Fukuda, T. *J. Am. Chem. Soc.* 2007, 129, 13347–13354.
- (5) (a) Roth, G. H.; Romero, N. A.; Nicewicz, D. A. *Synlett* 2016, 27, 714–723. (b) Isse, A. A.; Lin, C. Y.; Coote, M. L.; Gennaro, A. J. *Phys. Chem. B* 2011, 115, 678–684.
- (6) (a) Corrigan, N.; Shanmugam, S.; Xu, J.; Boyer, C. *Chem. Soc. Rev.* 2016, DOI: 10.1039/C6CS00185H. (b) Schultz, D. M.; Yoon, T. P. *Science* 2014, 343, 1239176. (c) Prier, C. K.; Rankic, D. A.; MacMillan, D. W. C. *Chem. Rev.* 2013, 113, 5322–5363. (d) Narayanam, J. M.

R.; Stephenson, C. R. *J. Chem. Soc. Rev.* 2011, 40, 102–113. (e) Yoon, T. P.; Ischay, M. A.; Du, J. *Nat. Chem.* 2010, 2, 527–532. (f) Juris, A.; Balzani, V.; Barigelletti, F.; Campagna, S.; Belser, P.; Von Zelewsky, A. *Coord. Chem. Rev.* 1988, 84, 85–277.

(7) (a) Wallentin, C.-J.; Nguyen, J. D.; Finkbeiner, P.; Stephenson, C. R. *J. Am. Chem. Soc.* 2012, 134, 8875–8884. (b) Furst, L.; Matsuura, B. S.; Narayanam, J. M. R.; Tucker, J. W.; Stephenson, C. R. *J. Org. Lett.* 2010, 12, 3104–3107.

(8) (a) Liu, X.; Zhang, L.; Cheng, Z.; Zhu, X. *Polym. Chem.* 2016, 7, 689–700. (b) Zhang, G.; Song, I. Y.; Ahn, K. H.; Park, T.; Choi, W. *Macromolecules* 2011, 44, 7594–7599.

(9) Nguyen, J. D.; Tucker, J. W.; Konieczynska, M. D.; Stephenson, C. R. *J. Am. Chem. Soc.* 2011, 133, 4160–4163.

(10) (a) Knorn, M.; Rawner, T.; Czerwieniec, R.; Reiser, O. *ACS Catal.* 2015, 5, 5186–5193. (b) Paria, S.; Reiser, O. *ChemCatChem* 2014, 6, 2477–2483. (c) Pirtsch, M.; Paria, S.; Matsuno, T.; Isobe, H.; Reiser, O. *Chem. - Eur. J.* 2012, 18, 7336–7340.

(11)(a) Yang, Q.; Dumur, F.; Morlet-Savary, F.; Poly, J.; Laleveé, J. *Macromolecules* 2015, 48, 1972–1980. (b) Treat, N. J.; Fors, B. P.; Kramer, J. W.; Christianson, M.; Chiu, C.-Y.; Read de Alaniz, J. R.; Hawker, C. J. *ACS Macro Lett.* 2014, 6, 580–584. (c) Fors, B. P.; Hawker, C. J. *Angew. Chem., Int. Ed.* 2012, 51, 8850–8853.

(12) (a) Chen, M.; Zhong, M.; Johnson, J. A. *Chem. Rev.* 2016, DOI: 10.1021/acs.chemrev.5b00671. (b) Pan, X.; Tasdelen, M. A.; Laun, J.; Junkers, T.; Yagci, Y.; Matyjaszewski, K. *Prog. Polym. Sci.* 2016, DOI: 10.1016/j.progpolymsci.2016.06.005. (c) Dadashi-Silab, S.; Doran, S.; Yagci, Y. *Chem. Rev.* 2016, DOI: 10.1021/acs.chemrev.5b00586. (d) Zivic, N.; Bouzrati-Zerelli, M.; Kermagoret, A.; Dumur, F.; Fouassier, J.-P.; Gimes, D.; Laleveé, J. *ChemCatChem* 2016, 8, 1617–1631.

- (13) (a) Joshi-Pangu, A.; Lévesque, F.; Roth, H. G.; Oliver, S. F.; Campeau, L.-C.; Nicewicz, D.; DiRocco, D. A. *J. Org. Chem.* 2016, DOI: 10.1021/acs.joc.6b01240. (b) Nicewicz, D. A.; Nguyen, T. M. *ACS Catal.* 2014, 4, 355–360. (c) Ravelli, D.; Fagnoni, M.; Albini, A. *Chem. Soc. Rev.* 2013, 42, 97–113. (d) Ravelli, D.; Fagnoni, M. *ChemCatChem* 2012, 4, 169–171. (e) Fagnoni, M.; Dondi, D.; Ravelli, D.; Albini, A. *Chem. Rev.* 2007, 107, 2725–2756.
- (14) Romero, N. A.; Nicewicz, D. A. *Chem. Rev.* 2016, DOI: 10.1021/acs.chemrev.6b00057.
- (15) Miyake, G. M.; Theriot, J. C. *Macromolecules* 2014, 47, 8255–8261.
- (16) (a) Yan, J.; Pan, X.; Schmitt, M.; Wang, Z.; Bockstaller, M. R.; Matyjaszewski, K. *ACS Macro Lett.* 2016, 5, 661–665. (b) Discekici, E. H.; Pester, C. W.; Treat, N. J.; Lawrence, J.; Mattson, K. M.; Narupai, B.; Toumayan, E. P.; Luo, Y.; McGrath, A. J.; Clark, P. G.; Read de Alaniz, J.; Hawker, C. J. *ACS Macro Lett.* 2016, 5, 258–262. (c) Pan, X.; Fang, C.; Fantin, M.; Malhotra, N.; So, W. Y.; Peteanu, L. A.; Isse, A. A.; Gennaro, A.; Liu, P.; Matyjaszewski, K. J. *Am. Chem. Soc.* 2016, 138, 2411–2425. (d) Pan, X.; Lamson, M.; Yan, J.; Matyjaszewski, K. *ACS Macro Lett.* 2015, 4, 192–196. (e) Treat, N. J.; Sprafke, H.; Kramer, J. W.; Clark, P. G.; Barton, B. E.; Read de Alaniz, J.; Fors, B. P.; Hawker, C. J. *J. Am. Chem. Soc.* 2014, 136, 16096–16101.
- (17) Theriot, J. C.; Lim, C.-H.; Yang, H.; Ryan, M. D.; Musgrave, C. B.; Miyake, G. M. *Science* 2016, 352, 1082–1086.
- (18) Prier, C. K.; Rankic, D. A.; MacMillan, D. W. C. *Chem. Rev.* 2013, 113, 5322–5363.
- (19) (a) Laursen, J. B.; Nielsen, J. *Chem. Rev.* 2004, 104, 1663–1686. (b) Palmer, B. D.; Rewcastle, G. W.; Atwell, G. J.; Baguley, B. C.; Denny, W. A. *J. Med. Chem.* 1988, 31, 707–712.
- (20) (a) Tanaka, H.; Shizu, K.; Miyazaki, H.; Adachi, C. *Chem. Commun.* 2012, 48, 11392–111394. (b) Park, Y.; Kim, B.; Lee, C.; Hyun, A.; Jang, S.; Lee, J.-H.; Gal, Y.-S.; Kim, T.

H.; Kim, K.-S.; Park, J. J. Phys. Chem. C 2011, 115, 4843–4850. (c) Okamoto, T.; Terada, E.; Kozaki, M.; Uchida, M.; Kikukawa, S.; Okada, K. Org. Lett. 2003, 5, 373–376.

(21) See the Supporting Information.

(22) Huber, J. R.; Mantulin, W. W. J. Am. Chem. Soc. 1972, 94, 3755–3760.

(23) (a) Liu, N.; Wang, B.; Chen, W.; Liu, C.; Wang, X.; Hu, Y. RSC Adv. 2014, 4, 51133. (b) Klein, J. C. L.; Conrad, M., III; Morris, S. A. Acta Crystallogr., Sect. C: Cryst. Struct. Commun. 1985, C41, 1202–1204.

(24) (a) Malinśka, M.; Nowacki, J.; Kapturkiewicz, A.; Wozniak, K. RSC Adv. 2012, 2, 4318–4328. (b) Borowicz, P.; Herbich, J.; Kapturkiewicz, A.; Anulewicz-Ostrowska, R.; Nowacki, J.; Grampp, G. Phys. Chem. Chem. Phys. 2000, 2, 4275–4280. (c) Borowicz, P.; Herbich, J.; Kapturkiewicz, A.; Opallo, M.; Nowacki, J. Chem. Phys. 1999, 249, 49–62.

(25) (a) Frick, E.; Anastasaki, A.; Haddleton, D. M.; Barner-Kowollik, C. J. Am. Chem. Soc. 2015, 137, 6889–6896. (b) Ribelli, G. G.; Konkolewicz, D.; Bernhard, S.; Matyjaszewski, K. J. Am. Chem. Soc. 2014, 136, 13303–13312.

(26) Chao, P.; Gu, R.; Ma, X.; Wang, T.; Zhao, Y. Polym. Chem. 2016, DOI: 10.1039/C6PY01095D.

(27) Liu, N.; Wang, B.; Chen, W.; Liu, C.; Wang, X.; Hu, Y. RSC Adv. **2014**, *4*, 51133-51139

(28) Pan, X.; Lamson, M.; Yan, J.; Matyjaszewski, K. ACS Macro Letters. **2015**, *2*, 192-196

(29) Zhu, Y.; Kulkarni, A. P.; Wu, P.-T.; Jenekhe, S. A. Chem. Mater. **2008**, *20*, 4200-4211.

(30) He, H.; Zapol, P.; Curtiss, L. A. The Journal of Physical Chemistry C **2010**, *114*, 21474.

(31) Tossell, J. A. Computational and Theoretical Chemistry **2011**, *977*, 123.

(32) Winget, P.; Cramer, C. J.; Truhlar, D. G. Theoretical Chemistry Accounts: Theory, Computation, and Modeling (Theoretica Chimica Acta) **2004**, *112*, 217.

(33) Zhao, Y.; Truhlar, D. *Theoretical Chemistry Accounts* **2008**, *120*, 215.

(34) Spackman, M. A. *J. Comput. Chem.* **1996**, *17*, 1.

Chapter 4 – Impact of Light Intensity on Control of Photoinduced Organocatalyzed Atom Transfer Radical Polymerization with Phenoxazine Catalysts

Overview

N-aryl phenoxazines have shown to successfully mediate organocatalyzed atom transfer radical polymerization (O-ATRP) in the presence of white LEDs. In this work we investigate to what extent does light intensity effect control over photo mediated O-ATRP and the resulting materials. Through the use of controlled dimming of white LEDs, we were able to systematically evaluate how irradiation conditions effect polymerization performance. In this work, 3,7-di(4-biphenyl) 1-naphthalene-10-phenoxazine was investigated. This study demonstrated that the phenoxazine photocatalyst is a robust catalyst compared to earlier catalyst variants such as perylene and could outperform the perylene in irradiation conditions 50% of that in perylene, and 25% of those employed in previous studies while being able to maintain control over the ATRP (dispersities < 1.50). These findings show that robust catalysts have been realized and can be employed in a wide scope of conditions, including those which might necessitate low light intensity irradiation.

Introduction

The following introduction was taken directly from the text and was co-written by Matthew D. Ryan and Ryan M. Pearson.

Controlled radical polymerization (CRP) methodologies have enabled the construction of well-defined and precise polymeric materials by providing synthetic approaches that produce polymers with well-defined molecular weight (MW), dispersity (\bar{D}), and composition.¹⁻⁵

Organocatalyzed atom transfer radical polymerization (O-ATRP) has recently emerged as a methodology to produce well-defined polymers without the use of metal catalysts.⁶ Since initial reports that perylene⁷ and phenylphenothiazine⁸ could operate O-ATRP, more organic photoredox catalysts (PCs) have been introduced, including several diaryl dihydrophenazine,⁹⁻¹¹ carbazole,¹² phenoxazine,¹³ anthracene/pyrene,¹⁴ and other phenothiazine¹⁵⁻¹⁸ derivatives. A proposed mechanism of O-ATRP proceeds through an oxidative quenching pathway which consists of five main processes: (1) photoexcitation of the ground state PC to a singlet excited state ($^1\text{PC}^*$); (2) intersystem crossing to a triplet excited state ($^3\text{PC}^*$);^{9,19} (3) direct reduction of an alkyl halide initiator or polymer chain end by $^3\text{PC}^*$, generating an active radical for polymerization propagation and formation of a radical cation/halide anion “deactivator” complex ($\text{PC}^{\bullet+}/\text{X}^-$); (4) polymer MW growth via polymerization propagation; and (5) oxidation of the active radical by $\text{PC}^{\bullet+}/\text{X}^-$ to reversibly deactivate the polymerization and regenerate PC (Figure 4.1).

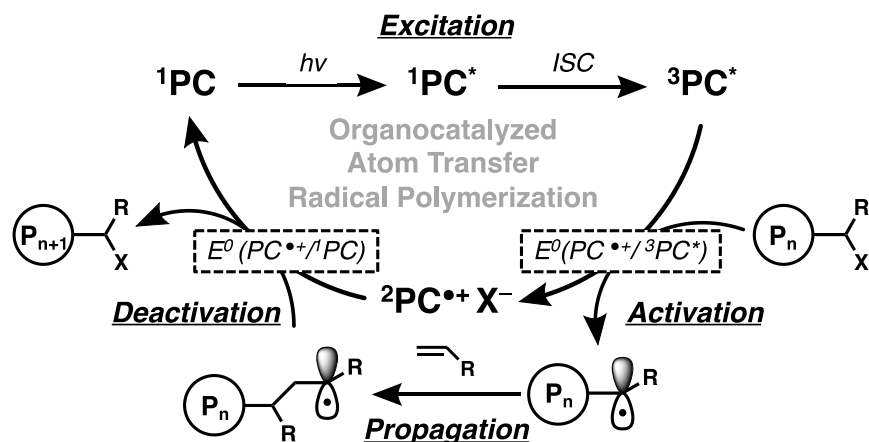


Figure 4.1. Proposed oxidative quenching cycle for O-ATRP mediated by photoredox catalysts

Maintaining a low radical concentration by favoring dormant polymer chains through an efficient radical deactivation process is critical for CRPs to produce well-defined polymers. Minimizing bimolecular termination pathways allows for the synthesis of polymers with

predictable MW and low Đ through a controlled polymerization, achieving a linear increase in polymer MW with monomer conversion. In an ideal polymerization, no exogenous additives would be necessary for the system to be controlled, but in practice CRPs can be greatly improved by the addition of deactivating species or reagents that regenerate active catalysts.^{20,21} For example, a strategy to maintain a low radical concentration in copper ATRP is the addition of excess or exclusively^{22,23} deactivator in the form of Cu(II) salts at the beginning of the polymerization.²⁴ Further, if excess Cu(II) species are not added, it is proposed that a steady-state Cu(II) concentration must be met before control over the system can be realized.²⁵ This approach influences the activation vs deactivation equilibrium to favor dormant polymer chains by increasing the concentration of the deactivating species that regenerates Cu(I) and the halide-capped polymer. If this condition is not met, deviation of the polymer MW from the theoretical values can be observed as a consequence of poor deactivation.²⁶ For O-ATRP, this translates to the requirement for a sufficient buildup of $PC^{\bullet+}/Br^-$ to be met to enable control over the polymerization. Holistically, the oxidizing power of this deactivator complex is also of importance, as the efficiency of deactivation is a function of both the concentration and reactivity of $PC^{\bullet+}/Br^-$.

In the O-ATRP mechanism, we hypothesize $^3PC^*$ is the predominant species responsible for reduction of the alkyl bromide and activation of the propagating radical for polymerization due to the longer excited state lifetime of the triplet state relative to the singlet state.²⁷ Thereafter, the resulting $PC^{\bullet+}Br^-$ ion pair must be sufficiently oxidizing to deactivate the propagating radical and realize a CRP. Furthermore, as is the case in all CRPs, the rate of deactivation (k_{deact}) must be equal to or greater than the rate of activation (k_{act}) to minimize undesirable termination pathways.²⁸ An idealized scenario to realize this balance of rates would involve the oxidized PC, $PC^{\bullet+}Br^-$, remaining associated with the same polymer chain after activating the radical and

rapidly deactivating the same radical. However, the ion pair can likely diffuse away from the neutral propagating radical and potentially deactivate other radicals in solution. Such diffusion between deactivating species and propagating radicals in CRPs has been experimentally confirmed through crossover studies in both polymerizations and model small molecule systems.²⁹⁻³² As such, a critical concentration of the deactivating species is required to achieve control over the polymerization, which can either be added at the onset of the polymerization or generated through the activation step.^{33,34} In photoredox mediated ATRP, the $\text{PC}^{\bullet+}\text{Br}^-$ deactivator is produced through the alkyl bromide reduction, which is dictated by the reduction potential and $[\text{}^3\text{PC}^*]$. In turn, $[\text{}^3\text{PC}^*]$ is influenced by a combination of the light intensity, initial PC loading, and the triplet quantum yield of the PC. In short, the $[\text{PC}^{\bullet+}\text{Br}^-]$, through controlling intensity of irradiation, in concert with the photophysical and thermodynamic properties of the photocatalyst, must be optimized for k_{deact} to be sufficiently large to realize a controlled process through efficient deactivation.

The PC used in this study of the effects of light intensity on the control over O-ATRP, 3,7-di(4-biphenyl) 1-naphthalene-10-phenoxazine, represents a successful PC designed to be highly reducing and absorptive under visible irradiation,¹³ respectively. By evaluating this PC directly under previously employed conditions, which have demonstrated different levels of success in the polymerization of methacrylate monomers, the impact of the light source on the control over O-ATRP can be evaluated more completely. This reaction parameter has not been systematically explored for O-ATRP systems, even though the photoexcitation event adds a rich level of complexity to the polymerization mechanism. Recently, irradiation conditions have been shown to be key optimization parameters for small molecule reactions mediated by a variety of photocatalysts.³⁵ For photoinduced O-ATRP, the photoexcitation process controls the efficiency

of activation directly and the efficiency of deactivation indirectly. The characteristics of absorption ($PC \rightarrow PC^*$), quantum yield, excited-state lifetime, and reduction potential of ${}^3PC^*$ are major factors in the efficiency of the polymerization catalytic cycle. Modulating the irradiation intensity influences the concentration of ${}^3PC^*$ in solution and the rate of initiation, with decreased light intensity lowering the rate of initiation. As such, the concentration of $PC^{\bullet+}/Br^-$ is decreased under lower irradiation, as this complex is generated through activation.³⁶ Herein, the influence of light intensity and PC concentration are investigated as factors that affect the performance of O- ATRP by its modulation of [${}^3PC^*$], using 3,7-di(4-biphenyl) 1-naphthalene-10-phenoxazine as a model catalyst for the polymerization of methyl methacrylate (MMA) (Figure 4.2).

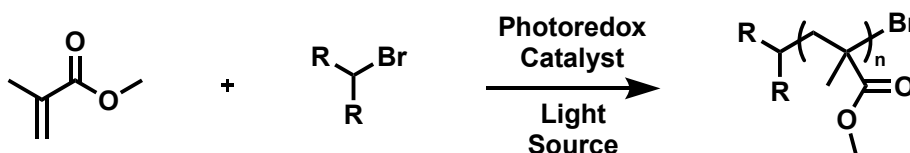


Figure 4.2. General reaction scheme for the O-ATRP of methyl methacrylate

Results and Discussion

The effects of varied light intensity on 3,7-Di(4-biphenyl) 1-naphthalene-10-phenoxazine (PC 1) were studied to investigate the activity of a photocatalyst that previously demonstrated superior performance in O-ATRP. The phenoxazine catalyst consistently produced polymer products with relatively low \bar{D} (<1.30) and predictable M_n in a highly efficient manner ($I^* > 90\%$).¹¹ In comparing the PCs, both perylene and phenoxazine have high molar extinction coefficients (>20000 L/(mol cm)) and absorption profiles in the visible region³⁷ but differ in other photophysical characteristics. The more reducing triplet excited state reduction potential of phenoxazine vs perylene (-1.93 V vs -0.78 V, respectively) likely results in a more efficient reduction of the alkyl bromide.

Overall, the phenoxazine photocatalyst used in this study is robust to broad changes in experimental conditions, as shown by maintaining a controlled O-ATRP in a wide range of irradiation intensities (100–25%) and catalyst concentrations (0.01–0.2 mol %). The catalyst loading could be significantly lowered and still effectively catalyze O-ATRP (Table 4.1). At 0.05 and 0.01 mol %, low \bar{D} and $I^* > 80\%$ are obtained, indicating maintained control over the polymerization across an order of magnitude of catalyst loading (runs 1–4). Increasing the amount of photocatalyst to 0.2 mol % also provides successful results ($I^* = 91.6\%$ and $\bar{D} = 1.22$), although 0.2 mol % is beyond the solubility for this catalyst and the polymerization becomes heterogeneous in PC. A number of general trends are observed for polymerizations mediated by this photocatalyst under the different irradiation conditions. By decreasing the intensity of irradiation from 100% to 5%, a significant decrease in I^* is observed from 96.3% to 31.0%. This lower I^* is accompanied by an increase in \bar{D} from 1.20 to 1.80 (Table 4.1, runs 5-7). Maintaining a controlled O-ATRP in a wide range of irradiation intensities (100–25%) and catalyst concentrations (0.01–0.2 mol %) makes this photocatalyst an attractive candidate for future applications of O-ATRP.

Table 4.1. Results of the O-ATRP of MMA Mediated by 3,7-Di(4-biphenyl) 1-naphthalene-10-phenoxazine with Varied PC Concentrations and Irradiation Intensities.

Run no.	$h\nu$ (intensity) ^a (%)	[I]:[PC] ^b	Time (h)	Conv. ^c (%)	M_w^d (kDa)	M_n^d (kDa)	\bar{D} (M_w/M_n) ^d	I^* ^c (%)
1	100	10:0.1	6	83.3	14.4	10.2	1.42	84.1
2	100	10:0.5	6	88.6	12.9	10.3	1.25	87.1
3	100	10:1	6	83.9	10.7	8.9	1.20	96.3
4	100	10:2	6	75.9	10.3	8.5	1.22	91.6
5	50	10:1	6	60.6	9.3	7.8	1.20	80.1
6	25	10:1	6	39.9	5.8	7.5	1.28	69.7
7	5	10:1	6	16.2	9.7	5.4	1.80	31.0

^aSee Supporting Information for details, polymerizations performed with 1.00 mL of MMA (1.87 M). ^bMolar ratio of initiator ([I]) to photocatalyst ([PC]). ^cMeasured by ¹H NMR. ^dMeasured by GPC coupled with light scattering. ^e $I^* = (\text{theoretical number-average MW})/(\text{experimentally measured number-average MW}) \times 100$.

Phenoxazine exhibits successful performance in O-ATRP under a much wider range of irradiation conditions (Figure 4.3). For O-ATRP mediated by phenoxazine, M_n growth is present from 100%, 50%, and 25% relative irradiation intensity (Figure 4.3A–C). When lowered to 5% relative intensity, there is a loss in control, as evidenced by a nonlinear growth in M_n with monomer conversion and high dispersity ($\mathcal{D} > 2.0$) (Figure 4.3D). Additionally, lower light intensity leads to lower rates of polymerization, and the first-order kinetic plots for the four different intensity trials remained linear, even at 5% relative intensity (Figure 4.4). Further, the degree of control does not significantly differ for polymerization in a photoreactor cooled by a fan (33 °C) and not cooled (50 °C). These kinetic and MW data prove that the highly performing photocatalyst can mediate a successful O-ATRP across broad irradiation intensities.

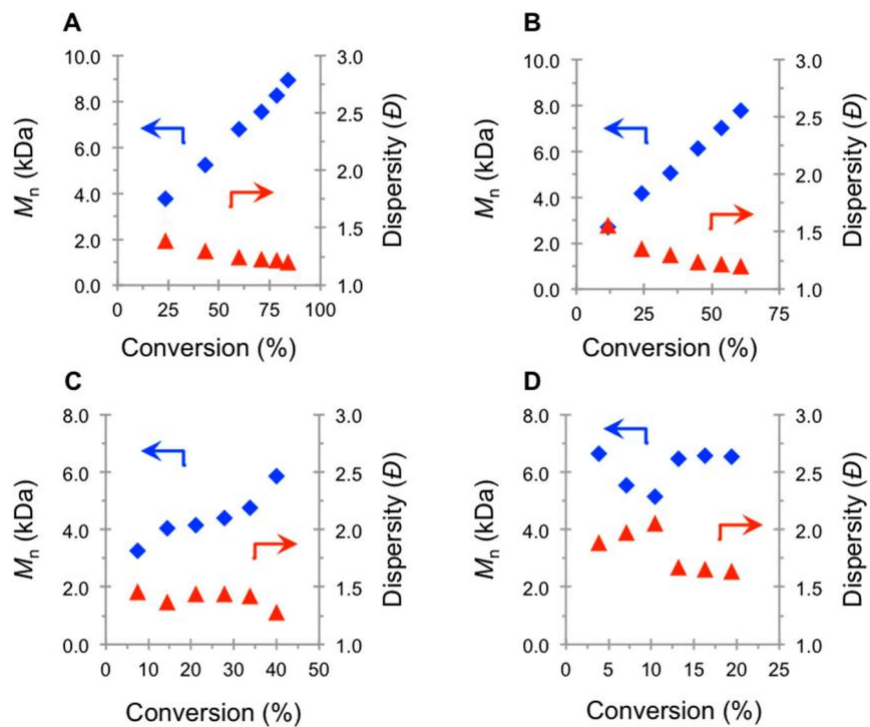


Figure 4.3. Plots of M_n (blue \blacklozenge) and \bar{D} (red \blacktriangle) as a function of monomer conversion at 100% (A), 50% (B), 25% (C), and 5% (D) relative irradiation intensity for the polymerization of MMA mediated by PC 2 (see Supporting Information for experimental details).

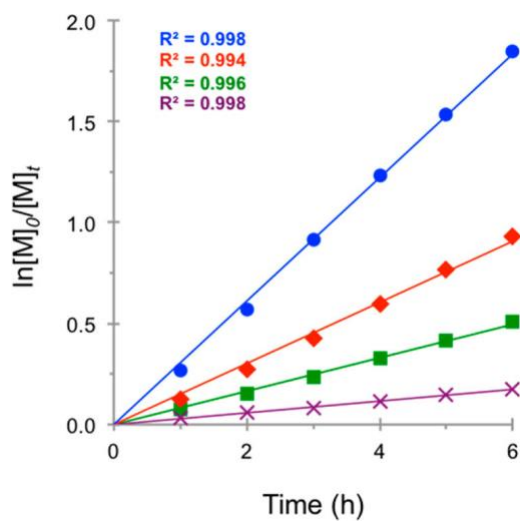


Figure 4.4. First-order kinetic plot for the polymerization of MMA using PC 2 at 100% (blue ●), 50% (red ◆), 25% (green ■), and 5% (violet ×) relative irradiation intensities (see Supporting Information for experimental details).

Conclusion

The intensity of light employed in O-ATRP has shown to have a significant effect on the control achieved throughout the polymerization. The 3,7-Di(4-biphenyl) 1-naphthalene-10-phenoxazine's ability to maintain growth in polymer molecular weight with respect to monomer conversion and linear first-order kinetics under decreased irradiation intensity proves the catalyst's ability to be implemented in a broad variety of applications.

Experimental

Materials: 3,7-bis(4-biphenyl) 1-naphthalene-10-phenoxazine was synthesized according to a previously reported procedure.¹ Dimethylacetamide (DMA) and methyl methacrylate (MMA), were dried over calcium hydride for 24 hours, and purified *via* vacuum distillation followed by three freeze-pump thaw cycles at -78 °C then stored in a N₂ glovebox. Ethyl α -bromophenylacetate (EBP) and diethyl 2-bromo-2-methylmalonate (DBMM) were purified *via* vacuum distillation followed by three freeze-pump thaw cycles at -78 °C, then stored in a N₂ glovebox.

General Polymerization Procedure For 3,7-Bis(4-biphenyl) 1-naphthalene-10-phenoxazine:

In a N₂ glovebox, a 20 mL scintillation vial equipped with stir bar was added phenoxazine catalyst (5.70 mg, 0.00935 mmol, 1.0 eq.) and 1.00 mL of DMA. Once the catalyst was fully dissolved, MMA (1.00 mL, 9.35 mmol, 1000 eq.) was pipetted into the vial followed by DBMM (17.9 μ L, 0.0935 mmol, 10 eq.). The vial was then sealed with a plastic lined cap and quickly placed into the

photo reactor shown in figure 4.5 with the indicated level of light intensity, as controlled by the LED dimmer. The temperature in the beaker with un-dimmed LEDs was approximately 50°C.

Time Point Collection for Kinetic Analysis: A 0.10 mL sample was taken from the polymerization reaction vial in an oxygen free environment and injected into a vial with 0.6 mL of CDCl₃ and 25 ppm butylated hydroxytoluene (BHT). This solution was then used directly for analysis. Nuclear magnetic resonance (NMR) spectra were recorded on a Varian 300 MHz instrument. Monomer conversions were determined by integrating the methyl ester protons of the monomer at ~3.50-3.55 ppm against polymer methyl ester protons at ~3.30-3.45 ppm.

Molecular Weight Characterization: After collecting NMR spectra, the sample was transferred into a 20 mL scintillation vial and the volatiles were removed. The resulting solid polymer was dissolved in 1 mL of HPLC grade THF and passed through a syringe filter before analysis *via* gel permeation chromatography (GPC) coupled with multi-angle light scattering (MALS), using an Agilent HPLC fitted with one guard column, three PLgel 5 µm MIXED-C gel permeation columns, a Wyatt Technology TrEX differential refractometer, and a Wyatt Technology miniDAWN TREOS light scattering detector, using THF as the eluent at a flow rate of 1.0 mL/min.

Measurement of LED Emission: The emission spectrum of the white LEDs was measured with an Ocean Optics ADC1000 spectrometer. Light from the LEDs was attenuated as needed by use of a continuously variable neutral density filter to prevent saturation of the detector. Emission was measured at the seven different light intensities. The light was guided into the spectrometer with a fiber-optic cable. Data from the seven different measurements were processed with a home-built LabView program, and the spectra overlaid.

Photo Reactor Set Up: A 45 cm strip of double-density white LEDs purchased from Creative Lighting Solutions (item no. CL-FRS120-5M-12V-WH) was wrapped around the inside of a 400 mL Pyrex beaker with a diameter of ~2.5 inches (Figure 4.5). The LED strip was powered by a 12VDC power Supply – 2.1A Commercial, 25W Power Supply by Creative Lighting Solutions LLC. A Dragonpad 12V12A inline mini LED dimmer control for single color LED strip lights with 7 dimmer settings was installed between the power supply and LED strips. The outside of the beaker was wrapped in aluminum foil. In this study the LEDs were dimmed from 100% to 50%, 25%, and 5% relative intensities (Figure 4.6).



Figure 4.5. A picture of the photoreactor used for O-ATRP, constructed from a 400mL beaker lined with 45 cm of white LEDs.



Figure 4.6. Picture of the relative light intensities used in this study, controlled by an LED dimmer. From left to right: 100%, 50%, 25%, 5% relative light intensity.

Measuring Light Intensity: To quantify the relative intensity of light emitted from the dimmed LEDs, lux readings were recorded by centering an LED lined beaker on the aperture of an integrating sphere diffuse reflectance accessory (Internal DRA-2500) equipped with a Amprobe LM-200 LED light meter with silicon photodiode and filter directed at the opening on the opposite side (Figure 4.7). The system was sealed to prevent light pollution from the surroundings. Measurement of the output from the various dimmer settings was repeated 10 times and the observed lux was averaged, with a standard deviation of $\pm 0.22\%$. The readings were plotted against intensity to calibrate our system (Figure 4.8).

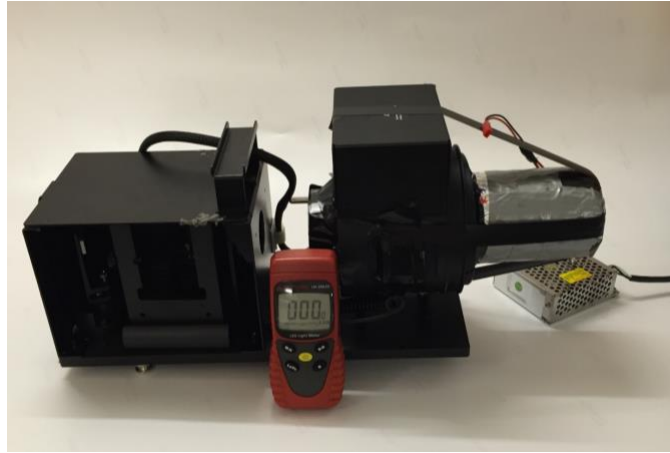


Figure 4.7. The set up used to measure lux at each dimmer setting, using an Amprobe LM-200 LED light meter and an integrating sphere diffuse reflectance accessory. The sealed system is shown, with no observed light pollution from the surroundings.

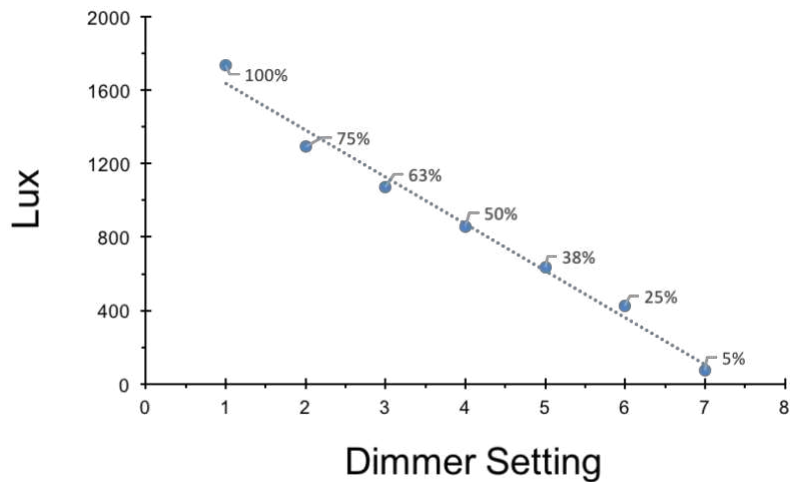


Figure 4.8. Plot of Lux as a function of dimmer setting, measured using the set up in Figure 7. The relative percent intensity reported as data point labels.

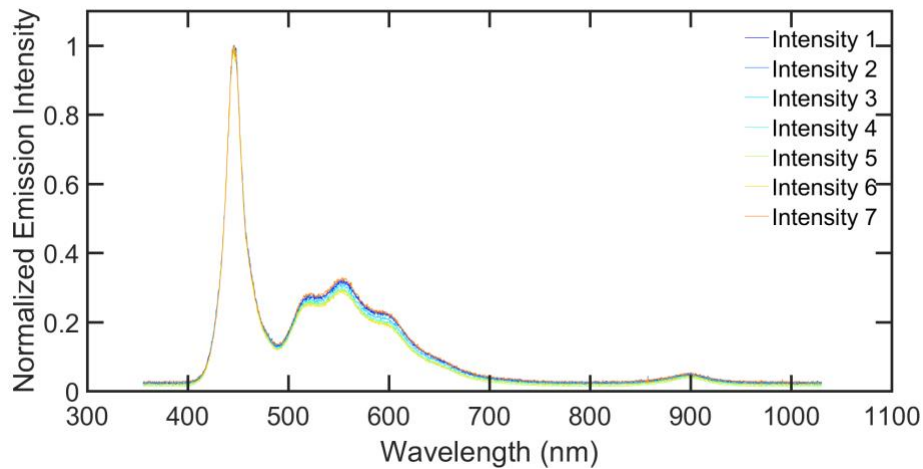


Figure 4.9. Overlaid plots of the normalized LED emission spectra at 7 different dimming settings. (Data collected by Steven Sartur at University of Colorado Boulder)

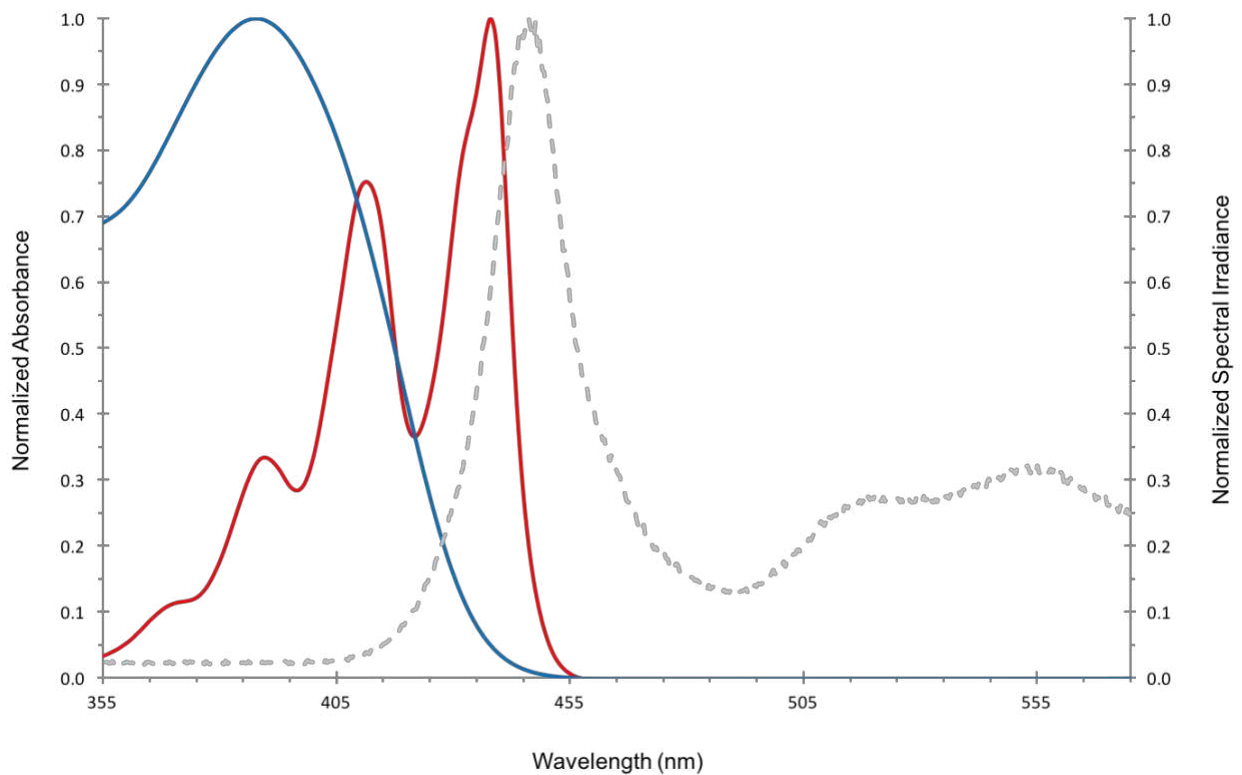


Figure 4.10. Overlaid normalized absorbance plots for PC 1 (red, $\epsilon = 37,961 \text{ M}^{-1}\text{cm}^{-1}$ @ 436 nm) and PC 2 (blue, $\epsilon = 26,635 \text{ M}^{-1}\text{cm}^{-1}$ @ 388 nm), and the normalized spectral irradiance of the white LED without dimming (gray).

References

- (1) Pan, X.; Tasdelen, M. A.; Laun, J.; Junkers, T.; Yagci, Y.; Matyjaszewski, K. Photomediated Controlled Radical Polymerization. *Prog. Polym. Sci.* 2016, 62, 73–125.
- (2) Chen, M.; Zhong, M.; Johnson, J. A. Light-Controlled Radical Polymerization: Mechanisms, Methods, and Applications. *Chem. Rev.* 2016, 116 (17), 10167–10211.
- (3) Matyjaszewski, K.; Tsarevsky, N. V. Macromolecular Engineering by Atom Transfer Radical Polymerization. *J. Am. Chem. Soc.* 2014, 136 (18), 6513–6533.
- (4) Braunecker, W. A.; Matyjaszewski, K. Controlled/Living Radical Polymerization: Features, Developments, and Perspectives. *Prog. Polym. Sci.* 2007, 32, 93–146.
- (5) Kamigaito, M.; Ando, T.; Sawamoto, M. Metal-Catalyzed Living Radical Polymerization. *Chem. Rev.* 2001, 101 (12), 3689–3746.
- (6) Theriot, J. C.; McCarthy, B. G.; Lim, C.-H.; Miyake, G. M. Organocatalyzed Atom Transfer Radical Polymerization: Perspectives on Catalyst Design and Performance. *Macromol. Rapid Commun.* 2017, 1700040.
- (7) Miyake, G. M.; Theriot, J. C. Perylene as an Organic Photocatalyst for the Radical Polymerization of Functionalized Vinyl Monomers through Oxidative Quenching with Alkyl Bromides and Visible Light. *Macromolecules* 2014, 47 (23), 8255–8261.
- (8) Treat, N. J.; Sprafke, H.; Kramer, J. W.; Clark, P. G.; Barton, B. E.; Read de Alaniz, J.; Fors, B. P.; Hawker, C. J. Metal-Free Atom Transfer Radical Polymerization. *J. Am. Chem. Soc.* 2014, 136 (45), 16096–16101.
- (9) Theriot, J. C.; Lim, C.-H.; Yang, H.; Ryan, M. D.; Musgrave, C. B.; Miyake. Organocatalyzed Atom Transfer Radical Polymerization Driven by Visible Light. *Science* 2016, 352, 1082–1086.

- (10) Lim, C.-H.; Ryan, M. D.; McCarthy, B. G.; Theriot, J. C.; Sartor, S. M.; Damrauer, N. H.; Musgrave, C. B.; Miyake, G. M. Intramolecular charge transfer and Ion pairing in N,N-Diaryl Dihydrophenazine Photoredox Catalysts for Efficient Organocatalyzed Atom Transfer Radical Polymerization. *J. Am. Chem. Soc.* 2017, 139 (1), 348–355.
- (11) Ryan, M. D.; Theriot, J. C.; Lim, C.-H.; Yang, H.; Lockwood, A. G.; Garrison, N. G.; Lincoln, S. R.; Musgrave, C. B.; Miyake, G. M. Solvent Effects on the Intramolecular Charge Transfer Character of N,N-Diaryl Dihydrophenazine Catalysts for Organocatalyzed Atom Transfer Radical Polymerization. *J. Polym. Sci., Part A: Polym. Chem.* 2017, DOI: 10.1002/pola.28574.
- (12) Huang, Z.; Gu, Y.; Liu, X.; Zhang, L.; Cheng, Z.; Zhu, X. Metal- Free Atom Transfer Radical Polymerization of Methyl Methacrylate with ppm Level of Organic Photocatalyst. *Macromol. Rapid Commun.* 2017, 38, 1600461.
- (13) Pearson, R. M.; Lim, C.-H.; McCarthy, B. G.; Musgrave, C. B.; Miyake, G. M. Organocatalyzed Atom Transfer Radical Polymerization Using N-Aryl Phenoxazines as Photoredox Catalysts. *J. Am. Chem. Soc.* 2016, 138 (35), 11399–11407.
- (14) Allushi, A.; Jockusch, S.; Yilmaz, G.; Yagci, Y. Photoinitiated Metal-Free Controlled/Living Radical Polymerization Using Poly- nuclear Aromatic Hydrocarbons. *Macromolecules* 2016, 49, 7785– 7792.
- (15) Pan, X.; Fang, C.; Fantin, M.; Malhotra, N.; So, W. Y.; Peteanu, L. A.; Isse, A. A.; Gennaro, A.; Matyjaszewski, K. Mechanism of Photoinduced Metal-Free Atom Transfer Radical Polymerization. *J. Am. Chem. Soc.* 2016, 138 (7), 2411–2425.
- (16) Pan, X.; Lamson, M.; Yan, J.; Matyjaszewski, K. Photoinduced Metal-Free Atom Transfer Radical Polymerization of Acrylonitrile. *ACS Macro Lett.* 2015, 4 (2), 192–196.

- (17) Dadashi-Silab, S.; Pan, X.; Matyjaszewski, K. Phenyl Benzo[b]-phenothiazine as a Visible Light Photoredox Catalyst for Metal-Free Atom Transfer Radical Polymerization. *Chem. - Eur. J.* 2017, 23, 5972.
- (18) Yan, J.; Pan, X.; Schmitt, M.; Wang, Z.; Bockstaller, M. R.; Matyjaszewski, K. Enhancing Initiation Efficiency in Metal-Free Surface-Initiated Atom Transfer Radical Polymerization (SI-ATRP). *ACS Macro Lett.* 2016, 5, 661–665.
- (19) Jockusch, S.; Yagci, Y. The Active Role of Excited States of Phenothiazines in Photoinduced Metal Free Atom Transfer Radical Polymerization: Singlet or Triplet Excited States? *Polym. Chem.* 2016, 7, 6039–6043.
- (20) Williams, V. A.; Ribelli, T. G.; Chmielarz, P.; Park, S.; Matyjaszewski, K. A Silver Bullet: Elemental Silver as an Efficient Reducing Agent for Atom Transfer Radical Polymerization of Acrylates. *J. Am. Chem. Soc.* 2015, 137 (4), 1428–1431.
- (21) Jakubowski, W.; Matyjaszewski, K. Activators Regenerated by Electron Transfer for Atom Transfer radical Polymerization of (Meth)acrylates and Related Block Copolymers. *Angew. Chem., Int. Ed.* 2006, 45, 4482–4486.
- (22) Wang, J.-S.; Matyjaszewski, K. Living^{*/}Controlled Radical Polymerization. Transition-Metal-Catalyzed Atom Transfer Radical Polymerization in the Presence of a Conventional Radical Initiator. *Macromolecules* 1995, 28 (22), 7572–7573.
- (23) Xia, J.; Matyjaszewski, K. Controlled^{*/}“Living^{*/}” Radical Polymerization. Homogenous Reverse Atom Transfer Radical Polymerization Using AIBN as the Initiator. *Macromolecules* 1997, 30 (25), 7692–7696.

- (24) Min, K.; Gao, H.; Matyjaszewski, K. Preparation of Homopolymers and Block Copolymers in Miniemulsion by ATRP Using Activators Generated by Electron Transfer (AGET). *J. Am. Chem. Soc.* 2005, 127 (11), 3825–2830.
- (25) Matyjaszewski, K.; Patten, T. E.; Xia, J. Controlled/“Living” Radical Polymerization. Kinetics of the Homogenous Atom Transfer Radical Polymerization of Styrene. *J. Am. Chem. Soc.* 1997, 119 (4), 674–680.
- (26) Matyjaszewski, K.; Nakagawa, Y.; Jasieczek, C. B. Polymerization of n-Butyl Acrylate by Atom Transfer Radical Polymerization. Remarkable Effect of Ethylene Carbonate and Other Solvents. *Macromolecules* 1998, 31, 1535–1541.
- (27) Arias-Rotondo, D. M.; McCusker, J. K. The Photophysics of Photoredox Catalysis: A Roadmap for Catalyst Design. *Chem. Soc. Rev.* 2016, 45, 5803–5820.
- (28) Matyjaszewski, K.; Paik, H. J.; Zhou, P.; Diamanti, S. Determination of Activation and Deactivation Rate Constants in Atom Transfer Radical Polymerization. *Macromolecules* 2001, 34, 5125–5131.
- (29) Wessely, I.; Mugnaini, V.; Bihlmeier, A.; Jeschke, G.; Brase, S.; Tsotsalas, M. Radical Exchange Reaction of Multi-Spin Isoindoline Nitroxides Followed by EPR Spectroscopy. *RSC Adv.* 2016, 6, 55715–55719.
- (30) Yamaguchi, G.; Higaki, Y.; Otsuka, H.; Takahara, A. Reversible Radical Ring-Crossover Polymerization of an Alkoxyamine-Containing Dynamic Covalent Macrocycle. *Macromolecules* 2005, 38, 6316–6320.
- (31) Turro, N. J.; Lem, G.; Zavarine, I. S. A Living Free Radical Exchange Reaction for the Preparation of Photoactive End-Labeled Monodisperse Polymers. *Macromolecules* 2000, 33, 9782–9785.

- (32) Hawker, C. J.; Barclay, G. G.; Dao, J. Radical Crossover in Nitroxide Mediated “Living” Free Radical Polymerizations. *J. Am. Chem. Soc.* 1996, 118 (46), 11467–11471.
- (33) Lacroix-Desmazes, P.; Lutz, J.-F.; Chauvin, F.; Severac, R.; Boutevin, B. Living Radical Polymerization: Use of an Excess of Nitroxide as a Rate Moderator. *Macromolecules* 2001, 34 (26), 8866– 8871.
- (34) Veregin, R. P. N.; Odell, P. G.; Michalak, L. M.; Georges, M. K. The Pivotal Role of Excess Nitroxide Radical in Living Free Radical Polymerizations with Narrow Polydispersity. *Macromolecules* 1996, 29 (8), 2746–2754.
- (35) Le, C.; Wismer, M. K.; Shi, Z.-C.; Zhang, R.; Conway, D. V.; Li, G.; Vachal, P.; Davies, I. W.; MacMillan, D. W. C. A General Small- Scale Reactor to Enable Standardization and Acceleration of Photocatalytic Reactions. *ACS Cent. Sci.* 2017, DOI: 10.1021/acscentsci.7b00159.
- (36) Lalevee, J.; Morlet-Savary, F.; Dietlin, C.; Graff, B.; Fouassier, J.- P. Photochemistry and Radical Chemistry under Low Intensity Visible Light Sources: Application to Photopolymerization Reactions. *Molecules* 2014, 19, 15026–15041.
- (37) George, C.; Streckowski, R. S.; Kleffmann, J.; Stemmler, K.; Ammann, M. Photoenhanced Uptake of Gaseous NO₂ on Solid Organic Compounds: A Photochemical Source of HONO? *Faraday Discuss.* 2005, 130, 195–210.

Overview

Photoredox catalysis has proven to be a versatile approach for the construction of challenging covalent bonds under mild reaction conditions. Much of this work has relied upon catalysts derived from iridium or ruthenium precious metals. As such, there is an urgent need to develop organic analogues as sustainable replacements. Although several organic photoredox catalysts have been introduced, there remains a lack of organic species that absorb visible light to yield a strongly reducing species. Herein, we report the critical photophysical and electrochemical characteristics of both a dihydrophenazine and a phenoxazine system that enables them to serve as strongly reducing visible light photoredox catalysts. Significantly, both the dihydrophenazine and the phenoxazine exhibit reversible redox behavior and access a charge transfer excited state, reminiscent of the metal-to-ligand charge transfer excited state in iridium and ruthenium complexes. While the dihydrophenazine possesses a sufficiently long excited state lifetime for photoredox catalysis of 4.3 μ s, the phenoxazine efficiently absorbs visible light to access a triplet excited state in 90 ± 10 % quantum yield with an impressively long lifetime of 480 μ s at room temperature while in solution. We further demonstrate that these organic photoredox catalysts catalyze demanding trifluoromethylations and dual photoredox/nickel catalyzed C-N and C-S cross-coupling reactions, which have been historically exclusive to precious metal photoredox catalysts.

Introduction

Visible-light photoredox catalysis has gained prominence orchestrating challenging chemical transformations under mild reaction conditions.¹ A large majority of this work has employed precious-metal polypyridyl iridium and ruthenium photoredox catalysts (PCs). The rapid establishment of these metal complexes as practical PCs leveraged their well-studied photophysical and photoredox properties, which in turn have enabled their incorporation in a range of applications including photovoltaics,² light emitting diodes,³ imaging and sensing in biological systems,⁴ therapeutics,⁵ and redox active antibiotics.⁶

In regards to photoredox catalysis, these metal complexes exhibit essential characteristics, including strong absorption of visible light by means of spin-allowed metal-to-ligand charge transfer (MLCT), efficient conversion to long-lived triplet MLCT excited states (³MLCT),⁷ and redox reversibility.^{7a,8} Furthermore, ligand and metal modifications tailor the redox properties of the ground and excited states.⁹ For example, *fac*-[Ir(ppy)₃] (tris[2-phenylpyridinato-*C*²,*N*]iridium(III), **1**, [ppy=2-phenylpyridine]) is amongst the strongest reducing PCs, while [Ru(bpy)₃]²⁺ (tris(2,2'-bipyridine)ruthenium(II), **2**, bpy=2,2'-bipyridine) possesses redox properties that enable it to function either as a reductant or as an oxidant from the ³MLCT state. However, iridium and ruthenium are precious metals and amongst the rarest elements on earth, escalating their costs and presenting concerns related to sustainability and scalability, driving the need to realize new PCs incorporating non-precious metals¹⁰ or to develop entirely organic replacements.¹¹ Several organic molecules have proven successful as visible-light PCs for small molecule and polymeric transformations.¹² The majority of these organic PCs, such as Eosin Y,¹³ rhodamine dyes,¹⁴ acridinium salts,¹⁵ perylene diimides,¹⁶ and carbazolyls¹⁷ are excited state

oxidants and operate through a reductive quenching cycle. Although a few strongly reducing organic PCs exist,¹⁸ many do not absorb visible light. PCs that operate using mild visible light and do not require sacrificial reductants are desired to minimize side reactions.

Our interest in organic PCs¹⁹ initiated with the development of organocatalyzed atom transfer radical polymerization (O-ATRP).²⁰ ATRP has historically been mediated by transition-metal catalysts, most commonly copper or ruthenium complexes, which can contaminate the polymer product and restrict applications.²¹ A primary challenge in developing a photoredox-mediated O-ATRP is presented by the strong reducing power that is required of the PC to activate a dormant alkyl halide.²² In general, PCs that possess such strong excited state reducing powers are rare, and this is particularly true for organic systems (*vide supra*).

To address this challenge, we have introduced visible-light organic PCs, including perylene,^{19a} *N,N*-diaryl dihydrophenazines,^{19b},²³ and *N*-aryl phenoxazines,²⁴ as organic PCs to mediate O-ATRP through an oxidative quenching pathway.²⁵ Dihydrophenazine and phenoxazine contain electron-rich chromophore motifs that form stable radical cations upon oxidation and enable them to be strong excited state reductants.²⁶ However, a detailed comprehension of the characteristics of these molecules in regards to catalysis or their ability to catalyze other transformations has not been established. Herein, through investigation of their photophysical and electrochemical properties, we report the critical characteristics of *N,N*-5,10-di(2-naphthalene)-5,10-dihydrophenazine (**3**) and 3,7-(4-biphenyl)-1-naphthalene-10-phenoxazine (**4**) that enable them to serve as successful PCs. We further establish **3** and **4** as PCs through their employment in atom transfer radical additions or substitutions with CF₃I to alkenes and heterocycles as well as dual photoredox/nickel-catalyzed C–N and C–S cross-coupling reactions.

Results and Discussion

The photophysical properties of **3** and **4** were investigated and compared to those of transition-metal complexes **1** and **2** (Figure 5.1). As photoexcitation is the first step in photoredox catalysis, PCs should be strong light absorbers. In *N,N*-dimethylacetamide (DMA), the molar absorptivities (ϵ) for transition-metal complexes **1** and **2** are 13 100 and 12 500 $\text{m}^{-1} \text{cm}^{-1}$ at their maximum peak wavelengths of absorption ($\lambda_{\text{max,abs}}$) of 377 nm and 454 nm, respectively (Figure 5.1 A). Dihydrophenazine **3** has a lower molar absorptivity ($\epsilon_{\text{max,abs}}=5950 \text{ m}^{-1} \text{cm}^{-1}$; $\lambda_{\text{max,abs}}=343$ nm) in comparison to **1** and **2**, while phenoxazine **4** is an excellent light absorber, possessing a higher molar absorptivity in the visible spectrum than the other three PCs ($\epsilon_{\text{max,abs}}=26\,600 \text{ m}^{-1} \text{cm}^{-1}$; $\lambda_{\text{max,abs}}=388$ nm). In a similar fashion to **1**, although the $\lambda_{\text{max,abs}}$ values are <400 nm, the absorption profiles of organic PCs **3** and **4** extend into the visible region and enable them to function as visible light PCs.

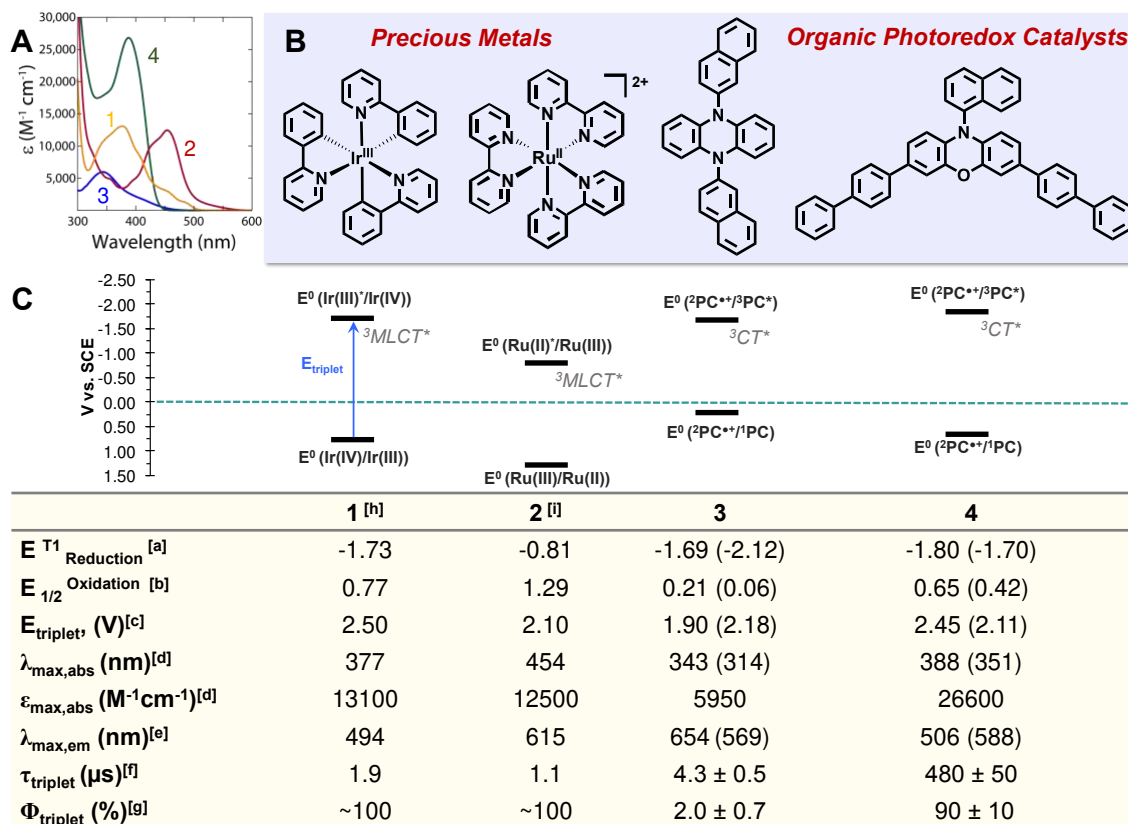


Figure 5.1. Photophysical and electrochemical properties of precious metal and organic photoredox catalysts. (A) UV-vis absorption spectra of PCs **1-4** in *N,N*-dimethylacetamide (DMA). (B) Structures of precious metal and organic PCs. (C) Values enclosed in parentheses are from density functional theory (DFT) calculations, computed at the improved M06/6-311+G(d,p)//M06/6-31+G(d,p) level of theory. Previously reported values for PCs **3** and **4** were computed at M06/6-31+G(d,p) and M06/6-311+G(d,p)//M06/Lanl2dz, respectively. All experimental values for PCs **3** and **4** were measured in DMA at room temperature. [a] Triplet excited state reduction potential, in units of V vs. SCE. [b] Ground state oxidation potential in units of V vs. SCE; typically approximated by the half wave potential $E_{1/2}$ in cyclic voltammetry measurements. [c] Triplet energy (E_{triplet}), in units of V; estimated from the fluorescence wavelength of the charge transfer singlet state. We note that the fluorescence wavelength from the charge transfer singlet state is used to estimate the energy of the charge transfer lowest triplet state, as the energies of the charge transfer lowest singlet and triplet states are expected to be nearly degenerate.^{15b} [d] Maximum absorption wavelength ($\lambda_{\text{max,abs}}$), in units of nm; molar absorptivity ($\epsilon_{\text{max,abs}}$) at $\lambda_{\text{max,abs}}$ in units of $M^{-1}cm^{-1}$. Acquired in DMA. [e] Emission maximum wavelength ($\lambda_{\text{max,em}}$), in units of nm. [f] Triplet excited state lifetime (τ_{triplet}), in units of μs . The reported lifetime is the average of three independently measured lifetimes with the error being twice the standard deviation of a given data set. [g] Quantum yield (Φ_{triplet}) of charge transfer triplet excited state ($^3CT^*$), and metal-ligand charge transfer triplet state ($^3MLCT^*$). [h] $\lambda_{\text{max,abs}}$ and $\epsilon_{\text{max,abs}}$ were measured in this work in DMA solvent. All other values were obtained from ref. ^{8a, 9b}, and were measured in acetonitrile, except for the $\lambda_{\text{max,em}}$, which was measured in alcoholic solvent at 77K. [i] $\lambda_{\text{max,abs}}$ and $\epsilon_{\text{max,abs}}$ were measured in this work in DMA solvent for $[Ru(\text{bpy})_3](PF_6)_2$. All other values were obtained from ref. ^{8b, 9a}, and were measured in acetonitrile.

Complex **1** is known to be one of the strongest excited state transition-metal PC reductants available, with an excited state reduction potential (E^{0*}) of $E^0(\text{Ir}^{\text{IV}}/\text{Ir}^{\text{III}*})=-1.73$ V vs. SCE (Figure 5.1C). Excitingly, organic PCs **3** and **4** are similarly reducing with $E^{0*}=E^0(2\text{PC}^+/\text{PC}^*)$ values of -1.69 and -1.80 V vs. SCE, respectively. Although **2** is not as reducing in the excited state [$E^{0*}=E^0(\text{Ru}^{\text{III}}/\text{Ru}^{\text{II}*})=-0.81$ V vs. SCE], the Ru^{III} generated after participating in a photoreduction event is strongly oxidizing, with an oxidation potential [$E^0_{\text{ox}}=E^0(\text{Ru}^{\text{III}}/\text{Ru}^{\text{II}})$] of 1.29 V vs. SCE. Notably, **1** and the organic PC **4** have similar E^0_{ox} values [$E^0(\text{Ir}^{\text{IV}}/\text{Ir}^{\text{III}})=0.77$ and $E^0(2\text{PC}^+/\text{PC})=0.65$ V vs. SCE, respectively], while **3** forms a rather stable radical cation [$E^0_{\text{ox}}=E^0(\text{PC}^+/\text{PC})=0.21$ V vs. SCE]. In regards to triplet energy (E_{triplet}), both **1** and **4** have energetic triplets with E_{triplet} of 2.50 and 2.45 V, respectively. Meanwhile, E_{triplet} of **2** and **3** are lower, with respective values of 2.10 and 1.90 V.

Upon photoexcitation, transition-metal complexes **1** and **2** form a MLCT excited state, which is suggested to facilitate electron-transfer mechanisms in photocatalytic cycles.^{8b,9} Recently, we reported that the lowest energy excited state of dihydrophenazine **3** is also CT in nature.²³ Specifically, intramolecular CT occurs from the electron-rich phenazine core (donor) to one of the 2-naphthyl *N*-substituents (acceptor). Here we show that phenoxazine PC **4** similarly undergoes photoinduced intramolecular CT, as evidenced by a significant solvatochromic effect in the emission (Figure 5.2A). Additionally, the broad and featureless emission peaks are characteristic of emission from a CT state (Figure 5.2B).²⁷

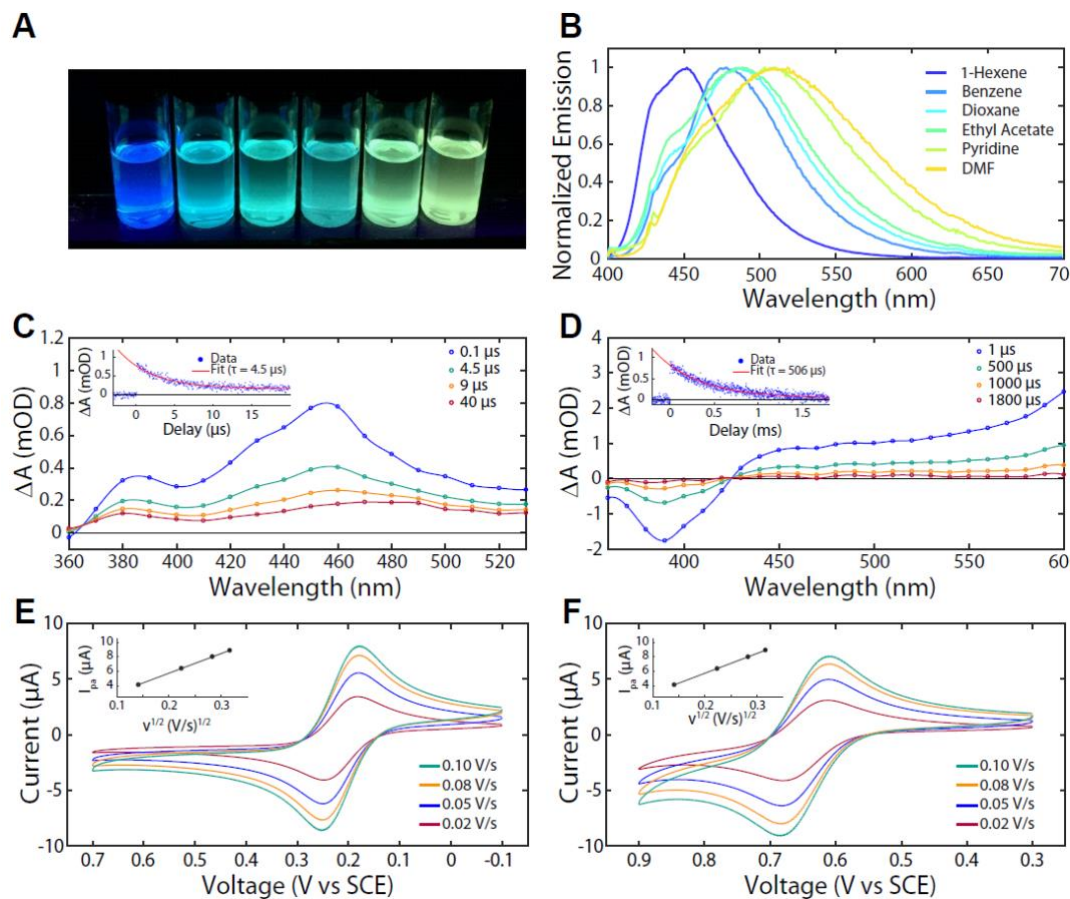


Figure 5.2. Photophysical properties of organic photoredox catalysts. (A) Photograph showing solvatochromic shifts in the emission of **4** when irradiated with 365 nm light in solvents of increasing polarity; from left to right: 1-hexene ($\epsilon_r = 2.07$), benzene ($\epsilon_r = 2.27$), dioxane ($\epsilon_r = 2.21$), ethyl acetate ($\epsilon_r = 6.02$), pyridine ($\epsilon_r = 13.0$), and DMF ($\epsilon_r = 37.2$); ϵ_r is dielectric constant of the solvent. (B) Normalized emission spectra of **4** in solvents of varying polarity. Transient absorption spectra of **3** (C) and **4** (D) in DMA at room temperature. The spectra consist of the global exponential fit to the raw data at timepoints indicated in the legend, connected by a spline function. The insets show the kinetic trace and the global exponential fit at 450 nm. Cyclic voltammetry (CV) experiments with various scan rates for (E) **3** and (F) **4**. CV measurements were performed in a 3-compartment electrochemical cell: reference electrode is Ag/AgNO₃ (0.01M) in MeCN and electrolyte is 0.1 M NBu₄PF₆. DMA was used as the solvent in the working electrode

compartment while platinum was used as both the working and counter electrodes. E (V vs. SCE) = E (V vs. Ag/AgNO₃ [0.01M]) + 0.298V.

The efficient access of a long-lived excited species by the PC enables sufficient time for bimolecular electron transfer with the desired substrate(s). In the case of transition-metal complexes **1** and **2**, ultrafast intersystem crossing produces the ³MLCT and is useful by way of extending excited state lifetimes (τ). Photoexcitation leads to a long-lived ³MLCT with quantitative yield. This ³MLCT state survives for 1.9 and 1.1 μ s in acetonitrile for **1** and **2**, respectively (Figure 5.1C). Using nanosecond transient-absorption (TA) spectroscopy performed in DMA at room temperature, we identified long-lived excited states for the organic PCs **3** and **4**. The τ of **3** was determined to be $4.3 \pm 0.5 \mu$ s (Figure 5.2C) whereas for **4**, it is a remarkable two orders of magnitude longer than that of **1**, **2**, or **3**, with $\tau = 480 \pm 50 \mu$ s (Figure 5.2D). By use of a triplet–triplet energy-transfer method (see Supporting Information), we have determined the triplet quantum yield (Φ_{triplet}) of **3** and **4** in DMA at ambient temperature: **3**'s Φ_{triplet} is relatively low at $2.0 \pm 0.7 \%$, while **4** has an impressively high Φ_{triplet} of $90 \% \pm 10 \%$.

Another critical characteristic for successful PCs is radical stability following single-electron-transfer events. Transition-metal complexes **1** and **2** exhibit reversible waves in cyclic voltammetry (CV), a property that indicates stability of the redox-altered catalyst.^{7a,8} Similarly, the CVs corresponding to the ²PC^{•+}/¹PC couple of **3** and **4** are reversible (Figure 5.2E and 5.2F). In particular, the difference between the anodic and cathodic peak potential (ΔE_p) for **3** is 67 mV (compared to theoretical value of 59 mV),²⁸ while the ratio of the peak anodic current (I_{pa}) to the peak cathodic current (I_{pc}) is 0.97 (compared to theoretical value of 1) (Figure 5.2E). Redox reversibility of **3** is in part attributed to the stability of **3**'s ²PC^{•+}, as indicated by low E^0_{ox} value of

0.21 V vs. SCE; this value is even lower than the redox couple producing ferrocenium ($E^0_{\text{ox}} \approx 0.4$ V vs. SCE).²⁹ Likewise, the CV of **4** reveals $\Delta E_p = 68$ mV and $I_{\text{pa}}/I_{\text{pc}} = 1.28$.³⁰ Additionally, a linear relationship between I_{pa} and the square root of the scan rate ($v^{1/2}$) reveals that the CV of **3** and **4** are diffusion limited (Figure 5.2E and 5.2F, insets); this supports the idea that electron transfer between the PC and the electrode (for either **3** or **4**) is fast and likely facilitated by small structural reorganization²⁴ between ^1PC and $^2\text{PC}^+$.

With the confirmation that **3** and **4** possess key photophysical and electrochemical characteristics critical for photoredox catalysis, we set out to establish their broader catalytic ability and potential to replace precious metal PCs through performing challenging chemical transformations, particularly ones that have been previously directed by polypyridyl iridium and ruthenium PCs such as **1** and **2**.

First, we investigated if the strongly reducing dihydrophenazine **3** could directly reduce CF_3I (peak reduction potential (E_p) of -1.52 V vs. SCE on glassy carbon),³¹ thereby generating $\text{CF}_3\cdot$ for the trifluoromethylation of unsaturated substrates (Figure 5.3A).³² Using white LED irradiation of **3** (1 to 5 mol %) in the presence of 1.5 equivalents of potassium formate (HCOOK), CF_3 was successfully installed onto five-membered heteroarenes (indoles, pyrroles), arenes, and alkenes at moderate to excellent yields (42 % to 98 %). For alkenes, the presence of HCOOK base affords the substitution product, while the absence of HCOOK favors the addition product. The reduction of $\text{CF}_3\text{CF}_2\text{I}$ was also accomplished, generating $\text{CF}_3\text{CF}_2\cdot$ for substitution onto indoles and alkenes. The trifluoromethylation of 3-methylindole was achieved with similar yield using natural sunlight. The substitution reaction between 10-undecene-1-ol and CF_3I could be performed using lower catalyst loading (0.25 mol %, 69 % yield) or on a larger 10 mmol scale (1.74 g product, 73 % yield) while maintaining good yields.

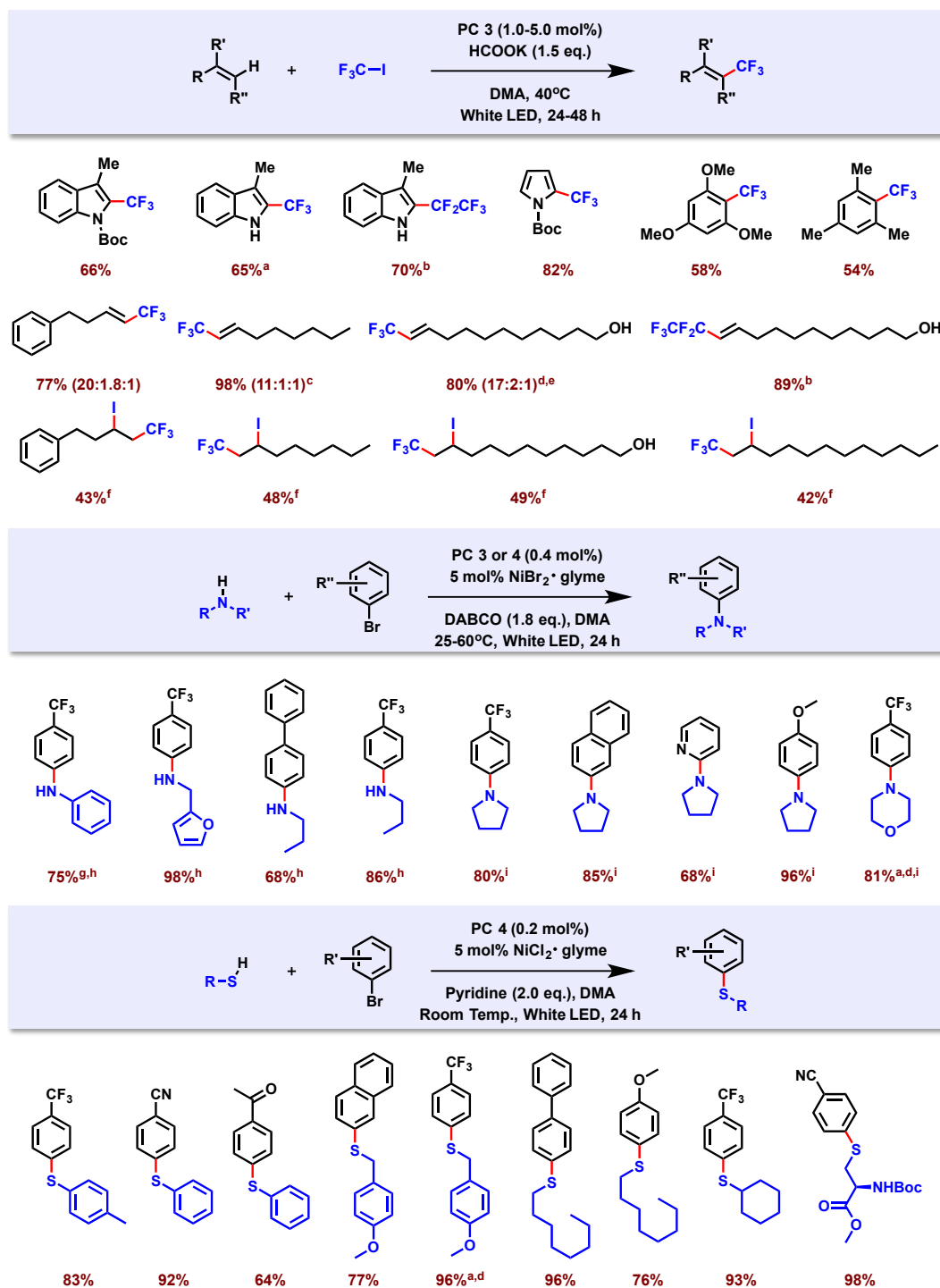


Figure 5.3. Photoredox-catalyzed transformations using organic PCs 3 and 4. A) Radical trifluoromethylations using PC 3 on alkenes, five-membered heteroarenes, arenes, and cross-addition on alkenes. B) Dual organic photoredox and nickel catalyzed C–N cross-coupling

reaction scope. C) Dual organic photoredox and nickel catalyzed C–S cross-coupling scope. Data reported as isolated yields. Values in parentheses are the ratio of Z:E:β-hydride elimination product. [a] Reaction was also conducted using sunlight for 1 week (67 % yield for trifluoromethylation, 83 % yield for C–N coupling, 94 % yield for C–S coupling). [b] CF₃CF₂I was used instead of CF₃I. [c] Reaction time 6 h. [d] Reaction was also conducted on a larger 10 mmol scale (73 % yield for trifluoromethylation, 53 % yield for C–N coupling, 98 % yield for C–S coupling). [e] Reaction was also conducted at reduced catalyst loading of 0.25 mol %, instead of standard 1.0 mol % (69 % yield for trifluoromethylation after 24 h). [f] Performed without HCOOK. [g] Reaction performed with 10 mol % pyrrolidine as the ligand and reduced nickel loading to 1.0 mol %. [h] Reaction catalyzed by PC 4. [i] Reaction catalyzed by PC 3.

Dual catalytic approaches integrating photoredox catalysis using iridium PCs and nickel-catalyzed cross-coupling reactions have enabled access to C–O,³³ C–S,³⁴ C–N,³⁵ and various C–C³⁶ bond forming reactions. Incorporating the photoredox cycle introduces redox or energy-transfer³⁷ mechanisms with the nickel complexes to complete otherwise demanding catalytic cycles. Cross-coupling reactions have traditionally been catalyzed by palladium complexes at elevated temperatures to construct such critical bonds.³⁸ Thus, to entirely remove precious metals out of cross-couplings through dual catalytic reactions, we sought to determine if organic PCs 3 and 4 could also enable such challenging reactions.

Previously, a dual photoredox/nickel catalytic approach employing 0.02 mol % of polypyridyl iridium PC [Ir{dF(CF)₃ppy}₂(dtbbpy)]PF₆ [dF(CF₃)ppy=2-(2,4-difluorophenyl)-5-(trifluoromethyl)pyridine; dtbbpy=4,4'-ditertbutyl-2,2'-bipyridine] in conjunction with NiBr₂·glyme could efficiently catalyze C–N bond formation under mild reaction conditions.^{35a} At

similar reaction conditions, albeit using a higher catalyst loading (0.4 mol %), PC **3** or PC **4** in combination with NiBr₂·glyme successfully catalyzed C–N coupling reactions at good to excellent yields (68 % to 96 %, Figure 5.3B). The scope of amines included both primary (aniline, furfurylamine, and propylamine) and secondary amines (pyrrolidine and morpholine) and were effectively coupled with electron-rich, electron-poor, and heterocyclic aryl bromides. For secondary amines, both PC **3** and **4** catalyzed C–N bond formations, although PC **3** generally gave slightly higher yields. Whilst PC **3** was unsuccessful in effecting C–N cross-coupling involving primary amines, PC **4** proved to be effective to couple primary amines in high yields.

In regards to C–S cross-coupling, the dual photoredox/nickel catalysis with 2 mol % [Ir{dF(CF)₃ppy}₂(dtbbpy)]PF₆ and NiCl₂·glyme produced C–S coupled products under mild conditions.³⁴ At analogous reaction conditions, phenoxazine PC **4** achieved C–S cross-couplings at good to excellent yields (64 % to 98 %, Figure 5.3C), but proved efficient at a much lower PC loading of 0.2 mol %. Aryl thiol (thiophenol), alkyl thiol (4-methoxybenzyl mercaptan, 1-octanethiol and cyclohexanethiol) and cysteine (*N*-(*tert*-butoxycarbonyl)-l-cysteine methyl ester) successfully coupled with a variety of aryl bromides. It is important to note that aryl bromide coupling partners were successfully incorporated with organic PC **4**, which were shown to be inactive when using [Ir{dF(CF)₃ppy}₂(dtbbpy)]PF₆.³⁴ PC **3** was unsuccessful in C–S coupling reactions, presumably due to its stable radical cation ($E^0_{\text{ox}}=0.21$ V vs. SCE) being unable to generate a thiol radical involved in the coupling reaction.³⁴

These photoredox/nickel C–N and C–S cross-coupling reactions could be driven by natural sunlight to obtain similarly high yield. Furthermore, both the C–N and C–S couplings could be performed on a larger 10 mmol scale reaction for C–N (1.22 g, 53 % yield) and C–S (2.92 g, 98 % yield) couplings. In these scaled reactions, C–S coupling maintained the high yield, while C–N

coupling suffered a 30 % drop in yield. This lower yield was attributed to limited light penetration owing to the opaque solution mixture compounded by the lower molar absorptivity of PC **3**.

Conclusion

In summary, photophysical and electrochemical characterizations on dihydrophenazine and phenoxazine PCs **3** and **4** reveal that these molecules possess the key attributes vital to successful photoredox catalysis, including redox reversibility and strong visible-light absorption to efficiently access a highly reducing triplet state through formation of CT excited state. The triplet excited state of these organic PCs are long-lived and accessed in 90 %±10 % quantum yield by PC **4**. Highlighting that **4** is an organic analogue of the iridium complex **1**, both PCs have almost identical E^{0*} , E^0_{ox} and E_{triplet} values. The potential for replacement of polypyridyl iridium and ruthenium complexes by organic PCs **3** and **4** is demonstrated by the ability of these organic analogues to catalyze trifluoromethylation reactions and dual photoredox/nickel C–N and C–S cross-coupling reactions using visible light, including natural sunlight.

Experimental

Materials and Methods

General Information

Unless otherwise stated, all commercially available chemicals were used without further purifications. 4-Biphenyl boronic acid was purchased from TCI America. Phenoxazine was purchased from Beantown Chemical. Glacial acetic acid was purchased from VWR. All other reagents were purchased from Sigma-Aldrich. Dimethylacetamide (DMA), pyrrolidine, and aniline were dried over calcium hydride overnight, filtered then distilled under vacuum followed

by three freeze-pump-thaw cycles and stored under nitrogen atmosphere. Dioxane, dimethylformamide (DMF) and tetrahydrofuran (THF) were purified using an mBraun MB-SPS-800 solvent purification system and kept under nitrogen atmosphere. Dicyclohexylphosphino-2,6-diisopropoxybiphenyl (RuPhos), tetrakis(triphenylphosphine)palladium(0), chloro-(2-dicyclohexylphosphino-2,6-diisopropoxy-1,1-biphenyl)[2-(2-aminoethyl)phenyl] palladium(II) - methyl-t-butyl ether adduct (RuPhos precatalyst) were stored under nitrogen atmosphere and used as received.

Nuclear magnetic resonance spectra were recorded on either a Bruker 300, Inova 400, or Inova 500 MHz instrument. Deuterated solvents were purchased from Cambridge Isotope Laboratories (Andover, MA) and used as received. All ^1H NMR experiments are reported in δ units, parts per million (ppm), and were measured relative to the signals for residual chloroform (7.26 ppm) in the deuterated solvent. All ^{13}C NMR spectra are reported in ppm relative to CDCl_3 (77.0 ppm). All ^{19}F NMR spectra are reported in ppm using ^1H NMR as absolute reference. The NMR yield of trifluoromethylation reaction was determined by ^{19}F NMR spectroscopy using 1-fluoro-3-nitrobenzene as an internal standard. Trimethoxybenzene was used as an internal standard for NMR yields from proton analysis for the nickel catalyzed reactions.

Flash column chromatography was performed by using a 100-150 times weight excess of flash silica gel 40-63 μm from Aldrich. Fractions were analyzed by TLC using TLC silica gel F254 250 μm precoated-plates from Merck and permanganate stain was used for UV-inactive compounds.

ESI mass spectrometry analysis was performed at the University of Colorado Boulder mass spectrometry facility using a Synapt G2 HDMS instrument, or Agilent 6220 TOF LC/MS with Agilent 1200 HPLC with multi-mode (combined ESI and APCI) at Colorado State University.

Photoreactor Setup

For trifluoromethylation: one 41 cm strip of double-density white LEDs, purchased from Creative Lighting Solutions (item no. CL-FRS1210-5M-12V-WH), was wrapped inside a 400 mL beaker and used as a visible light source, the LEDs naturally heat the reaction to ~40 °C. The beaker was then wrapped with aluminum foil on the outside (Figure 5.4, A). For nickel catalysis and 10 mmol scale up reactions: one 110 cm strip of double-density white LEDs, purchased from Creative Lighting Solutions (item no. CL-FRS120-5M-12V-WH) was wrapped inside a 400 mL beaker and used as a visible light source. The beaker was then wrapped with aluminum foil on the outside (Figure 5.4, B). Air was blown into the beaker to maintain room temperature where stated, or no air was blown into the set up to allow the LEDs to naturally heat the reaction to ~ 60 °C. Up to three 25 mL or 50 mL storage tubes were placed in one beaker on top of a stir plate (Figure 5.4, C). The reaction mediated by sunlight was shown in Figure 5.4, D.

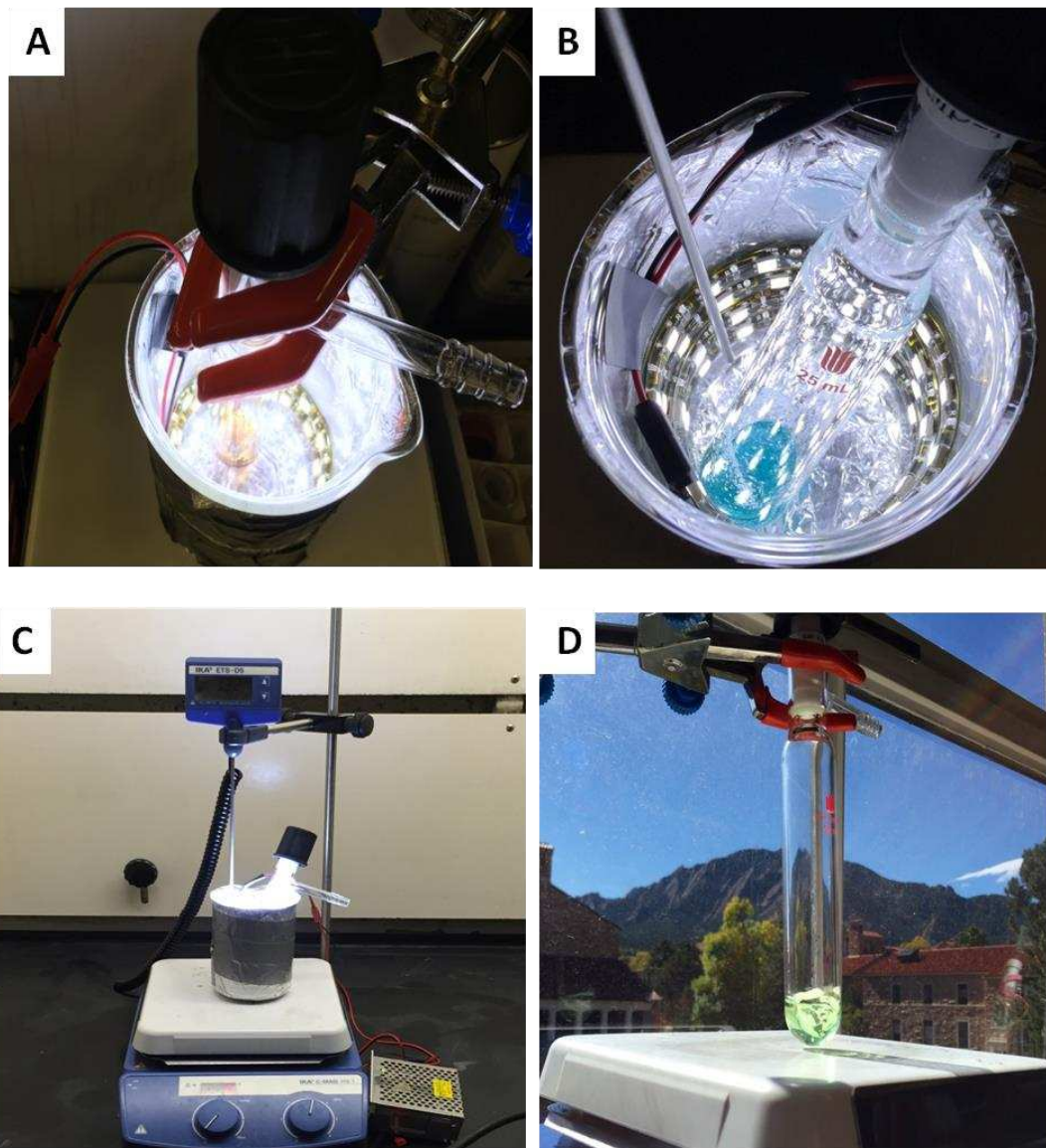


Figure 5.4. The photoreactor setup for trifluoromethylation (A), and Ni catalysis (B). View of the photoreactor is placed on the top of a stir plate (C), and the reaction mediated by sunlight (D).

Procedures

Photophysical Characterizations were performed by Collaborators at University of Colorado Boulder.

All samples were prepared in 1 x 1 cm quartz cuvettes and dissolved in anhydrous DMA. Samples were degassed prior to the experiment by bubbling argon for 15 minutes. All samples measured had optical densities near or below 0.1 at the excitation wavelength and were at ambient temperature (~23-25 °C). All reported lifetimes are the average of three independent measurements. Error is reported as two times the standard deviation of the respective sets of data.

Nanosecond to millisecond TA measurements were made using a home-built setup. A pulsed Nd:YAG laser (Continuum Surelite II) with a 10 Hz repetition rate, ~5 ns pulse width, and centered at 355 nm served either directly as the excitation source or was used to pump a Continuum Surelite optical parametric oscillator to obtain other excitation colors. The power was attenuated to between 0.5-8 mW at the sample as needed using neutral density filters and focused into the sample using a cylindrical lens (75 mm focal length). The spot size was measured with a knife-edge measurement and fit to a Gaussian profile. In the measurement of the TA spectra shown in Figure S5.3, the spot size was approximately ~ 4 mm by ~ 1 mm. The emission of a 100 W xenon arc lamp served as a broadband probe. This was focused onto the sample with a plano-convex lens (75 mm focal length). The pump and the probe were incident upon the cuvette at 90° relative to each other. Individual kinetic traces were obtained by selecting the wavelength with a monochromator (resolution of ± 1.7 nm) and measuring the signal from a PMT (Hamamatsu, R928-07) negatively biased at -1000 V with an oscilloscope (Lecroy, LC584AL). Traces were fit to a single-exponential model and in some cases were allowed to have a time-independent offset in order to account for longer-lived features. The model is global in the sense that a single lifetime

fit parameter is used to accommodate data at all wavelengths, while allowing the amplitudes to float. Shown spectra were created using wavelength-dependent values from the global exponential fit at a specified time-delay, connected by a spline function.

The long-lived TA feature of PC 3 in DMA

It was found that the TA signal of PC 3 in DMA does not decay to baseline but rather forms a long-lived shelf that persists with a lifetime of ~1 ms. The power dependence of this feature was investigated by taking the ratio of the amplitude of the exponentially decaying feature and the amplitude of the long-lived feature (fit as a constant offset) as a function of pump power (Figure 5.5). It was found that the long-lived feature becomes relatively less prominent as the pump power decreases. This behavior indicates that the long-lived component results from a multi-photon absorption event and thus is not considered to contribute to the photophysical understanding of the catalyst under typical catalytic conditions. It is the interpretation of the authors that the long-lived transient absorption signal following multi-photon absorption results from the transiently oxidized PC 3 with the most obvious redox partner being the solvent DMA.

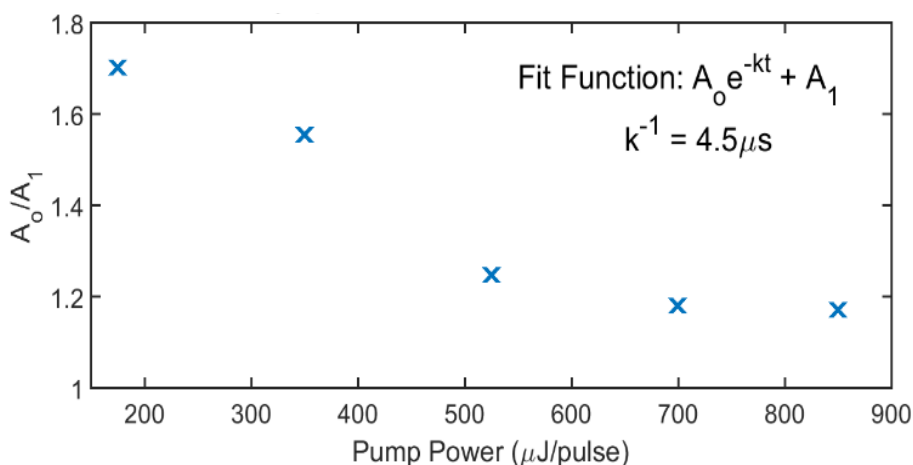


Figure 5.5. The ratio of the amplitude of the exponentially decaying feature over the long-lived TA feature (A_0/A_1) as a function of incident pump power. This data was collected at 480 nm where the amplitude of the long-lived feature is greatest.

Triplet Yield Measurement and Calculation via Triplet-Triplet Energy Transfer

The triplet yield (Φ_T) of a molecule, M, following a pulsed excitation can be defined as:

$$\Phi_T = [{}^3M^*] / [M^*]_0 \quad (1)$$

where $[{}^3M^*]$ is the concentration of M in the triplet excited state, and $[M^*]_0$ is the concentration of initially excited molecules. In a transient absorption (TA) experiment with a pulsed, monochromatic excitation source, the term $[M^*]_0$ can be determined the following equation:

$$[M^*]_0 = (\text{energy / pulse}) (\lambda / h c N_a) (1 - 10^{-A}) / (\sigma \ell) \quad (2)$$

where λ is the wavelength of the excitation pulse, σ is the spot size of the pulse, A is the absorbance of the sample at λ , ℓ is the path length, h is Planck's constant, c is the speed of light, and N_a is Avogadro's constant.

The other term in eq. 1, $[{}^3M^*]$, can be calculated using the Beer-Lambert law, but only provided that the molar absorptivity of ${}^3M^*$ (referred to as $\epsilon_{\text{triplet}}$) is known. One method for determining $\epsilon_{\text{triplet}}$ is via a triplet-triplet energy transfer (TTET) experiment.³ In this TA method, a donor molecule (D) of known triplet yield, $\Phi_{T,D}$, is used to promote the molecule of interest M into the triplet excited state via energy transfer, as shown in the following equations:



In eq. 4, Φ_{trans} refers to the yield of the TTET reaction (from $^3\text{D}^*$ to M) and it can be calculated in the following way:

$$\Phi_{\text{trans}} = 1 - ({}^3\tau)/({}^3\tau_0) \quad (5)$$

where ${}^3\tau_0$ is the triplet lifetime of D in the absence of M, and ${}^3\tau$ is the triplet lifetime of D in the presence of M. In order to determine $[{}^3\text{M}^*]$, one first calculates the initially excited concentration of D via eq. 2. Multiplying this value, $[{}^1\text{D}^*]_0$, by $\Phi_{\text{T,D}}$ will yield $[{}^3\text{D}^*]$. $[{}^3\text{D}^*]$ is then multiplied by Φ_{trans} to obtain the quantity that of $[{}^3\text{D}^*]$ that undergoes TTET, promoting M into the triplet excited state. This is shown more succinctly in the following expression:

$$[{}^3\text{M}^*] = [{}^1\text{D}^*]_0 \times \Phi_{\text{T,D}} \times \Phi_{\text{trans}} \quad (6)$$

$[{}^3\text{M}^*]$, thus calculated, is then related to an absorbance via the Beer-Lambert law in order to obtain $\epsilon_{\text{triplet}}$. Since ${}^3\text{M}^*$ is only transiently populated, the absorbance is measured via TA spectroscopy. Therefore, the measured observable is not a pure absorbance but rather is a change in absorbance, ΔA , which contains excited state absorbance, ground state bleach, and emission. This is furthermore complicated by the fact that the system for TTET contains two distinct species (D and M) which have their own unique ΔA profiles. Therefore, it is imperative that one select a wavelength region for observation in which there is an absence of overlapping ground-state bleach and emission from M. In which case, one can assume that the measured ΔA at the selected wavelength is uncontaminated and consists of only the absorbance of ${}^3\text{M}^*$. We will refer to this as $A_{\text{T,M}}(\lambda)$. Of course, one must also consider contribution in the measured absorbance from the donor

species. If the lifetime of $^3M^*$ is much longer than the timescale of its formation via TTET, one can simply measure $A_{T,M}(\lambda)$ via TA at a time delay that is chosen such that the signal is uncontaminated from the donor species. One can then calculate $\epsilon_{\text{triplet}}$ via the Beer-Lambert law:

$$\epsilon_{\text{triplet}}(\lambda) = A_{T,M}(\lambda) / ([^3M^*] \times \ell) \quad (7)$$

On the other hand, if the lifetime of $^3M^*$ is not significantly longer than the timescale of its formation, one cannot measure $A_{T,M}(\lambda)$ in a temporal regime in which $^3M^*$ is constant. In those cases, it is useful to consider a kinetic model in order to associate a given $A_{T,M}(\lambda)$ signal with a corresponding $[^3M^*]$.

Once $\epsilon_{\text{triplet}}(\lambda)$ is known, one can calculate the triplet yield of M by conducting a TA experiment in the absence of D. One can calculate $[^3M^*]$ by rearranging eq. 7, and $[M^*]_0$ can be calculated using eq. 2. The triplet yield of M can then be determined by taking the ratio of these two values, as shown in eq. 1.

In the present work, $\text{Ir}(\text{ppy})_3$ is used as the triplet donor since it possesses a higher energy triplet than PC 3 and PC 4, has a known triplet yield of 1, and has a ground state absorption spectrum that is sufficiently distinct from PC 3 and PC 4 such that it can be selectively excited.⁴ Furthermore, $\text{Ir}(\text{ppy})_3$ possess an intense phosphorescence band which provides a facile way to monitor its triplet lifetime.

Triplet Yield of PC 3

The triplet yield of PC 3 in DMA was determined using the TTET method described above. The triplet donor used was $\text{Ir}(\text{ppy})_3$, which possess a triplet state of quantitative yield and

sufficiently high energy to promote PC 3 into its triplet excited state. In all TTET measurements, Ir(ppy)₃ was excited using 475 nm light, a wavelength at which PC 3 is negligibly absorptive. The quenching of the triplet excited state of Ir(ppy)₃ (used to calculate Φ_{trans} via eq. 5) was measured by observing the change in lifetime of Ir(ppy)₃'s bright phosphorescence at 530 nm in the presence of PC 3. $A_{T,M}$ of PC 3 was determined by measuring ΔA at 450 nm at sufficiently long delays to ensure that the ΔA measured consisted of only the absorbance of the triplet excited state of PC 3. 450 nm was selected due to the low ΔA signal of Ir(ppy)₃ at this wavelength as well as the relatively strong ΔA of PC 3. However, due to the relatively short triplet lifetime of PC 3 (4.3 μs), the concentration of triplet species was not constant over the timescale measured. Therefore, the concentration of the triplet species had to be predicted using a kinetic model.

In the TTET system, the time-dependent concentration of the triplet state of the acceptor species, M, can be predicted from the following three equations:



where k_T is the rate constant for TTET, and k_M and k_D are the rate constants for the spontaneous decay of the triplet states of M and D, respectively.

From equations 8, 9, and 10, one can show that the time-dependent concentration of M can be represented by the following:

$$\frac{d[{}^3M]}{dt} = k_T[{}^3D(t=0)]e^{-t(k_T[M]+k_D)}[M] - k_M[{}^3M] \quad (11)$$

Integration of equation 11 yields:

$$[{}^3M(t)] = \frac{k_T*[M]*[{}^3D(t=0)]*(e^{-k_M t} - e^{-k_{D'} t})}{k_{D'} - k_M} \quad (12)$$

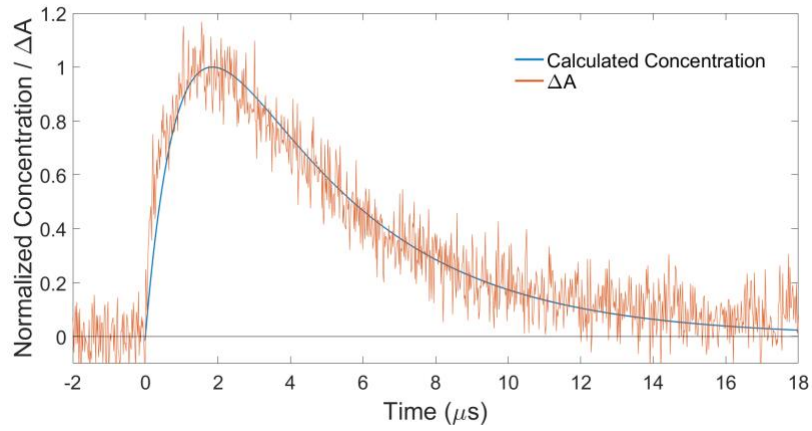
where $k_{D'} = k_D + [M] * k_T$. Since $k_{D'}$, k_M , and $[{}^3D(t=0)]$ are determined in the TTET experiment, $[{}^3M(t)]$ can be determined and used to calculate $\epsilon_{\text{triplet}}$.

Table 5.1: Data from three independent TA experiments of PC 3 and Ir(ppy)₃ mixture

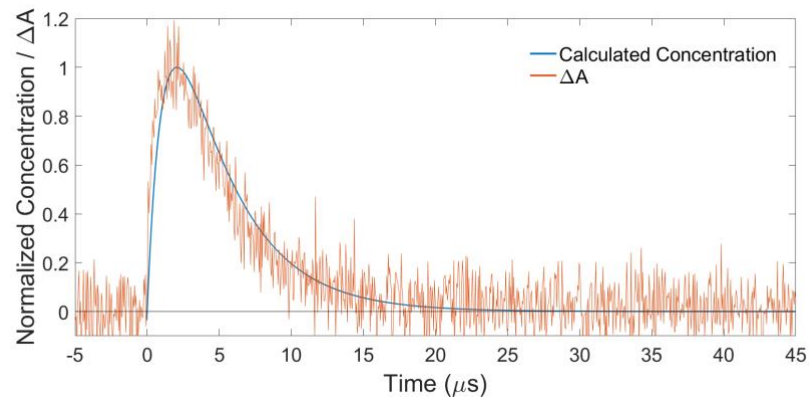
Experiment	#1	#2	#3
Abs @ 475 nm (OD)	0.103	0.124	0.087
Energy/pulse (μJ) ^{a,b}	158	184	158
Emissive lifetime of Ir(ppy) ₃ , τ_0 (μs)	1.50	1.50	1.50
Emissive lifetime of Ir(ppy) ₃ in the presence of PC 3, τ (μs)	1.00	1.20	1.09

^a Pump spot size FWHM: 2.41mm x 4.21 mm. ^b Pump wavelength: 475 nm

Experiment 1



Experiment 2



Experiment 3

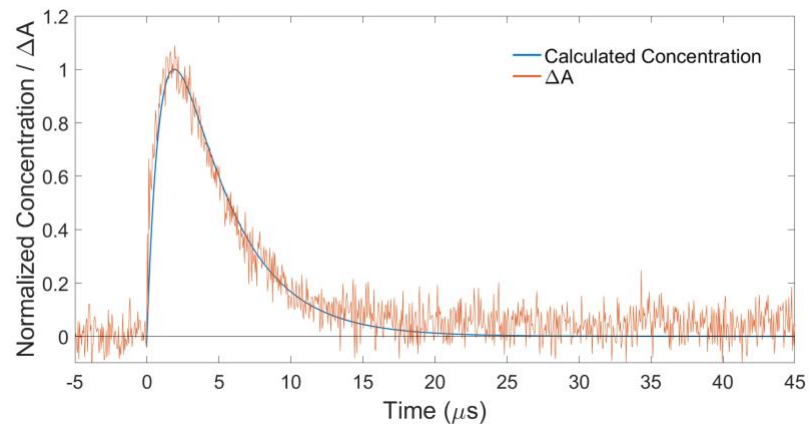


Figure 5.6. Comparison of the measured TA trace of PC 3 and Ir(ppy)₃ mixture with the kinetic model predicted by eq. 12. The orange curve is the normalized ΔA collected at 450 nm. The blue curve is the normalized concentration of PC 3 in the triplet excited state calculated using eq. 12.

From the modeled concentration and measured ΔA , $\epsilon_{\text{triplet}}$ was calculated using the Beer-Lambert law at each time point. After the first $\sim 2 \mu\text{s}$, the calculated value of $\epsilon_{\text{triplet}}$ was found to be constant for the duration of the ΔA signal. This value is reported in Table 5.2. The poor fit of the model at early times is attributed to contamination with a low intensity TA signal from Ir(ppy)₃.

Table 5.2: Calculated $\epsilon_{\text{triplet}}$ for PC 3

Experiment	1	2	3	Average	% Error
$\epsilon_{\text{triplet}}$ ($\text{M}^{-1} \text{cm}^{-1}$) @ 450 nm	15,042	17,565	14,873	15,827	15.56%

The $\epsilon_{\text{triplet}}$ ($\lambda = 450 \text{ nm}$) of PC 3 is found to be $16,000 \pm 2,500 \text{ M}^{-1} \text{cm}^{-1}$.

Table 5.3: The triplet yield of PC 3 using the average $\epsilon_{\text{triplet}}$ calculated from data from TA experiments of PC 3 in DMA.

Experiment	1	2	3	4	5	Average	% Error ^a	Total % Error ^b
Abs at 355 nm (OD)	0.177	0.138	0.122	0.182	0.094	----	----	----
Energy / pulse (μJ) ^{c,d}	373	390	442	120	120	----	----	----
ΔA at 450 nm (mOD) ^e	0.813	0.757	0.741	0.220	0.108	----	----	----
Triplet Yield	0.0206	0.0225	0.0216	0.017	0.0147	0.0193	30.7	34.4

^a The % error of the calculated triplet yield measurements using the average $\epsilon_{\text{triplet}}$ at 450 nm. ^b The total % error takes the uncertainty of $\epsilon_{\text{triplet}}$ into account. ^c Pump spot size FWHM: 1.53mm x

3.8mm. ^d Pump wavelength: 355 nm. ^eAll kinetic traces are fit to the exponential model: $A(t) = A_0 e^{-t/\tau} + A_1$. The reported ΔA values are the amplitude of the exponential portion of the fit, A_0 .

The triplet yield of PC 3, as observed at 450 nm in the TA spectrum, is 0.019 ± 0.0066 , or more conservatively, 0.02 ± 0.007 .

Triplet Yield of PC 4

The triplet yield of PC 4 in DMA was determined using the TTET method described above. The triplet donor used was Ir(ppy)₃, which possess a triplet state of quantitative yield and sufficiently high energy to promote PC 4 into its triplet excited state. In all TTET measurements, Ir(ppy)₃ was excited using 475 nm light, a wavelength at which PC 4 is negligibly absorptive. The quenching of the triplet excited state of Ir(ppy)₃ (used to calculate Φ_{trans} via eq. 5) was measured by observing the change in lifetime of Ir(ppy)₃'s bright phosphorescence at 530 nm in the presence of PC 4. The quantity $A_{\text{T,M}}(\lambda)$ for PC 4 was determined by measuring $\Delta A(\lambda)$ at the probe wavelengths 500 nm, 550 nm, and 600 nm, and at sufficiently long delays (> 3 μs) to ensure that the ΔA measured consisted of only the absorbance of the triplet excited state of PC 4. Due to the long triplet lifetime of PC 4, the concentration of triplet species was constant over the timescales measured.

Table 5.4: Data from three independent TA experiments for PC 4 and Ir(ppy)₃ mixture

Experiment	#1	#2	#3
Ir(ppy) ₃ Abs @ 475 nm (OD)	0.067	0.095	0.074
[PC 4] (mM) ^a	0.11	0.22	0.31
Energy/pulse (μJ) ^{b,c}	79	125	105
Emissive Lifetime of Ir(ppy) ₃ , τ_0 (μs)	1.50	1.49	1.51

Emissive Lifetime of Ir(ppy) ₃ in the presence of PC 4, τ (μ s)	1.01	1.12	1.31
ΔA @ 500 nm (mOD)	0.133	0.572	0.425
ΔA @ 550 nm (mOD)	0.161	0.698	0.596
ΔA @ 600 nm (mOD)	0.304	1.389	1.159

^a This value is not necessary for the calculations but is reported to demonstrate that these TTET experiments were conducted at a variety of concentrations of PC 4. ^b Pump spot size FWHM: 2.41mm x 4.21 mm. ^c Pump wavelength: 475 nm

Table 5.5. Calculated epsilons for PC 4

Experiment	#1	#2	#3	Average	% Error
$\epsilon_{\text{triplet}}$ at 500 nm ($M^{-1} \text{ cm}^{-1}$)	7.1315×10^3	7.5502×10^3	6.3162×10^3	7.00×10^3	14.6
$\epsilon_{\text{triplet}}$ at 550 nm ($M^{-1} \text{ cm}^{-1}$)	8.6309×10^3	9.2198×10^3	8.8584×10^3	8.90×10^3	5.5
$\epsilon_{\text{triplet}}$ at 600 nm ($M^{-1} \text{ cm}^{-1}$)	1.6321×10^4	1.8345×10^4	1.7219×10^4	1.73×10^4	9.6

From these epsilons, a triplet yield can be calculated from the TA data collected for PC 4 in the absence of the triplet sensitizer Ir(ppy)₃. This was done at 500, 550, and 600 nm using 355 nm light for excitation. However, due to the lower error in the 550 nm measurements, only these are reported below in Table S6.

Table 5.6. TA of PC 4 observed at 550 nm and calculated triplet yield

Experiment	#1	#2	#3	#4	Average	% Error ^a	Total Error ^b	%
Abs @ 355 nm	0.104	0.132	0.090	0.106	----	----	----	

Energy / pulse (μJ) ^{c,d}	55	29	29	29	----	----	----
ΔA @ 550 nm (mOD)	1.539	1.065	0.695	0.800	----	----	----
Triplet Yield	0.91	0.97	0.89	0.88	0.913	7.7	9.4

^a The % error of the calculated triplet yield measurements using the average $\epsilon_{\text{triplet}}$ at 550 nm. ^b The total % error takes the uncertainty of $\epsilon_{\text{triplet}}$ into account. ^c Pump spot size FWHM: 1.53mm x 3.8mm
^d Pump wavelength: 355 nm

The triplet yield of PC 4, as observed at 550 nm in the TA spectrum, is 0.91 ± 0.09 , or, more conservatively, 0.9 ± 0.1 .

Cyclic Voltammetry (Performed by Chern-Hooi Lim)

Cyclic voltammetry (CV) measurements were performed in a 3-compartment electrochemical cell: reference electrode is Ag/AgNO₃ (0.01M) in MeCN and electrolyte is 0.1 M NBu₄PF₆. DMA was used as the solvent in the working electrode compartment while platinum was used as both the working and counter electrodes. E (V vs. SCE) = E (V vs. Ag/AgNO₃ [0.01M]) + 0.298V. At the scan rate of 0.02V/s, the $i_{\text{pa}}/i_{\text{pc}}$ value of PC 4 in DMA is 1.28 (Figure 5.8), which deviates from 1 for system that exhibits reversible redox behavior. We attribute this deviation to the fact that oxidation of PC 4 occurs near the oxidation window of DMA solvent. For example, CV of PC 4 was scanned from 0.3V to 0.9V vs. SCE (Figure 5.8) while the onset of DMA oxidation occurs around 0.8V vs. SCE (Figure 5.7). DMF and THF have increasingly wider oxidation window, where these two solvents have negligible oxidation currents even at 1.2V vs. SCE (Figure 5.7). The $i_{\text{pa}}/i_{\text{pc}}$ value of PC 4 improves to 1.11 and 1.01, respectively in DMF (Figure 5.9) and THF (Figure 5.10).

Solvent Blank

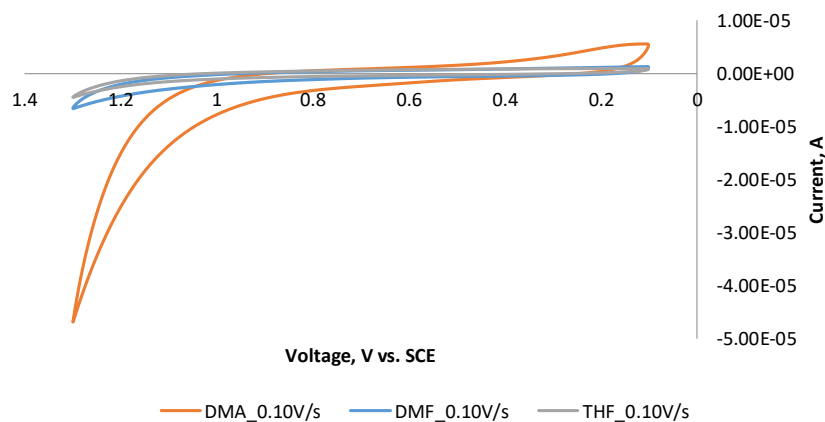
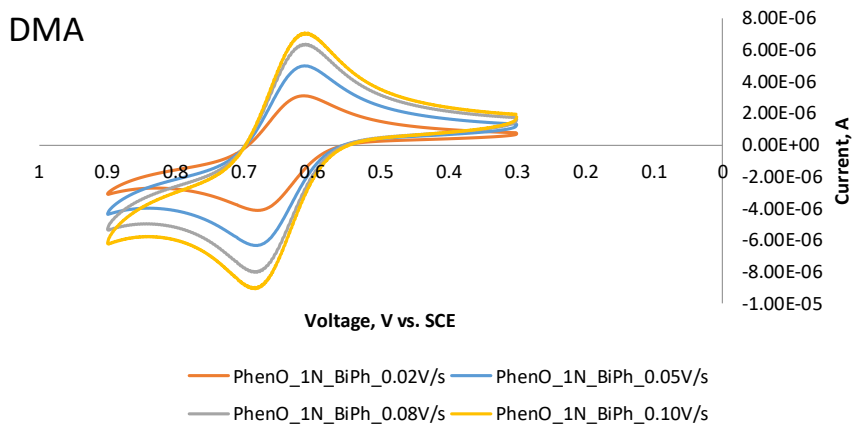


Figure 5.7. Solvent blank.

CV of PC 4 in DMA



V/s	E_{pa} (V)	E_{pc} (V)	i_{pa} (A)	i_{pc} (A)	i_{pa} / i_{pc}	ΔE_p (V)	$E_{1/2}$ (vs. SCE)
0.02	0.680	0.612	-4.13E-06	3.22E-06	1.28	0.068	0.64
0.05	0.681	0.611	-6.37E-06	5.07E-06	1.26	0.070	0.64
0.08	0.681	0.610	-7.99E-06	6.43E-06	1.24	0.071	0.64
0.10	0.683	0.611	-8.93E-06	7.13E-06	1.25	0.072	0.65

Figure 5.8. CV of PC 4 in DMA

CV of PC 4 in DMF

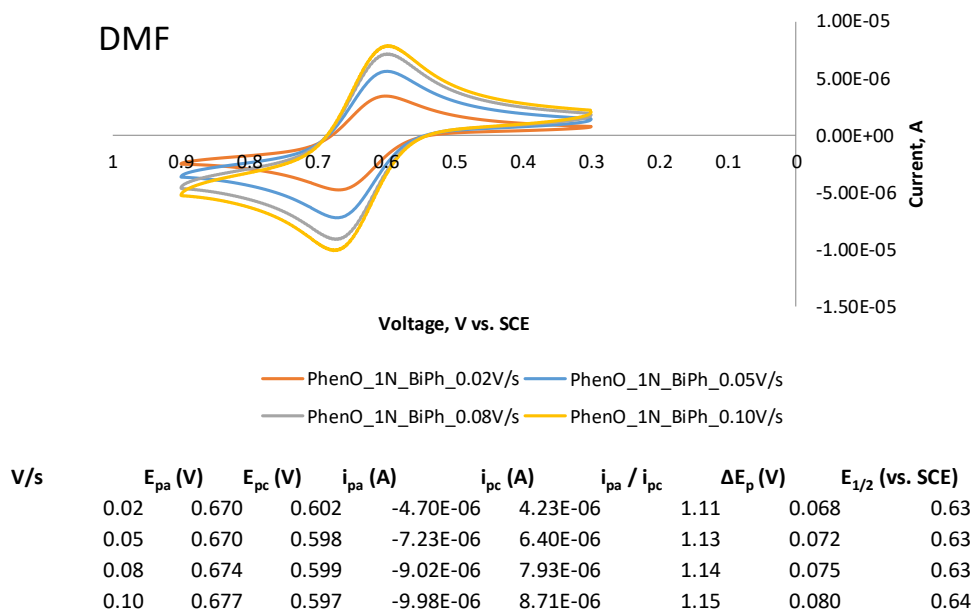


Figure 5.9. CV of PC 4 in DMF

CV of PC 4 in THF

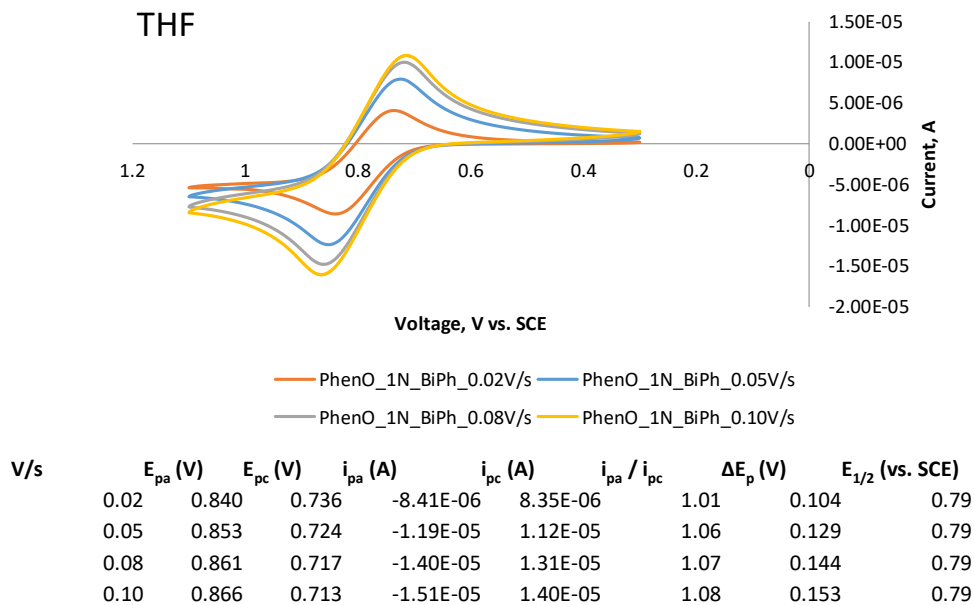
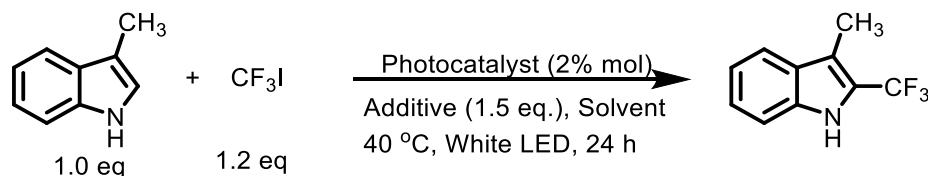


Figure 5.10. CV of PC 4 in THF

Optimization and Controls

Trifluoromethylations and Atom Transfer Radical Addition experiments performed by Ya Du

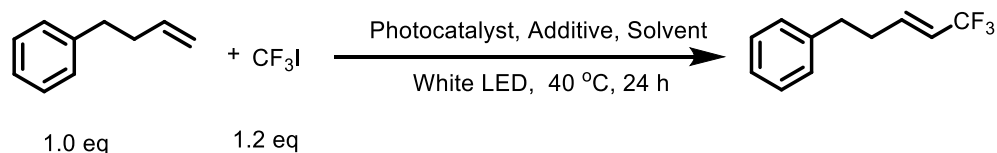
Optimization of Trifluoromethylation of 3-Methyl Indole



Entry ^a	PC	Solvent	Additive	Yield ^c
1	S1	DMA	-	17%
2	S2	DMA	-	31%
3	3	DMA	-	49%
4	S3	DMA	-	40%
5 ^d	S4	DMA	-	58%
6 ^d	S5	DMA	-	53%
7	None	DMA	-	NR
8 ^e	3	DMA	-	NR
9	3	DMSO	-	18%
10	3	DMF	-	48%
11	3	ACN	-	10%
12	3	Dioxane	-	9%
13	3	THF	-	36%
14	3	DMA	Et ₃ N	58%
15	3	DMA	CH ₃ COOK	53%
16	3	DMA	Cs ₂ CO ₃	12%
17	3	DMA	HCOOK	66%(65% ^f)
18 ^g	3	DMA	HCOOK	67%(67% ^f)
19	None	DMA	HCOOK	NR
20	S3	DMA	HCOOK	70%
21 ^d	S4	DMA	HCOOK	79%
22 ^d	S5	DMA	HCOOK	84%(82% ^f)

^a Reactions conducted in 25 mL storage tubes with 3-methyl indole (1 mmol, 1.0 eq.), CF₃I (0.6 M), and PC 0.02 mmol (2% mol) in solution of the designated solvent (2 mL) under N₂. ^bAdditive 1.5 eq. in relation to 3-methyl indole. ^c Yield determined by ¹⁹F NMR spectroscopy using the peak of 1-fluoro-3-nitrobenzene as an internal standard. ^d Light wavelength 365 nm. ^e Reaction in the dark (storage tube in aluminum foil). ^f Isolated yield. ^g Sunlight, with reaction time = 1 week.

Optimization of Trifluoromethylation of 4-Phenyl-1-Butene

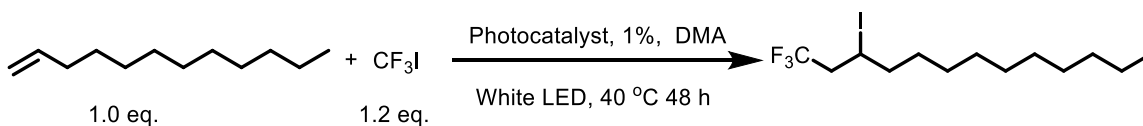


Entry ^a	PC	Solvent	Additive ^b	Yield ^c
1	None	DMA	-	NR
2	None	THF	HCOOK	NR
3	None	DMA	HCOOK	14%
4	3	DMA	HCOOK	89%
5 ^d	3	DMA	HCOOK	NR

^a Reactions conducted in 25 mL storage tubes with 4-phenyl-1-butene (1 mmol, 1.0 eq.), CF₃I (0.6 M), and PC 3 0.01 mmol (1 % mol) in solution of the designated solvent (2 mL) under N₂.

^bAdditive 1.5 eq. in relation to 4-phenyl-1-butene. ^c Yield determined by ¹⁹F NMR spectroscopy using the peak of 1-fluoro-3-nitrobenzene as an internal standard. *E* isomer: *Z* isomer: β-hydride elimination product = 20 : 1.8 : 1. ^d Reaction in the dark (storage tube in aluminum foil).

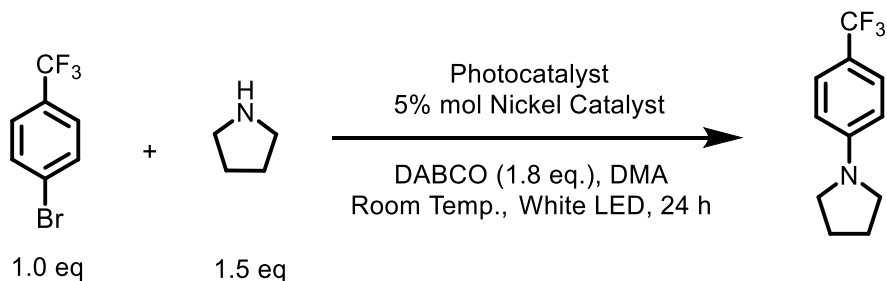
Cross-addition of Alkenes Catalyzed by Photoredox Catalysis



Entry ^a	PC	Solvent	Yield
1	None	DMA	NR
2	3	DMA	42%
3 ^b	3	DMA	NR

^a Reactions conducted in 25 mL storage tubes with 4-phenyl-1-butene (1 mmol, 1.0 eq.), CF₃I (0.6 M) and PC 3 0.01 mmol (1 % mol) in DMA(2 mL) under N₂. ^b Reaction performed in the dark (storage tube in aluminum foil).

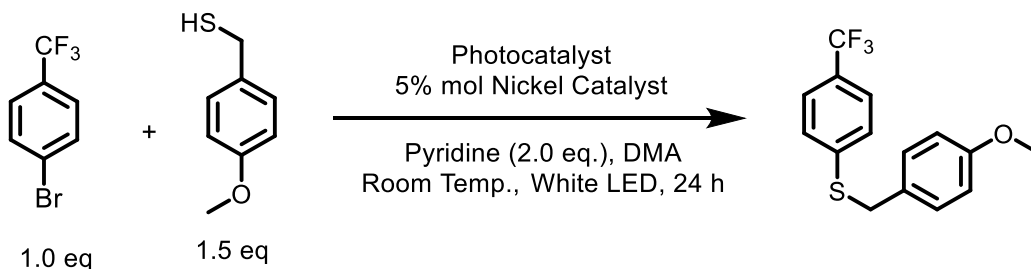
Optimization of C-N Coupling Reaction



Entry ^a	PC	Nickel Cat.	Yield ^b
1	0.2% mol 3	NiBr ₂ *glyme	86%
2	0.2% mol 4	NiBr ₂ *glyme	65%
3 ^c	0.2% mol 3	NiBr ₂ *glyme	92%
4	0.2% mol 3	Ni(COD) ₂	79%
5 ^d	0.2% mol 3	NiBr ₂ *glyme	NR
6	No PC	NiBr ₂ *glyme	NR
7	0.2% mol 3	No Nickel	NR
8	0.4% mol 3	5 NiBr ₂ *glyme	95%

^a Reactions conducted in 50 mL storage tubes with 4-bromobenzotrifluoride (1.2 mmol, 1.0 eq.), dry pyrrolidine (1.8 mmol, 1.5 eq.), 1,4-diazabicyclo[2.2.2] octane (2.16 mmol, 1.8 eq) in DMA (3 mL) under N₂. ^b Yields were obtained via ¹H NMR using trimethoxybenzene (100.9 mg, 0.60 mmol, 0.5 eq) as an internal standard, which was added to the worked up reaction mixtures. The standard and remaining solids/oils were fully dissolved in the needed amount of deuterated chloroform (typically 2.0 mL). Aromatic peaks of the trimethoxybenzene and 1-(4-(trifluoromethyl)phenyl)pyrrolidine product were compared to get NMR Yield. ^c Run at 60 °C. ^d Reaction run in the dark (storage tube in aluminum foil).

Optimization of C-S Coupling Reaction

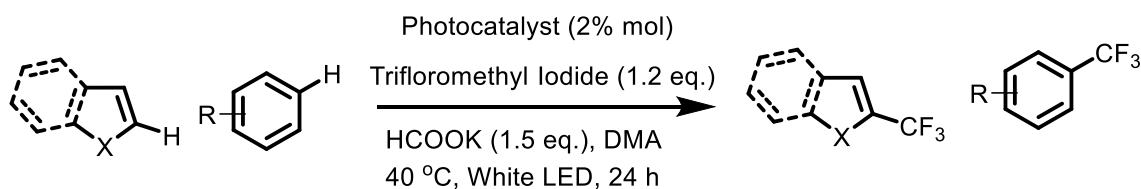


Entry ^a	PC	Nickel Cat.	Yield ^b
1	1.0% mol 3	NiCl ₂ *glyme	NR
2	1.0% mol 4	NiCl ₂ *glyme	98%
3 ^c	1.0% mol 4	NiCl ₂ *glyme	NR
4	1.0% mol 4	Ni(COD) ₂	NR
5 ^d	1.0% mol 4	NiCl ₂ *glyme	NR
6	None	NiCl ₂ *glyme	NR
7	1.0% mol 4	No Nickel	NR
8	0.2% mol 4	NiCl*glyme	98%

^a Reactions conducted in 50 mL storage tubes with 4-bromobenzotrifluoride (1.2 mmol, 1.0 eq.), 4-methoxybenzyl mercaptan (1.8 mmol, 1.5 eq.) dry pyridine (2.4 mmol, 2.0 eq.), Nickel catalyst and photocatalyst in DMA (3 mL) under N₂. ^b Yields were obtained via ¹H NMR using trimethoxybenzene (100.9 mg, 0.60 mmol, 0.5 eq) as an internal standard, which was added to the worked up reaction mixtures. The standard and remaining solids/oils were fully dissolved in the needed amount of deuterated chloroform (typically 2.0 mL). Aromatic peaks of the trimethoxybenzene and 4-methoxyphenyl(4-(trifluoromethyl)phenyl)sulfane product were compared to get NMR yield. ^c Run with DABCO instead of pyridine. ^d Reaction run in the dark (storage tube in aluminum foil).

General Synthesis Procedures

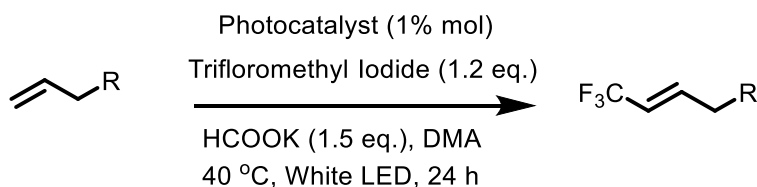
General Procedure A for C-CF₃ Bond Formation of (Hetero) Arenes



To an oven-dried 25 mL storage flask was added a stir bar, photocatalyst 3 (0.02 mmol, 2% mol.), potassium formate (126.2 mg, 1.5 mmol, 1.5 eq.), and (hetero) arenes (1.0 mmol, 1.0 eq.). The flask was degassed by quickly alternating vacuum evacuation and argon backfill (x3) before a CF₃I

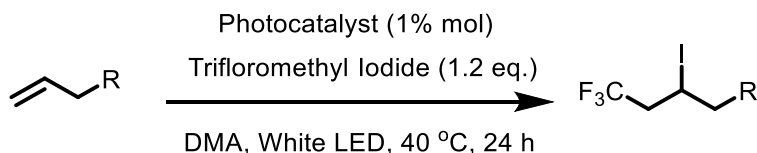
solution in DMA (CF₃I/DMA solution is pre-made and stored under N₂) (2 mL, 0.6 M, 1.2 eq.) was added by syringe. The flask was sealed and placed in the photo reactor with white LEDs as described for the trifluoromethylation reaction, and allowed to stir at 40 °C for 24 hours (Figure S5.2, A). After which the reaction was removed from light and quenched with water (10 mL) and extracted with Et₂O (20 mL x 3) except when specified and the combined organic layers were dried over Na₂SO₄. The crude material was then purified by column chromatography on silica gel using the noted solvent mixture to isolate the desired product.

General Procedure B for C-CF₃ Bond Formation of Olefins



This procedure is identical to General Procedure A except for the use of 1% loading of photoredox catalyst 3.

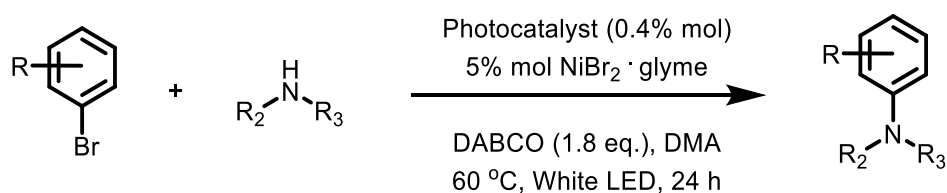
General Procedure C for Cross Addition of Trifluoromethyl Iodide



To an oven-dried 25 mL storage flask was equipped with a magnetic stir bar, PC 3(0.01 equiv), and olefin (1 mmol, 1eq.). The tube was degassed by quickly alternating vacuum evacuation and argon backfill (x3) before a CF₃I solution in DMA (CF₃I/DMA solution is prepaid and stored under N₂) (2.0 mL, 0.6 M) was added by syringe. The tube was sealed and placed in a 400 ml beaker with one 41 cm strip of double-density LEDs (white), wrapped inside (Figure S5.2, A).

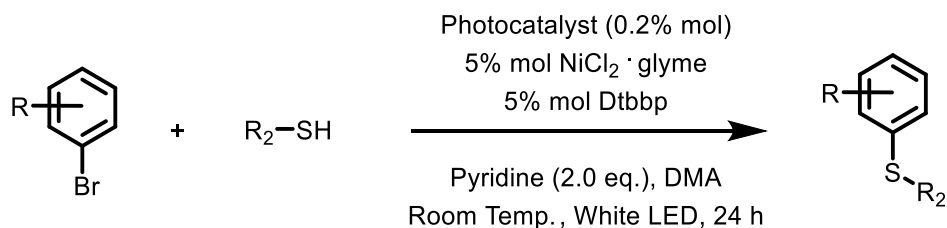
After 48 hours, the reaction was quenched with water (10 mL) and extracted with Et₂O (20 mL×3) and the combined organic layers were dried over Na₂SO₄. The crude material was then purified by column chromatography on silica gel using the noted solvent mixture to isolate the desired cross-addition products.

General Procedure D for C-N Bond Formation



To an oven-dried 50 mL storage flask was added a stir bar, PC 3 (2.1 mg, 0.0048 mmol, 0.4% mol) for secondary amines or PC 4 (3.0 mg, 0.0048 mmol, 0.4%) for primary amines, aryl halide (1.20 mmol, 1.0 eq.), and amine (1.80 mmol, 1.5 eq.). The reagents were then freeze pump thawed and backfilled with nitrogen three times before being brought into a glove box where Nickel(II) bromide 2-methoxyethyl ether complex (18.5 mg, 0.06 mmol, 5.0% mol), in 1.0 mL of a DMA stock solution was added, 1,4-diazabicyclo[2.2.2]octane (242.3 mg, 2.16 mmol, 1.8 eq.) then an additional 2.0 mL of DMA. The flask was sealed then removed from the glove box and placed in a photo reactor described for nickel coupling and allowed to stir at the temperature of the LEDs (55-60 °C) for 24 hours (Figure S5.2, B). After which the reaction was removed from the photoreactor, diluted with 25 mL of dichloromethane, washed twice with approximately 50 mL of water, then a 50/50 mixture of saturated brine solution/water, dried over MgSO₄ and concentrated under vacuum. The crude material was purified by column chromatography on silica gel using the noted solvent mixture to isolate the desired C-N coupled product.

General Procedure E for C-S Bond Formation



To an oven-dried 50 mL storage flask was added a stir bar, PC 4 (1.5 mg, 0.0024 mmol, 0.2% mol), 4,4'-di-tert-butyl-2,2'-dipyridyl (16.1 mg, 0.06 mmol, 5.0% mol), pyridine (193.7 μ L, 2.4 mmol, 2.0 eq.), aryl halide (1.20 mmol, 1.0 eq.), and thiol (1.80 mmol, 1.5 eq.). The reagents were then degassed with two freeze pump thaw cycles and backfilled with nitrogen before being brought into the glovebox where nickel(II) chloride 2-methoxyethyl ether complex (13.2 mg, 0.06 mmol, 5.0% mol) in 1 mL of a DMA stock solution was added, then an additional 2 mL of DMA. The flask was sealed then removed from the glovebox and placed in a photo reactor described for nickel coupling and allowed to stir at the temperature of the LEDs (55-60 $^{\circ}$ C) for 24 hours (Figure S5.2, B). After which the reaction was removed from light, diluted with 25 mL of dichloromethane then washed twice with \sim 50 mL of water, then a 50/50 mixture of saturated brine solution/water, dried over MgSO₄ and concentrated under vacuum. The crude material was then purified by column chromatography on silica gel using the noted solvent mixture to isolate the desired C-S coupled product.

General Procedure F for Sunlight-driven Reactions

Once all reagents were mixed followed the general procedure, instead of being placed in a 400 mL beaker with LEDs, the reaction vessel was put in a window-sill that received approximately 7 hours of sunlight a day (Figure S5.2, D). These reactions were allowed to react for 7 days after

which the workup described in the general procedures for LED driven reactions was followed exactly.

General Procedure G for Scale Up

To an oven-dried 100 mL storage flask was added a stir bar, and 8.34 times the amount specified reagents given for the nickel dual catalysis for both C-S and C-N coupling, or 10 times specified reagents for trifluoromethylation reaction (10mmol scale). These reactions were allowed to stir for 24 hours after which the workup described in the general procedures for LED driven reactions was scaled appropriately and followed.

3. Substrate Scope

Procedure of (Hetero)arenes and Olefins Preparation and Characterization

Boc Protection Substrates Preparation

Di-tert-butyl dicarbonate ((Boc)₂O) (3.9 g, 17.85 mmol) and 4-(dimethylamino) pyridine (DMAP), (0.25 g, 2.24 mmol) were added to the (hetero)arenes (14.9 mmol) in THF (20 mL) under argon. After the addition was completed, the mixture was stirred at room temperature for two hours. Evaporation of the solvent and subsequent column chromatography afforded product as a colorless liquid.

tert-Butyl 1H-pyrrole-1-carboxylate The general procedure was followed using pyrrole as the substrate. The purification was done by flash chromatography on silica gel, eluting with hexane: ethyl acetate = 40:1 (R_f = 0.43) to give the product tert-butyl 1H-pyrrole-1-carboxylate as a

colorless liquid, with 82% yield. ^1H NMR (300 MHz, CDCl_3) δ 7.24 (dd, $J = 2.7, 2.0$ Hz, 1H), 6.22 (dd, $J = 2.6, 2.1$ Hz, 2H), 1.60 (s, 9H). ^1H NMR data matched previously reported.⁵

tert-Butyl 1H-indole-1-carboxylate The general procedure was followed using indole as the substrate. The product tert-butyl 1H-indole-1-carboxylate was purified by flash chromatography on silica gel, eluting with hexane: ethyl acetate = 100:1 ($R_f = 0.13$) as a colorless liquid with 72% yield. ^1H NMR (300 MHz, CDCl_3): δ 8.15 (d, $J = 8.2$ Hz, 1H), 7.70 – 7.49 (m, 2H), 7.39 – 7.13 (m, 2H), 6.57 (dd, $J = 3.7, 0.8$ Hz, 1H), 1.68 (s, 9H). ^1H NMR data matched previously reported.⁶

tert-Butyl 3-methyl-1H-indole-1-carboxylate The general procedure was followed using 3-methyl indole as the substrate. The product tert-butyl 3-methyl-1H-indole-1-carboxylate was purified by flash chromatography on silica gel, eluting with hexane: ethyl acetate = 100:1 ($R_f = 0.13$) as a colorless liquid with 75% yield. ^1H NMR (300 MHz, CDCl_3) δ 8.11 (d, $J = 8.1$ Hz, 1H), 7.60 – 7.45 (m, 1H), 7.39 – 7.28 (m, 2H), 7.27 – 7.21 (m, 2H), 2.27 (d, $J = 1.3$ Hz, 3H), 1.66 (s, 9H). ^1H NMR data *matched* previously reported.⁶

Protecting Product Preparation

Undec-10-en-1-yl acetate Ac_2O (7.04 mmol, 0.664 mL) was added into the 10 mL DCM solution of 10-undecene-1-ol (5.87 mmol, 1.0 g), Et_3N (7.04 mmol, 0.98 mL) and DMAP (0.11 mmol, 14 mg) at 0 °C. The above mixture was stirred for 1 h at r.t.. After completion, the reaction was quenched with water (50 mL), and the mixture was extracted with hexanes (50 mL \times 3). The organic layer was separated, washed with water (50 mL \times 2), brine (50 mL) and dried over anhydrous Na_2SO_4 . Evaporation of the solvent under reduced pressure gave the crude product;

further purification using column chromatography gave the pure product with 86% yield. $R_f = 0.76$ (hexane: ethyl acetate 4:1). $^1\text{H NMR}$ (400 MHz, CDCl_3) δ 5.81 (ddt, $J = 16.8, 10.2, 6.6$ Hz, 1H), 5.07 – 4.83 (m, 2H), 4.05 (t, $J = 6.8$ Hz, 2H), 2.08 – 1.95 (m, 5H), 1.60 (dd, $J = 14.2, 7.2$ Hz, 2H), 1.43 – 1.17 (m, 12H). $^1\text{H NMR}$ data *matched* previously reported.⁷

((Undec-10-en-1-yloxy)methyl) benzene At 0 °C, NaH (60%) was added into the 10 mL THF solution of 10-undecene-1-ol (5.87 mmol, 1.0 g). To the above solution, BnBr (5.58 mmol, 0.66 mL) was added at 0 °C and the reaction was stirred at r.t. overnight. The reaction was quenched with water (50 mL), and the mixture was extracted with hexanes (50 mL \times 3). The organic layer was separated, washed with water (50 mL \times 2), brine (50 mL) and dried over anhydrous Na_2SO_4 . Evaporation of the solvent under reduced pressure gave the crude product; further purification using column chromatography gave the pure product with 70% yield. $R_f = 0.15$ (hexane: ethyl acetate 50:1). $^1\text{H NMR}$ (400 MHz, CDCl_3) δ 7.40 – 7.23 (m, 5H), 5.81 (ddt, $J = 16.9, 10.2, 6.7$ Hz, 1H), 5.05 – 4.87 (m, 2H), 4.50 (s, 2H), 3.46 (t, $J = 6.7$ Hz, 2H), 2.11 – 1.96 (m, 2H), 1.68 – 1.51 (m, 2H), 1.44 – 1.08 (m, 12H). $^1\text{H NMR}$ data *matched* previously reported.⁸

tert-Butyldimethyl(undec-10-en-1-yloxy)silane TBSCl (6.457 mmol, 0.973) was added into the 10 mL DCM solution of 10-undecene-1-ol (5.87 mmol, 1.0 g), Et_3N (7.04 mmol, 0.98 mL) and DMAP (0.11 mmol, 14 mg) at 0 °C. The above mixture was stirred for 1 h at r.t.. After completion, the reaction was quenched with water (50 mL), and the mixture was extracted with hexanes (3 \times 50 mL). The organic layer was separated, washed with water (2 \times 50 mL), brine (50 mL) and dried over anhydrous Na_2SO_4 . Evaporation of the solvent under reduced pressure gave the crude product; further purification using column chromatography gave the pure product with 92% yield.

$R_f = 0.29$ (hexane: DCM 12:1). $^1\text{H NMR}$ (400 MHz, CDCl_3) δ 5.97 – 5.58 (m, 1H), 5.11 – 4.80 (m, 2H), 3.59 (td, $J = 6.6, 0.8$ Hz, 2H), 2.04 (tdd, $J = 7.9, 6.0, 1.3$ Hz, 2H), 1.60 – 1.19 (m, 14H), 0.89 (d, $J = 0.8$ Hz, 9H), 0.04 (d, $J = 0.8$ Hz, 6H). $^1\text{H NMR}$ data *matched* previously reported.⁹

Radical Trifluoromethylation of (Hetero)Arenes

3-methyl-2-(trifluoromethyl)-1H-indole General procedure A was followed using 3-methyl indole as the substrate. Purification was done by chromatography on silica gel, eluting with hexanes: dichloromethane = 10 : 1 ($R_f = 0.12$) to give the product as a white solid with 65% yield. $^1\text{H NMR}$ (300 MHz, CD_3CN) δ 9.73 (s, 1H), 7.64 (dd, $J = 8.0, 1.0$ Hz, 1H), 7.46 (dt, $J = 8.3, 1.0$ Hz, 1H), 7.31 (ddd, $J = 8.2, 6.9, 1.2$ Hz, 1H), 7.16 (ddd, $J = 8.0, 7.0, 1.0$ Hz, 1H), 2.42 (q, $J = 1.9$ Hz, 3H). $^{13}\text{C NMR}$ (75 MHz, CDCl_3) δ 135.33, 127.61, 124.86, 122.78 (q, $J = 269$ Hz), 121.61 (q, $J = 36.81$ Hz), 120.48, 120.20, 114.16 (q, $J = 3.0$ Hz), 111.70, 8.40. $^{19}\text{F NMR}$ (282 MHz, CD_3CN) δ -58.42 (q, $J = 2.0$ Hz). $^1\text{H NMR}$, $^{13}\text{C NMR}$ and $^{19}\text{F NMR}$ data *matched* those previously reported.¹⁰

2-(trifluoromethyl)-1H-pyrrole The general procedure A was followed using pyrrole as the substrate. The 99% NMR yield in 6 h was determined by $^{19}\text{F NMR}$ spectroscopy using 1-fluoro-3-nitrobenzene as an internal standard. Purification was done by chromatography on silica gel, eluting with pentane: diethyl ether = 95:5 ($R_f = 0.25$) to give the product 2-(trifluoromethyl)-1H-pyrrole as a colorless liquid. $^1\text{H NMR}$ (400 MHz, CD_2Cl_2) δ 8.69 (t, $J = 52.0$ Hz, 1H), 6.93 (q, $J = 2.4$ Hz, 1H), 6.60 (dq, $J = 2.7, 1.3$ Hz, 1H), 6.25 (dp, $J = 2.7, 0.9$ Hz, 1H). $^{19}\text{F NMR}$ (376 MHz, CD_2Cl_2) δ -59.55 (s, 3F). HRMS (APCI): calculated for $\text{C}_5\text{H}_4\text{F}_3\text{N}$ ($[\text{M}+\text{Cl}]^+$) 169.9990, found 169.9992. $^1\text{H NMR}$ and $^{19}\text{F NMR}$ data *matched* those previously reported.¹¹

tert-Butyl 2-(trifluoromethyl)-1H-pyrrole-1-carboxylate General procedure A was followed using tert-butyl 1H-pyrrole-1-carboxylate as the substrate. Purification was done by chromatography on silica gel, eluting with hexanes: ethyl acetate = 40:1 (R_f = 0.36) to give the product as a colorless liquid with 82% yield. ^1H NMR (400 MHz, CDCl_3) δ 7.44 (dd, J = 3.3, 1.9 Hz, 1H), 6.73 (ddd, J = 3.7, 1.9, 0.7 Hz, 1H), 6.25 – 6.16 (m, 1H), 1.61 (s, 9H). ^{19}F NMR (376 MHz, CDCl_3) δ -58.33 (s, 3F). ^1H NMR and ^{19}F NMR data matched those previously reported.¹²

2-(trifluoromethyl)-1H-indole General procedure A was followed using indole as the substrate. Purification was done by flash chromatography on silica gel, eluting with hexanes: dichloromethane = 10:1 (R_f = 0.10) to give the sole product 2-(trifluoromethyl)-1H-indole as a white solid with 45% yield. ^1H NMR (300 MHz, CDCl_3) δ 8.40 (s, 1H), 7.69 (dt, J = 8.0, 1.0 Hz, 1H), 7.44 (dq, J = 8.3, 1.0 Hz, 1H), 7.34 (ddd, J = 8.2, 7.0, 1.2 Hz, 1H), 7.20 (ddd, J = 8.0, 7.0, 1.1 Hz, 1H), 6.94 (dp, J = 2.4, 1.3 Hz, 1H), ^{13}C NMR (101 MHz, CDCl_3) δ 136.04, 126.55, 125.7 (q, J = 38.9 Hz), 124.78, 122.08, 121.23 (q, J = 265 Hz), 121.13, 111.68, 104.27 (q, J = 3.4 Hz). ^{19}F NMR (376 MHz, CDCl_3) δ -60.55 (d, J = 1.3 Hz, 3F). ^1H NMR, ^{13}C NMR and ^{19}F NMR data matched those previously reported.¹³

tert-Butyl 2-(trifluoromethyl)-1H-indole-1-carboxylate General procedure A was followed using tert-butyl 1H-indole-1-carboxylate as the substrate. Purification was done by chromatography on silica gel, eluting with hexane: diethyl ether = 100:1 (R_f = 0.18) to give the product tert-butyl 2-(trifluoromethyl)-1H-indole-1-carboxylate as a colorless liquid with 53% yield. ^1H NMR (300 MHz, CDCl_3) δ 8.28 (dq, J = 8.5, 0.8 Hz, 1H), 7.66 – 7.59 (m, 1H), 7.45 (ddd,

$J = 8.6, 7.2, 1.3$ Hz, 1H), 7.30 (ddd, $J = 7.8, 7.2, 1.0$ Hz, 1H), 7.14 (t, $J = 0.7$ Hz, 1H), 1.67 (s, 9H). ^{19}F NMR (282 MHz, Chloroform- d) δ -58.16(s, 3F). ^1H NMR and ^{19}F NMR data matched those previously reported.¹⁵ HRMS (ESI): calculated for $\text{C}_{14}\text{H}_{14}\text{F}_3\text{NO}_2([\text{M}+\text{Li}]^+)$ 292.1137, found 292.1151.

tert-Butyl 3-methyl-2-(trifluoromethyl)-1H-indole-1-carboxylate General procedure A was followed using tert-butyl 3-methyl-1H-indole-1-carboxylate as the substrate. Purification was done by chromatography on silica gel, eluting with hexane: diethyl ether = 100:1 ($R_f = 0.20$) to give the product tert-butyl 3-methyl-2-(trifluoromethyl)-1H-indole-1-carboxylate as a colorless liquid with 66% yield. ^1H NMR (300 MHz, CDCl_3) δ 8.19 (dt, $J = 8.5, 0.9$ Hz, 1H), 7.60 (dt, $J = 7.9, 1.0$ Hz, 1H), 7.45 (ddd, $J = 8.5, 7.2, 1.3$ Hz, 1H), 7.31 (ddd, $J = 8.0, 7.2, 1.0$ Hz, 1H), 2.45 (q, $J = 3.0$ Hz, 3H), 1.66 (s, 9H). ^{19}F NMR (282 MHz, CDCl_3) δ -54.12 (q, $J = 3.0$ Hz, 3F). HRMS (ESI): calculated for $\text{C}_{15}\text{H}_{16}\text{F}_3\text{NO}_2([\text{M}+\text{Li}]^+)$ 306.1294, found 306.1295. ^1H NMR and ^{19}F NMR data matched those previously reported.¹⁶

1,3,5-trimethyl-2-(trifluoromethyl)benzene General procedure A was followed using 1,3,5-trimethyl benzene as the substrate. Purification was done by chromatography on silica gel, eluting with pure pentane ($R_f = 0.62$) to give the product 1,3,5-trimethyl-2-(trifluoromethyl) benzene as a colorless liquid with 54% yield. ^1H NMR (400 MHz, CDCl_3) δ 6.91 (s, 2H), 2.45 (q, $J = 3.4$ Hz, 6H), 2.30 (s, 3H). ^{19}F NMR (376 MHz, CDCl_3) δ -53.73 (t, $J = 3.7$ Hz, 3F). HRMS (ESI): calculated for $\text{C}_{10}\text{H}_{11}\text{F}_3\text{O}([\text{M} + \text{Li}]^+)$ 195.0967, found 195.0965. ^1H NMR and ^{19}F NMR data matched those previously reported.¹⁷

1,3,5-trimethoxy-2-(trifluoromethyl)benzene General procedure A was followed using 1, 3, 5-trimethoxy benzene as the substrate. Purification was done by chromatography on silica gel, eluting with hexane: ethyl acetate = 40: 1 (R_f = 0.20) to give the product 1,3,5-trimethoxy-2-(trifluoromethyl)benzene as a white solid with 58% yield. ^1H NMR (300 MHz, Chloroform- d) δ 6.12 (d, J = 0.7 Hz, 2H), 3.82 (d, J = 1.2 Hz, 9H). ^{19}F NMR (282 MHz, CD_2Cl_2) δ -54.04 (s, 3F). HRMS (ESI): calculated for $\text{C}_{10}\text{H}_{11}\text{F}_3\text{O}_3$ ($[\text{M}+\text{Li}]^+$) 243.0821, found 243.0823. ^1H NMR and ^{19}F NMR data matched those previously reported.¹⁷

1,2,3-trimethoxy-5-methyl-4-(trifluoromethyl)benzene General procedure A was followed using 1,2,3-trimethoxy-5-methyl benzene as the substrate. Purification was done by chromatography on silica gel, eluting with hexane: diethyl ether =100: 1 (R_f = 0.07) to give the product 1,2,3-trimethoxy-5-methyl-4-(trifluoromethyl)benzene as a colorless liquid with 33% yield. ^1H NMR (300 MHz, CDCl_3) δ 6.49 (s, 1H), 3.91 (s, 3H), 3.88 (s, 3H), 3.84(s, 3H), 2.42 (qd, J = 3.5, 0.7 Hz, 3H). ^{19}F NMR (282 MHz, CDCl_3) δ -54.29 (q, J = 3.5 Hz, 3F). HRMS (ESI): calculated for $\text{C}_{11}\text{H}_{13}\text{F}_3\text{O}_3$ ($[\text{M}+\text{Li}]^+$) 257.0977, found 257.0981. ^1H NMR and ^{19}F NMR data matched those previously reported.¹⁸

2,6-di-tert-butyl-4-(trifluoromethyl)phenol General procedure A was followed using 2, 6-di-tert-butyl phenol as the substrate. Purification was done by chromatography on silica gel, eluting with hexane: diethyl ether = 200:1 (R_f = 0.54) to give the product 2,6-di-tert-butyl-4-(trifluoromethyl)phenol as a colorless liquid with 23% yield. ^1H NMR (300 MHz, CDCl_3) δ 7.43 (d, J = 0.8 Hz, 2H), 5.57 (s, 1H), 1.47 (s, 20H). ^{19}F NMR (282 MHz, CDCl_3) δ -61.15 (s, 3F).

HRMS (ESI): calculated for C₁₅H₂₁F₃O ([M+H]⁺) 275.1618, found 275.1608. ¹H NMR and ¹⁹F NMR data matched those previously reported.¹⁸

3-methyl-2-(perfluoroethyl)-1H-indole General procedure A was followed using 3-methyl indole as the substrate, and the CF₃CF₂I instead of CF₃I. Purification was done by chromatography on silica gel, eluting with hexane: CH₂Cl₂ = 9:1 (*R_f* = 0.20) to give the product 3-methyl-2-(perfluoroethyl)-1H-indole as a white solid with 70% yield. ¹H NMR (400 MHz, CDCl₃) δ 8.15 (s, 1H), 7.71 (d, *J* = 8.0 Hz, 1H), 7.40 (qd, *J* = 8.3, 1.5 Hz, 2H), 7.26 (ddd, *J* = 8.0, 6.4, 1.7 Hz, 1H), 2.49 (t, *J* = 2.3 Hz, 3H). ¹³C NMR (101 MHz, CDCl₃) δ 135.78, 128.33, 124.82, 120.35, 119.99, 119.25(qt, *J* = 40.3, 284.2 Hz), 119.24 (t, *J* = 28.2 Hz), 116.14 (t, *J* = 3.3 Hz), 112.06 (tq, *J* = 40.3, 284.2 Hz), 111.49, 8.41. ¹⁹F NMR (376 MHz, CDCl₃) δ -84.77 – -84.84 (t, *J* = 3.5 Hz, 3F), -112.86 (p, *J* = 2.9 Hz, 2F). HRMS (APCI): calculated for C₁₁H₇F₅N ([M-H]⁻) 248.0504, found 248.0500.

Radical Trifluoromethylation of Olefins

(*E*)-1,1,1-trifluoronon-2-ene The general procedure B was followed using 1-octene as the substrate. The 98% NMR yield was determined by ¹⁹F NMR spectroscopy using 1-fluoro-3-nitrobenzene as an internal standard. Purification was done by chromatography on silica gel, eluting with pure pentane to give the product 1,1,1-trifluoronon-2-ene as a colorless liquid (*E* : *Z* : β-hydride elimination product = 11 : 1 : 1). ¹H NMR (400 MHz, CDCl₃) δ 6.37 (dddt, *J* = 13.7, 6.8, 4.6, 2.2 Hz, 1H), 5.60 (dqt, *J* = 16.1, 6.5, 1.7 Hz, 1H), 2.15 (dddd, *J* = 12.1, 7.0, 2.5, 1.8 Hz, 2H), 1.43 (dtd, *J* = 8.3, 7.0, 6.5, 3.5 Hz, 2H), 1.36 – 1.23 (m, 6H), 0.95 – 0.83 (m, 3H). ¹³C NMR (101 MHz, CDCl₃) δ 140.83 (q, *J* = 6.6 Hz), 123.13 (q, *J* = 269.2 Hz), 118.22 (q, *J* = 33.1 Hz), 31.55,

31.45, 28.69, 27.91, 22.53, 14.04. ^{19}F NMR (376 MHz, CDCl_3) δ -63.49 (m, 3F). ^1H NMR, ^{13}C NMR and ^{19}F NMR data matched those previously reported.¹⁹

(E)-1,1,1-trifluorotridec-2-ene General procedure B was followed using 1-dodecene as the substrate. Purification was done by chromatography on silica gel, eluting with pure hexane (R_f = 0.82) to give 1,1,1-trifluorotridec-2-ene as a colorless liquid with 85% yield ($E : Z : \beta$ -hydride elimination product = 11 : 1 : 1). ^1H NMR (400 MHz, CDCl_3) δ 6.37 (dtd, J = 15.9, 6.8, 2.4 Hz, 1H), 5.60 (m, 1H), 2.22 – 1.92 (m, 2H), 1.50 – 1.04 (m, 16H), 0.88 (t, J = 6.6 Hz, 3H). ^{13}C NMR (101 MHz, CDCl_3) δ 141.00 (q, J = 6.5 Hz), 123.28 (q, J = 269.0 Hz), 118.37 (q, J = 33.1 Hz), 32.05, 31.61, 29.73, 29.67, 29.51, 29.47, 29.19, 28.10, 22.84, 14.28. ^{19}F NMR (376 MHz, CDCl_3) δ -64.07 (m, 3F). ^1H NMR, ^{13}C NMR and ^{19}F NMR data matched those previously reported.²⁰

(E)-(5,5,5-trifluoropent-3-en-1-yl)benzene General procedure B was followed using 4-phenyl-1-butene as the substrate. Purification was done by chromatography on silica gel, eluting with pure hexane (R_f = 0.60) to give the product 5,5,5-trifluoropent-3-en-1-ylbenzene as a colorless liquid with 77% yield ($E : Z : \beta$ -hydride elimination product = 20 : 1.8 : 1). ^1H NMR (300 MHz, CDCl_3) δ 7.50 – 6.96 (m, 6H), 6.42 (dtq, J = 15.7, 6.6, 2.1 Hz, 1H), 5.63 (dqt, J = 15.9, 6.4, 1.6 Hz, 1H), 2.76 (dd, J = 8.9, 6.7 Hz, 2H), 2.56 – 2.39 (m, 2H). ^{19}F NMR (282 MHz, CDCl_3) δ -64.05 (m, 3F). HRMS (ESI): calculated for $\text{C}_{11}\text{H}_{11}\text{F}_3$ ($[\text{M}+\text{Li}]^+$) 207.0973, found 207.0974. ^1H NMR and ^{19}F NMR data matched those previously reported.²¹

(E)-12-bromo-1,1,1-trifluorododec-2-ene General procedure B was followed using bromo-1-undecene as the substrate. Purification was done by chromatography on silica gel, eluting with pure hexane (R_f = 0.63) to give the product 12-bromo-1,1,1-trifluorododec-2-ene as a colorless

liquid with 53% yield (*E* : *Z* : β -hydride elimination product = 33 : 2.7 : 1). ^1H NMR (300 MHz, CDCl_3) δ 6.37 (dddt, $J = 13.7, 6.9, 4.6, 2.2$ Hz, 1H), 5.69 – 5.50 (m, 1H), 3.41 (t, $J = 6.8$ Hz, 2H), 2.14 (dtd, $J = 11.5, 4.6, 2.2$ Hz, 2H), 1.95 – 1.76 (m, 2H), 1.43-1.30 (s, 12H). ^{13}C NMR (75 MHz, CDCl_3) δ 140.91 (q, $J = 6.4$ Hz), 123.27 (q, $J = 269.1$ Hz), 118.47 (q, $J = 33.1$ Hz), 45.31, 34.16, 33.67, 32.95, 31.58, 29.41, 29.12, 28.86, 28.28. ^{19}F NMR (282 MHz, CDCl_3) δ -61.43 – -65.88 (m, 3F), HRMS (TOF): calculated for $\text{C}_{12}\text{H}_{20}\text{BrF}_3$ ($[\text{M} + \text{Cl}]^-$) 335.0394, found 335.0410.

(*E*)-12-bromo-1, 1, 1-trifluorododec-2-ene General procedure B was followed using 10-undecene-1-ol as the substrate. Purification was done by chromatography on silica gel, eluting with hexane: ethyl acetate = 4 : 1 ($R_f = 0.32$) to give the product 12-bromo-1,1,1-trifluorododec-2-ene as a colorless product with 80% yield (*E* : *Z* : β -hydride elimination product 17 : 2 : 1). ^1H NMR (300 MHz, CDCl_3) δ 6.35 (dtq, $J = 15.8, 6.8, 2.2$ Hz, 1H), 5.58 (dqt, $J = 15.9, 6.2, 1.6$ Hz, 1H), 3.60 (t, $J = 6.6$ Hz, 2H), 2.20 – 2.03 (m, 2H), 1.92 (s, 1H), 1.65 – 1.47 (m, 2H), 1.45 – 1.11 (m, 12H). ^{13}C NMR (75 MHz, CDCl_3) δ 140.74 (q, $J = 6.5$ Hz), 123.09 (q, $J = 269.02$ Hz), 118.23 (q, $J = 33.2$ Hz), 62.84, 32.68, 31.36, 29.39, 29.32, 29.22, 28.93, 27.89, 27.88. ^{19}F NMR (282 MHz, CDCl_3) δ -63.95 (m, 3F). HRMS (ESI): calculated for $\text{C}_{12}\text{H}_{21}\text{F}_3\text{O}$ ($[\text{M} + \text{Li}]^+$) 244.1696, found 244.1688.

This reaction was also conducted using 10-undecene-1-ol (2 ml, 10 mmol), CF_3I (0.6 M in DMA, 20 mL) HCOOK (15 mmol, 1.264 g) in 50 mL storage flask. The reaction was allowed to stir for 24 hours, after which was washed with 100 mL of water and extracted by ethyl acetate 3 times before being washed with brine, dried over MgSO_4 and concentrated under vacuum. Purification was done by chromatography on silica gel, eluting with above noted solvents to give the product

12-bromo-1,1,1-trifluorododec-2-ene as a colorless product with 73% yield (1.74 g). This reaction was also conducted using cat.3 with 0.25% catalyst loading; the yield reached 69% after 24 h.

(E)-12,12,12-trifluorododec-10-en-1-yl acetate General procedure B was followed using undec-10-en-1-yl acetate as the substrate. Purification was done by chromatography on silica gel, eluting with hexane: ethyl acetate =10:1 (R_f =0.52) to give the product 12,12,12-trifluorododec-10-en-1-yl acetate as a colorless liquid with 88% yield ($E : Z : \beta$ -hydride elimination product = 50 : 6.5 : 1). ^1H NMR (300 MHz, CDCl_3) δ 6.37 (dtq, $J = 15.9, 6.8, 2.2$ Hz, 1H), 5.74 – 5.44 (m, 1H), 4.05 (t, $J = 6.8$ Hz, 2H), 2.14 (ddt, $J = 7.7, 4.0, 2.5$ Hz, 2H), 2.04 (s, 3H), 1.57 (s, 3H), 1.50 – 1.20 (m, 11H). ^{13}C NMR (101 MHz, CDCl_3) δ 171.15, 140.78 (q, $J = 6.5$ Hz), 123.16 (q, $J = 268.9$ Hz), 118.32 (q, $J = 33.1$ Hz), 64.58, 31.46, 29.40, 29.29, 29.23, 29.02, 28.62, 27.96, 25.92, 20.90. ^{19}F NMR (282 MHz, CDCl_3) δ -63.92 (m, 3F). HRMS (ESI) calculated for $\text{C}_{14}\text{H}_{23}\text{F}_3\text{O}_2$ ($[\text{M}+\text{Li}]^+$) 287.1811, found 287.1811.

(E)-(((12,12,12-trifluorododec-10-en-1-yl)oxy)methyl)benzene General procedure B was followed using ((undec-10-en-1-yloxy) methyl) benzene as the substrate. Purification was done by chromatography on silica gel, eluting with hexane: ethyl acetate = 50: 1 ($R_f = 0.14$) to give the product ((12, 12, 12-trifluorododec-10-en-1-yl) oxy) methyl benzene as a colorless liquid with 75% yield ($E : Z : \beta$ -hydride elimination product = 100 : 7 : 1). ^1H NMR (400 MHz, CDCl_3) δ 7.41 – 7.26 (m, 5H), 6.39 (dddt, $J = 13.7, 6.8, 4.6, 2.2$ Hz, 1H), 5.62 (dqt, $J = 16.1, 6.5, 1.7$ Hz, 1H), 4.52 (s, 2H), 3.49 (t, $J = 6.6$ Hz, 2H), 2.22 – 1.99 (m, 2H), 1.75 – 1.56 (m, 2H), 1.52 – 1.18 (m, 12H). ^{13}C NMR (75 MHz, CDCl_3) δ 140.95 (q, $J = 6.5$ Hz), 138.86, 128.47, 127.74, 127.59, 123.28 (q, $J = 268.9$ Hz), 118.42 (q, $J = 33.1$ Hz), 73.00, 70.63, 31.57, 29.91, 29.56(2C), 29.42,

29.13, 28.08 (q, $J = 1.2$ Hz), 26.32. ^{19}F NMR (376 MHz, CDCl_3) δ -63.88 (m, 3F). HRMS (ESI): calculated for $\text{C}_{19}\text{H}_{27}\text{F}_3\text{O}$ ($[\text{M}+\text{Li}]^+$) 335.2174, found 335.2175.

(E)-tert-butyldimethyl((12,12,12-trifluorododec-10-en-1-yl)oxy)silane General procedure B was followed using tert-butyldimethyl(undec-10-en-1-yloxy)silane as the substrate. Purification was done by chromatography on silica gel, eluting with hexane: DCM 12:1 ($R_f = 0.28$) to give the product as a colorless liquid with 70% yield ($E : Z : \beta$ -hydride elimination product = 100 : 7 : 1). ^1H NMR (300 MHz, CDCl_3) δ 6.37 (dddt, $J = 13.7, 6.8, 4.5, 2.2$ Hz, 1H), 5.69 – 5.51 (m, 1H), 3.60 (t, $J = 6.6$ Hz, 2H), 2.14 (ddp, $J = 9.1, 6.8, 2.1$ Hz, 2H), 1.62 – 1.16 (m, 14H), 0.89 (s, 9H), 0.05 (s, 6H). ^{19}F NMR (282 MHz, CDCl_3) δ -63.90 (dq, $J = 6.8, 2.4$ Hz). ^{13}C NMR (101 MHz, CDCl_3) δ 140.90 (q, $J = 6.5$ Hz), 123.29 (q, $J = 269.0$ Hz), 118.48 (q, $J = 33.2$ Hz), 63.42, 33.05, 31.62, 29.67, 29.57, 29.48, 29.20, 28.14, 26.12(3C), 25.97, 18.53, -5.15(2C). ^{19}F NMR (282 MHz, CDCl_3) δ -63.90 (m, 3F). HRMS (ESI): calculated for $\text{C}_{18}\text{H}_{35}\text{F}_3\text{OSi}$ ($[\text{M}+\text{Li}]^+$) 359.2570, found 359.2569.

(E)-12,12,13,13,13-pentafluorotridec-10-en-1-ol General procedure B was followed using 10-undecene-1-ol as the substrate, and the $\text{CF}_3\text{CF}_2\text{I}$ instead of CF_3I . Purification was done by chromatography on silica gel, eluting with hexane: ethylacetate = 5:1 ($R_f = 0.20$) to give the product 12,12,13,13,13-pentafluorotridec-10-en-1-ol as a white solid with 89% yield ($E : Z = 7.36 : 1$). ^1H NMR (400 MHz, CDCl_3) δ 6.59 – 6.20 (m, 1H), 5.54 (td, $J = 16.0, 11.8$ Hz, 1H), 3.59 (dt, $J = 11.6, 6.5$ Hz, 2H), 2.23 – 2.07 (m, 2H), 1.65 – 1.10 (m, 14H). ^{13}C NMR (101 MHz, CDCl_3) δ 143.08 (t, $J = 8.6$ Hz), 118.96 (qt, $J = 285.2, 38.5$ Hz), 116.41 (t, $J = 23.0$ Hz), 112.12 (tq, $J = 285.2, 38.2$ Hz), 62.72, 32.65, 31.89, 29.40, 29.33, 29.21, 28.88, 28.87, 25.68. ^{19}F NMR (376 MHz, CDCl_3) δ

-85.51 (d, $J = 4.7$ Hz, 3F), -115.13 (dd, $J = 10.6, 3.4$ Hz, 2H). HRMS (APCI): calculated for $C_{13}H_{21}F_5O$ ($[M+Cl]^-$) 323.1207, found 323.1204.

Cross-Addition Reaction of Olefins

1,1,1-trifluoro-3-iodoheptane General procedure C was followed using 1-hexene as the substrate. Purification was done by chromatography on silica gel, eluting with pentane ($R_f = 0.65$) to give the product 1,1,1-trifluoro-3-iodoheptane as a colorless liquid with 45% yield. 1H NMR (400 MHz, $CDCl_3$) δ 4.32 – 4.10 (m, 1H), 3.00 – 2.68 (m, 2H), 1.76 (dtt, $J = 14.5, 9.7, 4.9$ Hz, 2H), 1.58 – 1.19 (m, 4H), 0.93 (t, $J = 7.2$ Hz, 3H). ^{13}C NMR (75 MHz, $CDCl_3$) δ 125.61 (q, $J = 278.7$ Hz), 44.94 (q, $J = 28.1$ Hz), 39.41, 31.52, 21.75 (q, $J = 2.9$ Hz), 21.66, 13.85. ^{19}F NMR (282 MHz, $CDCl_3$) δ -63.98 (t, $J = 10.3$ Hz, 3F). 1H NMR, ^{13}C NMR and ^{19}F NMR data matched those previously reported.²²

1,1,1-trifluoro-3-iodononane General procedure C was followed using 1-octene as the substrate. Purification was done by chromatography on silica gel, eluting with pentane ($R_f = 0.64$) to the product 1,1,1-trifluoro-3-iodononane as a colorless liquid with 48 % yield. 1H NMR (400 MHz, $CDCl_3$) δ 4.19 (d, $J = 5.4$ Hz, 1H), 2.99 – 2.67 (m, 2H), 1.91 – 1.64 (m, 3H), 1.30 (dt, $J = 10.3, 3.3$ Hz, 8H), 0.89 (t, $J = 7.2$ Hz, 3H). ^{13}C NMR (101 MHz, $CDCl_3$) δ 125.59 (q, $J = 278.7$ Hz), 44.90 (q, $J = 28.3$ Hz), 39.67, 31.56, 29.39, 28.19, 22.55, 21.93 (q, $J = 2.7$ Hz), 14.03. ^{19}F NMR (376 MHz, $CDCl_3$) δ -63.99 (t, $J = 10.3$ Hz, 3F). HRMS (APCI): calculated for $C_9H_{16}F_3I$ ($[M+ Cl]^-$) 324.9943, found 324.9941.

1,1,1-trifluoro-3-iodotridecane General procedure C was followed using 1-dodecene as the substrate. Purification was done by chromatography on silica gel, eluting with hexane ($R_f = 0.63$) to give the product 1, 1, 1-trifluoro-3-iodotridecane as a colorless liquid with 42% yield. $^1\text{H NMR}$ (500 MHz, CDCl_3) δ 4.19 (ddd, $J = 13.6, 8.3, 4.2$ Hz, 1H), 2.90 (dt, $J = 16.7, 10.6, 5.3$ Hz, 1H), 2.78 (dq, $J = 15.5, 10.0, 7.6$ Hz, 1H), 1.76 (dq, $J = 28.1, 9.7, 4.7$ Hz, 2H), 1.59 – 1.07 (m, 16H), 0.88 (t, $J = 6.8$ Hz, 3H). $^{13}\text{C NMR}$ (101 MHz, CDCl_3) δ 125.75 (q, $J = 278.7$ Hz), 45.06 (q, $J = 28.2$ Hz), 39.83, 32.05, 29.71, 29.69, 29.58, 29.53, 29.47, 22.84, 22.08, 22.06, 14.28. $^{19}\text{F NMR}$ (376 MHz, CDCl_3) δ -64.01 (t, $J = 10.3$ Hz, 3F). $^1\text{H NMR}$, $^{13}\text{C NMR}$ and $^{19}\text{F NMR}$ data matched those previously reported.²¹

(5, 5, 5-trifluoro-3-iodopentyl)benzene General procedure C was followed using 4-phenyl-1-butene as the substrate. Purification was done by chromatography on silica gel, eluting with pure hexane ($R_f = 0.41$) to give the product (5, 5, 5-trifluoro-3-iodopentyl) benzene as a colorless liquid with 43% yield. $^1\text{H NMR}$ (300 MHz, CDCl_3) δ 7.66 – 7.08 (m, 5H), 4.17 (t, $J = 6.8$ Hz, 1H), 3.15 – 2.61 (m, 4H), 2.13 (dt, $J = 8.3, 6.0$ Hz, 2H). $^{13}\text{C NMR}$ (101 MHz, CDCl_3) δ 140.06, 128.75, 128.63, 125.65 (q, $J = 278.1$ Hz), 126.52, 45.07 (q, $J = 28.3$ Hz), 41.28, 35.66, 21.15, 21.14 (q, $J = 2.64$ Hz). $^{19}\text{F NMR}$ (282 MHz, CDCl_3) δ -63.73 (t, $J = 10.3$ Hz, 3F). $^1\text{H NMR}$, $^{13}\text{C NMR}$ and $^{19}\text{F NMR}$ data matched those previously reported.²³

Tert-butyldimethyl((12,12,12-trifluoro-10-iodododecyl)oxy)silane General procedure C was followed using tert-butyldimethyl(undec-10-en-1-yloxy)silane. Purification was done by chromatography on silica gel, eluting with hexane: DCM = 30: 1 ($R_f = 0.15$) to give the product tert-butyldimethyl((12,12,12-trifluoro-10-iodododecyl) -oxy)silane as a colorless liquid with 69%

yield. ^1H NMR (300 MHz, CDCl_3) δ 4.36 – 4.11 (m, 1H), 3.60 (t, J = 6.6 Hz, 2H), 3.07 – 2.59 (m, 2H), 1.95 – 1.65 (m, 2H), 1.42 (d, J = 73.6 Hz, 14H), 0.90 (s, 9H), 0.05 (s, 6H). ^{19}F NMR (282 MHz, CDCl_3) δ -63.96 (t, J = 10.3 Hz, 3F). ^{13}C NMR (75 MHz, CDCl_3) δ 125.60 (q, J = 278.7 Hz), 63.28, 44.95 (q, J = 28.2 Hz), 39.71, 32.87, 29.48, 29.41, 29.36, 29.30, 28.50, 25.99, 25.77, 21.80 (q, J = 2.9 Hz), 18.37, -5.26. HRMS (ESI): calculated for $\text{C}_{18}\text{H}_{36}\text{F}_3\text{IOSi}$ ($[\text{M} + \text{H}]^+$) 481.1605, found 481.1611.

12,12,12-trifluoro-10-iodododecyl acetate General procedure C was followed using undec-10-en-1-yl acetate. Purification was done by chromatography on silica gel, eluting with hexane: ethyl acetate = 10: 1 (R_f = 0.48) to give the product 12,12,12-trifluoro-10-iodododecyl acetate as a colorless liquid with 50% yield. ^1H NMR (300 MHz, CDCl_3) δ 4.19 (tdd, J = 8.1, 6.2, 4.6 Hz, 1H), 4.05 (t, J = 6.7 Hz, 2H), 3.03 – 2.68 (m, 2H), 2.04 (s, 3H), 1.85 – 1.46 (m, 4H), 1.44 – 1.16 (m, 14H). ^{13}C NMR (75 MHz, CDCl_3) δ 171.16, 125.58 (q, J = 278.7 Hz), 64.57, 44.90 (q, J = 28.2 Hz), 39.64, 29.36, 29.33, 29.23, 29.14, 28.57, 28.44, 25.85, 21.77 (q, J = 3.0 Hz), 20.98. ^{19}F NMR (282 MHz, CDCl_3) δ -63.98 (t, J = 10.3 Hz, 3F). HRMS (ESI): calculated for $\text{C}_{14}\text{H}_{24}\text{F}_3\text{IO}_2$ ($[\text{M} + \text{Li}]^+$) 415.0928, found 415.0934.

C-N Bond Formation Substrate Scope

1-(4-(trifluoromethyl)phenyl)pyrrolidine General procedure D was followed using 4-bromobenzotrifluoride as the aryl halide, and pyrrolidine as the amine. The reaction was run at room temperature instead of 60 °C. Purification was done by flash chromatography on silica gel, eluting with a gradient of 0-3% diethyl ether/hexanes to give the product as a white solid (207 mg, 80%). ^1H NMR (400 MHz, CDCl_3) δ 7.44 (d, J = 8.5, 2H), 6.55 (d, J = 8.6, 2H), 3.32 (m, 4H),

2.04 (m, 4H). ^{13}C NMR (101 MHz, CDCl_3) δ 149.9, 126.5 (d, $J_{\text{C-F}} = 3.8$ Hz), 116.7 (q, $J_{\text{C-F}} = 32.5$ Hz), 110.9, 47.6, 25.6. ^{19}F NMR (376 MHz, CDCl_3) δ -60.6 (s, 3F). HRMS (ESI): calculated for $\text{C}_{11}\text{H}_{12}\text{F}_3\text{N}$ ($[\text{M}+\text{H}]^+$) 216.0922, found 216.0995. ^1H NMR, ^{13}C NMR and ^{19}F NMR data matched those previously reported.²⁴

***N*-phenyl-4-(trifluoromethyl)aniline** General procedure D was followed with slight modification: 4-bromobenzotrifluoride was used as the aryl halide and aniline as the amine. Dry pyrrolidine (10.1 μL , 0.12 mmol, 0.1 eq.) was added to act as a ligand. $\text{Ni}(\text{II})\text{Br}_2 \cdot \text{glyme}$ (3.7 mg, 0.012 mmol, 1.0% mol) was decreased by 80%. Purification was done by flash chromatography on silica gel, eluting with a gradient of 0-10% diethyl ether/hexanes to give the product as an off-white solid (212 mg, 75%). ^1H NMR (400 MHz, CDCl_3) δ = 7.48 (d, $J = 8.5$ Hz, 2H), 7.34 (dd, $J = 8.4, 7.3$ Hz, 2H), 7.16 (d, $J = 7.3$ Hz, 2H), 7.06 (m, 3H), 5.92 (s, 1H). ^{13}C NMR (101 MHz, CDCl_3) δ = 146.9, 141.2, 129.7, 126.8, 124.7 (q, $J = 270.7$ Hz) 123.1, 121.8 (q, $J = 32.7$ Hz) 120.1, 115.4. ^{19}F NMR (376 MHz, CDCl_3) δ = -61.5 (s, 3F). HRMS (ESI): calculated for $\text{C}_{13}\text{H}_{10}\text{F}_3\text{N}$ ($[\text{M}+\text{H}]^+$) 238.0765, found 238.0839. ^1H NMR, ^{13}C NMR and ^{19}F NMR data matched those previously reported.²⁴

4-(4-(trifluoromethyl)phenyl)morpholine General procedure D was followed using 4-bromobenzotrifluoride as the aryl halide and morpholine as the amine. The reaction was run at room temperature instead of 60 $^\circ\text{C}$. Purification was done by flash chromatography on silica gel, eluting with a gradient of 0-20% diethyl ether/hexanes to give the product as a white crystalline solid (223 mg, 81%, [230 mg, 83% yield using general procedure F]). ^1H NMR (400 MHz, CDCl_3) δ 7.50 (d, $J = 8.4$ Hz, 2H), 6.92 (d, $J = 8.6$ Hz, 2H), 3.87 (m, 4H), 3.24 (m, 4H). ^{13}C NMR (101

MHz, CDCl₃) δ 153.5, 126.6 (q, $J = 3.8$ Hz), 124.8 (q, $J = 270.4$ Hz), 121.2 (q, $J = 32.7$ Hz), 114.4, 66.8, 48.3. ¹⁹F NMR (376 MHz, CDCl₃) δ -61.4 (s, 3F). HRMS (ESI): Calculated for C₁₁H₁₃F₃NO ([M+H]⁺) 232.0871, found 232.0944. ¹H NMR, ¹³C NMR and ¹⁹F NMR data matched those previously reported.²⁴

This reaction was also conducted using 4-bromobenzotrifluoride (10 mmol), as the aryl halide and morpholine as the amine. The reaction was run at room temperature for 24 hours. Purification was done by flash chromatography on silica gel, eluting with a gradient of 0-20% diethyl ether/hexanes to give the product as a white crystalline solid (1.216 g, 53%).

1-(4-methoxyphenyl)pyrrolidine General procedure D was followed using 4-bromoanisole as the aryl halide and dry pyrrolidine as the amine. Purification was done by flash chromatography on silica gel, eluting with a gradient of 0-5% diethyl ether/pentane to give the product as an off-white solid (204 mg, 96%). ¹H NMR (400 MHz, CDCl₃) δ = 6.85 (d, $J = 9.0$ Hz, 2H), 6.54 (d, $J = 9.0$ Hz, 2H), 3.76 (s, 3H), 3.24 (m, 4H), 1.99 (m, 4H). ¹³C NMR (101 MHz, CDCl₃) δ = 150.8, 143.3, 115.1, 112.7, 56.1, 48.4, 25.5. HRMS (ESI): Calculated for C₁₁H₁₅NO ([M+H]⁺) 178.1154, found 178.1227. ¹H NMR, ¹³C NMR and ¹⁹F NMR data matched those previously reported.²⁵

1-(2-naphthalenyl)pyrrolidine General procedure D was followed using 2-bromonaphthalene as the aryl halide and pyrrolidine as the amine. Purification was done by flash chromatography on silica gel, eluting with a gradient of 0-10% diethyl ether/pentane to give the product as an off-white solid (202 mg, 85% yield). ¹H NMR (400 MHz, CDCl₃) δ 7.72 (m, 2H), 7.68 (d, $J = 8.4$ Hz, 1H), 7.40 (t, $J = 7.6$ Hz, 1H), 7.21 (t, $J = 7.5$ Hz, 1H), 7.04 (dd, $J = 9.0, 2.4$ Hz, 1H), 6.81 (s, 1H), 3.44 (m, 4H), 2.08 (m, 4H). ¹³C NMR (101 MHz, CDCl₃) δ 146.0, 135.4, 128.9, 128.0, 127.7,

126.2, 125.9, 121.3, 115.8, 104.7, 47.9, 25.6. HRMS (ESI): calculated for C₁₄H₁₅N ([M+H]⁺) 198.1278, found 198.1276. ¹H NMR, ¹³C NMR and ¹⁹F NMR data matched those previously reported.²⁶

2-(1-pyrrolidinyl)pyridine General procedure D was followed using 2-bromopyridine as the aryl halide and dry pyrrolidine as the amine. Purification was done by flash chromatography on silica gel, eluting with a gradient of 1:2 ethyl acetate/hexanes to give the product as a yellow liquid (121mg, 68%). ¹H NMR (400 MHz, CDCl₃) δ 8.15 (m, 1H), 7.41 (m, 1H), 6.50 (m, 1H), 6.34 (m, 1H), 3.44 (m, 4H), 2.00 (m, 4H). ¹³C NMR (101 MHz, CDCl₃) δ 157.5, 148.3, 137.0, 111.1, 106.6, 46.8, 25.7. HRMS (ESI): calculated for C₉H₁₂N₂ ([M+H]⁺) 149.1000, found 149.1074. ¹H NMR, ¹³C NMR and ¹⁹F NMR data matched those previously reported.²⁷

N-[4-(trifluoromethyl)phenyl]2-furanmethanamine General procedure D was followed using 4-bromobenzonitrile as the aryl halide and furfurylamine as the amine. Purification was done by flash chromatography on silica gel, eluting with a gradient of a gradient of 10% ethyl acetate/hexanes to give the product as a white solid. (233 mg, 98%). ¹H NMR (300 MHz, CDCl₃) δ 7.50-7.32 (m, 3H), 6.69 (d, *J* = 8.7, 2H), 6.34 (dd, *J* = 3.2, 1.8 Hz, 1H), 6.25 (td, *J* = 3.0, 1.5 Hz, 1H), 4.36 (s, 3H). ¹³C NMR (101 MHz, CDCl₃) δ 151.9, 150.1, 142.3, 126.7 (q, *J* = 3.7 Hz), 125.0 (q, *J* = 270.4 Hz), 119.6 (q, *J* = 32.7 Hz), 112.3, 110.6, 107.5, 41.0. ¹⁹F NMR (376 MHz, CDCl₃) δ -61.09. HRMS (ESI): calculated for C₁₂H₁₀F₃NO ([M+H]⁺) 240.0631, found 240.0636.

N-propyl-4-(trifluoromethyl)Benzenamine General procedure D was followed using 4-bromobenzotrifluoride as the aryl halide and propylamine as the amine. Purification was done by

flash chromatography on silica gel, eluting with a gradient of 10% ethyl acetate/hexanes to give the product as a yellow liquid (210 mg, 86%). ¹H NMR (400 MHz, CDCl₃) δ 7.40 (d, *J* = 8.9, 2H), 6.59 (d, *J* = 8.6, 2H), 3.99 (s, 1H), 3.12 (t, *J* = 7.1, 2H), 1.66 (m, 2H), 1.02 (t, *J* = 7.4, 3H). ¹³C NMR (400 MHz, CDCl₃) δ 151.0, 126.7 (q, *J* = 3.8), 125.2 (q, *J* = 270.2), 118.5 (q, *J* = 32.5), 111.8, 45.4, 22.6, 11.6. ¹⁹F NMR (376 MHz, CDCl₃) δ -60.93. HRMS (ESI): calculated for C₁₀H₁₂F₃N ([M+H]⁺) 204.1000, found 204.1011

***N*-propyl-[1,1'-biphenyl]-4-amine** General procedure D was adjusted slightly using 4-bromobiphenyl as the aryl halide and propylamine as the amine. However the reaction was run for 48 hours instead of the normal 24 h. Purification was done by flash chromatography on silica gel, eluting with a gradient of 0-10% ethyl acetate in hexanes to give the product as a yellow solid (172 mg, 68%). ¹H NMR (400 MHz, CDCl₃) δ 7.65-7.52 (m, 2H), 7.53-7.37 (m, 4H), 7.33-7.20 (m, 1H), 6.78-6.62 (m, 2H), 3.75 (s, 1H), 3.15 (t, *J* = 7.1 Hz, 2H), 1.96-1.53 (m, 2H), 1.05 (t, *J* = 7.4 Hz, 3H). ¹³C NMR (101MHz, CDCl₃) δ 148.0, 141.4, 130.0, 128.7, 128.0, 126.4, 126.3, 126.1, 113.0, 45.9, 22.8, 11.8. HRMS (ESI): calculated for C₁₅H₁₇N ([M+H]⁺) 212.1439, found 212.1438.

C-S Bond Formation Substrate Scope

4-methoxyphenyl phenyl sulfide General procedure E was followed using 4-bromoanisole as the aryl halide and thiophenol as the thiol. Purification was done by flash chromatography on silica gel, eluting with a gradient of 0-4% EtOAc/hexanes to give the product as a clear oil (114 mg, 44%). ¹H NMR (400 MHz, CDCl₃) δ 7.42 (d, *J* = 8.8 Hz, 2H), 7.23 (d, *J* = 7.7 Hz, 2H), 7.20-7.10 (m, 3H), 6.90 (d, *J* = 8.8 Hz, 2H), 3.82 (s, 3H). ¹³C NMR (101M Hz, CDCl₃) δ 159.9, 138.7, 135.5,

129.1, 128.3, 125.9, 124.4, 115.1, 55.5. HRMS (ESI): calculated for C₁₃H₁₂OS ([M+H]⁺) 217.0609, found 217.0687. ¹H NMR and ¹³C NMR data matched those previously reported.²⁸

4-cyanophenyl phenyl sulfide General procedure E was followed using 4-bromobenzonitrile as the aryl halide and thiophenol as the thiol. Purification was done by flash chromatography on silica gel, eluting with 4% EtOAc/hexanes to give the product as a clear oil (233 mg, 92%). ¹H NMR (400 MHz, CDCl₃) δ 7.54-7.40 (m, 7H), 7.16 (d, *J* = 8.5 Hz, 2H). ¹³C NMR (101 MHz, CDCl₃) δ 145.8, 134.5, 132.4, 130.8, 130.0, 129.4, 127.3, 118.9, 108.7. HRMS (ESI): calculated for C₁₃H₉NS ([M+H]⁺) 212.0456, found 212.0534. ¹H NMR, ¹³C NMR data matched those previously reported.²⁸

4-Phenylsulfanylacetophenone General procedure E was followed using 4-bromoacetophenone as the aryl halide and thiophenol as the thiol. Purification was done by flash chromatography on silica gel, eluting with a gradient of 4-10% EtOAc/hexanes to give the product as a white solid (174mg, 64%). ¹H NMR (400 MHz, CDCl₃) δ 7.82 (d, *J* = 8.5, 2H), 7.54-7.46 (m, 3H), 7.44-7.35 (m, 2H), 7.21 (d, *J* = 8.5 Hz, 2H). ¹³C NMR (101 MHz, CDCl₃) δ 197.3, 145.1, 134.6, 134.0, 132.2, 129.8, 129.0, 128.9, 127.6, 26.6. HRMS (ESI): calculated for C₁₄H₁₂OS ([M+H]) 229.0609, found 229.0682. ¹H NMR and ¹³C NMR data matched those previously reported.²⁹

4-Methoxyphenyl(4-(trifluoromethyl)phenyl)sulfane General procedure E was followed using 4-bromobenzotrifluoride as the aryl halide and 4-methoxybenzyl mercaptan as the thiol. Purification was done by flash chromatography on silica gel, eluting with 3.5% EtOAc/hexanes to give the product as a slightly yellow solid (347 mg, 96% [338 mg, 94% using general procedure F]). ¹H

NMR (400 MHz, CDCl₃) δ = 7.49 (d, J = 8.5 Hz, 2H), 7.35 (d, J = 8.9 Hz, 2H), 7.27 (d, J = 8.5 Hz, 2H), 6.85 (d, J = 8.8 Hz, 2H), 4.15 (s, 2H), 3.80 (s, 3H). ¹³C NMR (101 MHz, CDCl₃) δ = 159.1, 142.4, 130.7, 130.0, 128.3, 128.0, 127.6, 125.7, 114.2, 55.4, 37.6. ¹⁹F NMR (376 MHz, CDCl₃) δ -62.45 (s). HRMS (ESI): calculated for C₁₅H₁₃F₃OS ([M+H]⁺) 299.0639, found 299.0717. ¹H NMR, ¹³C NMR and ¹⁹F NMR data matched those previously reported.²⁸

This reaction was also conducted using 4-bromobenzotrifluoride (10 mmol) as the aryl halide and 4-methoxybenzyl mercaptan as the thiol. The reaction was run at room temperature for 24 hours. Purification was done by flash chromatography on silica gel, eluting with 3.5% EtOAc/hexanes to give the product as a slightly yellow solid (2.923g, 98% yield).

1-methoxy-4-[(2-naphthalenythio)methyl]benzene General procedure E was followed using 2-bromonaphthalene as the aryl halide and 4-methoxybenzyl mercaptan as the thiol. Purification was done by flash chromatography on silica gel, eluting with 4% EtOAc/hexanes to give the product as a white solid (260 mg, 77%). ¹H NMR (400 MHz, CDCl₃) δ 7.79 (d, J = 7.9 Hz, 1H), 7.79 – 7.69 (m, 3H), 7.50 – 7.37 (m, 3H), 7.26 (d, J = 8.5 Hz, 2H), 6.83 (d, J = 8.5 Hz, 2H), 4.19 (s, 2H), 3.78 (s, 3H). ¹³C NMR (101 MHz, CDCl₃) δ 158.9, 134.2, 133.8, 132.0, 130.1, 129.3, 128.4, 127.8, 127.8, 127.6, 127.3, 126.6, 125.8, 114.1, 55.4, 38.4. HRMS (ESI): calculated for C₁₈H₁₆OS ([M+H]⁺) 281.0922, found 281.1000.

4-(octylthio)1,1'-biphenyl General procedure E was followed using 4-bromobiphenyl as the aryl halide and 1-octanethiol as the thiol. Purification was done by flash chromatography on silica gel, eluting with 2% EtOAc/hexanes to give the product as a white solid (345 mg, 96%). ¹H NMR (400 MHz, CDCl₃) δ 7.64-7.58 (m, 2H), 7.55 (d, J = 8.4 Hz, 2H), 7.49-7.31 (m, 5H), 2.98 (t, J = 7.4),

1.72 (p, $J = 7.4$ Hz, 2H), 1.54-1.41 (m, 2H), 1.40-1.20 (m, 8H), 1.07-0.78 (m, 3H). ^{13}C NMR (101 MHz, CDCl_3) δ 140.6, 138.6, 136.4, 129.1, 128.9, 127.6, 127.3, 127.0, 33.6, 31.9, 29.3 (3C), 29.0, 22.8, 14.3. HRMS (ESI): calculated for $\text{C}_{20}\text{H}_{26}\text{S}$ ($[\text{M}+\text{H}]^+$) 299.1755, found 299.1828.

1-(octylthio)-4-(methoxy)benzene General procedure E was followed using 4-bromoanisole as the aryl halide and 1-octanethiol as the thiol. Purification was done by flash chromatography on silica gel, eluting with 2% EtOAc/hexanes to give the product as an oil (230 mg, 76%). ^1H NMR (400 MHz, CDCl_3) δ 7.33 (d, $J = 8.8$ Hz, 2H), 6.84 (d, $J = 8.8$ Hz, 2H), 3.79 (s, 3H), 2.81 (t, $J = 7.5$), 1.58 (dt, $J = 15.0, 7.3$ Hz, 2H) 1.38 (m, 2H), 1.30-1.21 (s, 8H), 0.87 (t, $J = 7.1$ Hz, 3H). ^{13}C NMR (101 MHz, CDCl_3) δ 158.8, 133.0, 127.1, 114.6, 55.4, 36.0, 31.9, 29.5, 29.3 (2C), 28.9, 22.8, 14.3. HRMS (ESI): calculated for $\text{C}_{15}\text{H}_{24}\text{OS}$ ($[\text{M}+\text{H}]^+$) 253.1548, found 253.1621.

S-(4-trifluoromethylphenyl)-N-[(1,1-dimethylethoxy)carbonyl]-methyl ester General procedure E was followed using 4-bromobenzonitrile as the aryl halide and *N*-(tert-butoxycarbonyl)-L-cysteine methyl ester as the thiol. Purification was done by flash chromatography on silica gel, eluting with 1:9 ethyl acetate/hexanes to give the product as a white solid (394 mg, 98%). ^1H NMR (400 MHz, CDCl_3) δ = 7.52 (dd, $J = 8.5, 1.7$ Hz, 2H), 7.38 (dd, $J = 8.5, 1.7$ Hz, 2H), 5.36 (m, 1H), 4.60 (m, 1H), 3.65 (d, $J = 1.6$, 3H), 3.45 (m, 2H), 1.39 (d, $J = 1.39$, 9H). ^{13}C NMR (101 MHz, CDCl_3) δ 170.6, 154.9, 143.0, 132.4, 128.4, 118.6, 109.3, 80.4, 53.3, 52.7, 35.2, 28.3. HRMS (ESI): calculated for $\text{C}_{16}\text{H}_{20}\text{N}_2\text{O}_4\text{S}$ ($[\text{M}+\text{Li}]^+$) 343.1304, found 343.1297.

S-(4-cyanophenyl)-N-[(1,1-dimethylethoxy)carbonyl]-methyl ester General procedure E was followed using 4-bromobenzotrifluoride as the aryl halide and *N*-(tert-butoxycarbonyl)-L-cysteine methyl ester as the thiol. Purification was done by flash chromatography on silica gel,

eluting with 1:9 ethyl acetate/hexanes to give the product as a white solid (373 mg, 82%). ¹H NMR (400 MHz, CDCl₃) δ = 7.53 (d, *J* = 8.5 Hz, 2H), 7.46 (d, *J* = 8.3 Hz, 2H), 5.31 (d, *J* = 7.8 Hz, 1H), 4.61 (dd, *J* = 8.2, 4.6, 1H), 3.62 (s, 3H), 3.45 (qd, *J* = 14.1, 4.8 Hz, 2H), 1.41 (s, 9H). ¹³C NMR (101 MHz, CDCl₃) δ = 170.9, 155.0, 140.6, 129.5, 128.7 (q, *J* = 32.6), 125.9 (q, *J* = 3.8), 124.0 (q, *J* = 271.8). ¹⁹F NMR (376 MHz, CDCl₃) δ – 62.61. HRMS (ESI): calculated for C₁₆H₂₀F₃NO₄S ([M+Li]⁺) 380.1226, found 380.1222.

1-[(4-methylphenyl)thio]-4-(trifluoromethyl)-benzene General procedure E was followed using 4-bromobenzotrifluoride as the aryl halide and 4-methylbenzenethiol as the thiol. Purification was done by flash chromatography on silica gel, eluting with hexanes to give the product as a white solid (267 mg, 83%). ¹H NMR (400 MHz, CDCl₃) δ 7.49 (m, 4H), 7.27 (m, 4H), 2.44 (s, 3H). ¹³C NMR (101 MHz, CDCl₃) δ 144.1 (d, *J* = 1.6 Hz), 139.4, 134.4, 130.7, 128.4, 127.5, 125.8 (q, *J* = 3.8 Hz), 124.3 (q, *J* = 279.6 Hz), 21.3. ¹⁹F NMR (376 MHz, CDCl₃) δ -62.36. HRMS (ESI): calculated for C₁₄H₁₁F₃S ([M]⁺) 268.0533, found 268.0522.

1-(cyclohexylthio)-4-(trifluoromethyl)-benzene General procedure E was followed using 4-bromobenzotrifluoride as the aryl halide and cyclohexanethiol as the thiol. Purification was done by flash chromatography on silica gel, eluting with hexanes to give the product as a colorless liquid (290 mg, 93 %). ¹H NMR (400 MHz, CDCl₃) δ 7.51 (m, 2H), 7.42 (m, 2H), 3.25 (m, 1H), 2.02, (m, 2H), 1.79 (m, 2H), 1.64 (m, 1H), 1.37 (m, 5H). ¹³C NMR (101 MHz, CDCl₃) δ 144.4 (d, *J* = 1.6 Hz), 129.8, 128.0 (q, *J* = 32.6 Hz), 125.7 (q, *J* = 3.8 Hz), 124.3 (q, *J* = 279.6 Hz), 45.7, 33.2, 26.1, 25.8. ¹⁹F NMR (376 MHz, CDCl₃) δ -62.47. HRMS (ESI): calculated for C₁₃H₁₅F₃S([M]⁺) 260.0847, found 260.0836.

References

- (1) a) J. W. Tucker, C. R. J. Stephenson, *J. Org. Chem.* 2012, *77*, 1617-1622; b) C. K. Prier, D. A. Rankic, D. W. C. MacMillan, *Chem. Rev.* 2013, *113*, 5322-5363; c) D. M. Schultz, T. P. Yoon, *Science* 2014, *343*, 1239176.
- (2) a) Y. You, W. Nam, *Chem. Soc. Rev.* 2012, *41*, 7061-7084; b) B. O'Regan, M. Gratzel, *Nature* 1991, *353*, 737-740; c) P. Wang, S. M. Zakeeruddin, J. E. Moser, M. K. Nazeeruddin, T. Sekiguchi, M. Gratzel, *Nat. Mater.* 2003, *2*, 402-407.
- (3) C. Adachi, M. A. Baldo, M. E. Thompson, S. R. Forrest, *J. Appl. Phys.* 2001, *90*, 5048-5051.
- (4) a) M. R. Gill, J. Garcia-Lara, S. J. Foster, C. Smythe, G. Battaglia, J. A. Thomas, *Nat. Chem.* 2009, *1*, 662-667; b) K. K.-W. Lo, *Acc. Chem. Res.* 2015, *48*, 2985-2995.
- (5) C. S. Allardyce, P. J. Dyson, *Platin. Met. Rev.* 2001, *45*, 62-69.
- (6) F. Li, J. G. Collins, F. R. Keene, *Chem. Soc. Rev.* 2015, *44*, 2529-2542.
- (7) a) D. M. Arias-Rotondo, J. K. McCusker, *Chem. Soc. Rev.* 2016, *45*, 5803-5820; b) S. Lamansky, P. Djurovich, D. Murphy, F. Abdel-Razzaq, R. Kwong, I. Tsyba, M. Bortz, B. Mui, R. Bau, M. E. Thompson, *Inorg. Chem.* 2001, *40*, 1704-1711.
- (8) a) L. Flamigni, A. Barbieri, C. Sabatini, B. Ventura, F. Barigelletti, in *Photochemistry and Photophysics of Coordination Compounds II* (Eds.: V. Balzani, S. Campagna), Springer Berlin Heidelberg, Berlin, Heidelberg, 2007, pp. 143-203; b) A. Juris, V. Balzani, F. Barigelletti, S. Campagna, P. Belser, A. von Zelewsky, *Coord. Chem. Rev.* 1988, *84*, 85-277.
- (9) a) C. R. Bock, J. A. Connor, A. R. Gutierrez, T. J. Meyer, D. G. Whitten, B. P. Sullivan, J. K. Nagle, *J. Am. Chem. Soc.* 1979, *101*, 4815-4824; b) K. A. King, P. J. Spellane, R. J. Watts, *J. Am. Chem. Soc.* 1985, *107*, 1431-1432.

- (10) a) R. F. Higgins, S. M. Fatur, S. G. Shepard, S. M. Stevenson, D. J. Boston, E. M. Ferreira, N. H. Damrauer, A. K. Rappé, M. P. Shores, *J. Am. Chem. Soc.* 2016, *138*, 5451-5464; b) Q. M. Kainz, C. D. Matier, A. Bartoszewicz, S. L. Zultanski, J. C. Peters, G. C. Fu, *Science* 2016, *351*, 681-684.
- (11) a) N. A. Romero, D. A. Nicewicz, *Chem. Rev.* 2016, *116*, 10075-10166; b) M. Neumann, S. Földner, B. König, K. Zeitler, *Angew. Chem. Int. Ed.* 2011, *50*, 951-954.
- (12) a) N. Corrigan, S. Shanmugam, J. Xu, C. Boyer, *Chem. Soc. Rev.* 2016, *45*, 6165-6212; b) M. Chen, M. Zhong, J. A. Johnson, *Chem. Rev.* 2016, *116*, 10167-10211; c) M. H. Shaw, J. Twilton, D. W. C. MacMillan, *J. Org. Chem.* 2016, *81*, 6898-6926.
- (13) a) D. P. Hari, B. König, *Chem. Comm.* 2014, *50*, 6688-6699; b) R. S. Rohokale, B. Koenig, D. D. Dhavale, *J. Org. Chem.* 2016, *81*, 7121-7126; c) A. U. Meyer, K. Straková, T. Slanina, B. König, *Chem. Eur. J.* 2016, *22*, 8694-8699.
- (14) E. Yoshioka, S. Kohtani, T. Jichu, T. Fukazawa, T. Nagai, A. Kawashima, Y. Takemoto, H. Miyabe, *J. Org. Chem.* 2016, *81*, 7217-7229.
- (15) a) J. K. Matsui, G. A. Molander, *Org. Lett.* 2017, *19*, 950-953; b) A. Joshi-Pangu, F. Lévesque, H. G. Roth, S. F. Oliver, L.-C. Campeau, D. Nicewicz, D. A. DiRocco, *J. Org. Chem.* 2016, *81*, 7244-7249; c) E. Alfonzo, F. S. Alfonso, A. B. Beeler, *Org. Lett.* 2017, *19*, 2989-2992; d) K. A. Margrey, D. A. Nicewicz, *Acc. Chem. Res.* 2016, *49*, 1997-2006; e) H. Kotani, K. Ohkubo, S. Fukuzumi, *J. Am. Chem. Soc.* 2004, *126*, 15999-16006.
- (16) I. Ghosh, T. Ghosh, J. I. Bardagi, B. König, *Science* 2014, *346*, 725-728.
- (17) a) J. Luo, J. Zhang, *ACS Catal.* 2016, *6*, 873-877; b) H. Uoyama, K. Goushi, K. Shizu, H. Nomura, C. Adachi, *Nature* 2012, *492*, 234-238.

- (18) a) S. O. Poelma, G. L. Burnett, E. H. Discekici, K. M. Mattson, N. J. Treat, Y. Luo, Z. M. Hudson, S. L. Shankel, P. G. Clark, J. W. Kramer, C. J. Hawker, J. Read de Alaniz, *J. Org. Chem.* 2016, *81*, 7155-7160; b) N. J. Treat, H. Sprafke, J. W. Kramer, P. G. Clark, B. E. Barton, J. Read de Alaniz, B. P. Fors, C. J. Hawker, *J. Am. Chem. Soc.* 2014, *136*, 16096-16101; c) E. H. Discekici, N. J. Treat, S. O. Poelma, K. M. Mattson, Z. M. Hudson, Y. Luo, C. J. Hawker, J. R. de Alaniz, *Chem. Commun.* 2015, *51*, 11705-11708.
- (19) a) G. M. Miyake, J. C. Theriot, *Macromolecules* 2014, *47*, 8255-8261; b) J. C. Theriot, C.-H. Lim, H. Yang, M. D. Ryan, C. B. Musgrave, G. M. Miyake, *Science* 2016, *352*, 1082-1086.
- (20) a) K. Matyjaszewski, J. Xia, *Chem. Rev.* 2001, *101*, 2921-2990; b) M. Ouchi, T. Terashima, M. Sawamoto, *Chem. Rev.* 2009, *109*, 4963-5050.
- (21) S. Shanmugam, C. Boyer, *Science* 2016, *352*, 1053-1054.
- (22) A. A. Isse, C. Y. Lin, M. L. Coote, A. Gennaro, *J. Phys. Chem. B* 2011, *115*, 678-684.
- (23) C.-H. Lim, M. D. Ryan, B. G. McCarthy, J. C. Theriot, S. M. Sartor, N. H. Damrauer, C. B. Musgrave, G. M. Miyake, *J. Am. Chem. Soc.* 2017, *139*, 348-355.
- (24) R. M. Pearson, C.-H. Lim, B. G. McCarthy, C. B. Musgrave, G. M. Miyake, *J. Am. Chem. Soc.* 2016, *138*, 11399-11407.
- (25) J. C. Theriot, B. G. McCarthy, C.-H. Lim, G. M. Miyake, *Macromol. Rapid Commun.* 2017, 1700040.
- (26) a) S. Hiraoka, T. Okamoto, M. Kozaki, D. Shiomi, K. Sato, T. Takui, K. Okada, *J. Am. Chem. Soc.* 2004, *126*, 58-59; b) Y. Zhu, A. P. Kulkarni, P.-T. Wu, S. A. Jenekhe, *Chem. Mater.* 2008, *20*, 4200-4211.
- (27) a) M. D. Ryan, J. C. Theriot, C.-H. Lim, H. Yang, A. G. Lockwood, N. G. Garrison, S. R. Lincoln, C. B. Musgrave, G. M. Miyake, *J. Polym. Sci. A Polym. Chem.* 2017, DOI:

10.1002/pola.28574; b) U. Resch-Genger, M. Grabolle, S. Cavaliere-Jaricot, R. Nitschke, T. Nann, *Nat. Methods* 2008, 5, 763-775.

(28) A. J. Bard, L. R. Faulkner, *Electrochemical Methods: Fundamentals and Applications*, Second ed., Wiley, 2001.

(29) N. G. Connelly, W. E. Geiger, *Chem. Rev.* 1996, 96, 877-910.

(30) The oxidation of **4** occurs near the oxidation window of DMA, which causes the i_{pa}/i_{pc} to deviate from 1; **4**'s i_{pa}/i_{pc} values improve to 1.11 in DMF and 1.01 in THF with increasingly wider solvent oxidation window (see supporting information).

(31) C. P. Andrieux, L. Gelis, M. Medebielle, J. Pinson, J. M. Saveant, *J. Am. Chem. Soc.* 1990, 112, 3509-3520.

(32) a) N. Iqbal, S. Choi, E. Ko, E. J. Cho, *Tetrahedron Lett.* 2012, 53, 2005-2008; b) J. D. Nguyen, J. W. Tucker, M. D. Konieczynska, C. R. J. Stephenson, *J. Am. Chem. Soc.* 2011, 133, 4160-4163; c) P. V. Pham, D. A. Nagib, D. W. C. MacMillan, *Angew. Chem. Int. Ed.* 2011, 50, 6119-6122; d) C.-J. Wallentin, J. D. Nguyen, P. Finkbeiner, C. R. J. Stephenson, *J. Am. Chem. Soc.* 2012, 134, 8875-8884; e) T. Koike, M. Akita, *Top. Catal.* 2014, 57, 967-974.

(33) J. A. Terrett, J. D. Cuthbertson, V. W. Shurtleff, D. W. C. MacMillan, *Nature* 2015, 524, 330-334.

(34) M. S. Oderinde, M. Frenette, D. W. Robbins, B. Aquila, J. W. Johannes, *J. Am. Chem. Soc.* 2016, 138, 1760-1763.

(35) a) E. B. Corcoran, M. T. Pirnot, S. Lin, S. D. Dreher, D. A. DiRocco, I. W. Davies, S. L. Buchwald, D. W. C. MacMillan, *Science* 2016, 353, 279-283; b) M. S. Oderinde, N. H. Jones, A. Juneau, M. Frenette, B. Aquila, S. Tentarelli, D. W. Robbins, J. W. Johannes, *Angew. Chem. Int. Ed.* 2016, 55, 13219-13223.

(36) a) B. J. Shields, A. G. Doyle, *J. Am. Chem. Soc.* 2016, *138*, 12719-12722; b) C. C. Le, D. W. C. MacMillan, *J. Am. Chem. Soc.* 2015, *137*, 11938-11941; c) A. Noble, S. J. McCarver, D. W. C. MacMillan, *J. Am. Chem. Soc.* 2015, *137*, 624-627; d) M. Jouffroy, D. N. Primer, G. A. Molander, *J. Am. Chem. Soc.* 2016, *138*, 475-478; e) J. C. Tellis, D. N. Primer, G. A. Molander, *Science* 2014, *345*, 433-436; f) Z. Zuo, D. T. Ahneman, L. Chu, J. A. Terrett, A. G. Doyle, D. W. C. MacMillan, *Science* 2014, *345*, 437-440; g) M. H. Shaw, V. W. Shurtleff, J. A. Terrett, J. D. Cuthbertson, D. W. C. MacMillan, *Science* 2016, *352*, 1304-1308.

(37) E. R. Welin, C. Le, D. M. Arias-Rotondo, J. K. McCusker, D. W. C. MacMillan, *Science* 2017, *355*, 380-385.

(38) a) N. Miyaura, A. Suzuki, *Chem. Rev.* 1995, *95*, 2457-2483; b) P. Ruiz-Castillo, S. L. Buchwald, *Chem. Rev.* 2016, *116*, 12564-12649; c) Á. Molnár, *Chem. Rev.* 2011, *111*, 2251-2320; d) R. Jana, T. P. Pathak, M. S. Sigman, *Chem. Rev.* 2011, *111*, 1417-1492.

References in Experimental

(1) Theriot, J. C.; Lim, C.-H.; Yang, H.; Ryan, M. D.; Musgrave, C. B.; Miyake, G. M. *Science* 2016, *352*, 1082.

(2) Pearson, R. M.; Lim, C.-H.; McCarthy, B. G.; Musgrave, C. B.; Miyake, G. M. *J. Am. Chem. Soc.* 2016, *138*, 11399.

(3) R. Bonneau, I. C. a. G. L. H. *Pure Appl. Chem.* 1991, *63*, 289.

(4) Yersin, T. H. a. H. *Inorg. Chem.* 2010, *49*, 9290.

(5) Salman, H.; Abraham, Y.; Tal, S.; Meltzman, S.; Kapon, M.; Tessler, N.; Speiser, S.; Eichen, Y. *Eur. J. Org. Chem.* 2005, 2207.

(6) Dhanak, D.; Reese, C. B. *J. Chem. Soc., Perkin Trans.* 1986, *2*, 2181.

- (7) Wang, P.; Blank, D. H.; Spencer, T. A. *J. Org. Chem.* 2004, *69*, 2693.
- (8) Vyvyan, J. R.; Meyer, J. A.; Meyer, K. D. *J. Org. Chem.* 2003, *68*, 9144.
- (9) Sinha, S. C.; Sinha-Bagchi, A.; Keinan, E. *J. Org. Chem.* 1993, *58*, 7789.
- (10) Choi, W. J.; Choi, S.; Ohkubo, K.; Fukuzumi, S.; Cho, E. J.; You, Y. *Chem. Sci.* 2015, *6*, 1454.
- (11) Baar, M.; Blechert, S. *Chem. Eur. J.* 2015, *21*, 526.
- (12) Seo, S.; Taylor, J. B.; Greaney, M. F. *Chem. Commun.* 2013, *49*, 6385.
- (13) Pedroni, J.; Cramer, N. *Org. Lett.* 2016, *18*, 1932.
- (14) Wiehn, M. S.; Vinogradova, E. V.; Togni, A. *J. Fluorine Chem.* 2010, *131*, 951.
- (15) Arimori, S.; Shibata, N. *Org. Lett.* 2015, *17*, 1632.
- (16) Mormino, M. G.; Fier, P. S.; Hartwig, J. F. *Org. Lett.* 2014, *16*, 1744.
- (17) Natte, K.; Jagadeesh, R. V.; He, L.; Rabeah, J.; Chen, J.; Taeschler, C.; Ellinger, S.; Zaragoza, F.; Neumann, H.; Brückner, A.; Beller, M. *Angew. Chem., Int. Ed.* 2016, *55*, 2782.
- (18) Li, L.; Mu, X.; Liu, W.; Wang, Y.; Mi, Z.; Li, C.-J. *J. Am. Chem. Soc.* 2016, *138*, 5809.
- (19) Chu, L.; Qing, F.-L. *Org. Lett.* 2010, *12*, 5060.
- (20) Sladojevich, F.; McNeill, E.; Börgel, J.; Zheng, S.-L.; Ritter, T. *Angew. Chem., Int. Ed.* 2015, *54*, 3712.
- (21) Iqbal, N.; Choi, S.; Kim, E.; Cho, E. J. *J. Org. Chem.* 2012, *77*, 11383.
- (22) Fuchikami, T.; Ojima, I. *Tetrahedron Letters* 1984, *25*, 303.
- (23) Hang, Z.; Li, Z.; Liu, Z.-Q. *Org. Lett.* 2014, *16*, 3648.
- (24) Corcoran, E. B.; Pirnot, M. T.; Lin, S.; Dreher, S. D.; DiRocco, D. A.; Davies, I. W.; Buchwald, S. L.; MacMillan, D. W. C. *Science* 2016, *353*, 279.

- (25) Hamid, M. H. S. A.; Allen, C. L.; Lamb, G. W.; Maxwell, A. C.; Maytum, H. C.; Watson, A. J. A.; Williams, J. M. J. *J. Am. Chem. Soc.* 2009, *131*, 1766.
- (26) So, C. M.; Zhou, Z.; Lau, C. P.; Kwong, F. Y. *Angew. Chem., Int. Ed.* 2008, *47*, 6402.
- (27) Londregan, A. T.; Jennings, S.; Wei, L. *Org. Lett.* 2010, *12*, 5254.
- (28) Prasad, D. J. C.; Sekar, G. *Org. Lett.* 2011, *13*, 1008.
- (29) Sperotto, E.; van Klink, G. P. M.; de Vries, J. G.; van Koten, G. *J. Org. Chem.* 2008, *73*, 5625.

Chapter 6 – Summary

The work presented in this dissertation focused on the design and synthesis of photoredox catalysts for organo-catalyzed atom transfer polymerization and a variety of small molecule reactions. These photoredox catalysts offer sustainable alternatives to precious metal-containing photoredox catalysts.

Since the report of the first phenoxazine photoredox catalysts, our group has further investigated how we could utilize both the N (10-) position of the phenoxazine core as well as the 3- and 7- positions on the core to install substituents to modify the photoredox properties and ability to access a charge transfer excited state- a property which was shown to be important in the seminal *N,N*-diaryl dihydrophenazine paper.¹⁻³ Through this study we have realized catalysts which have excited state reduction potentials ranging from -1.42 V vs .SCE to -2.11 V vs. SCE. In a later study we investigated how the nature of the charge transfer excited state affects the triplet quantum yield of these catalysts.

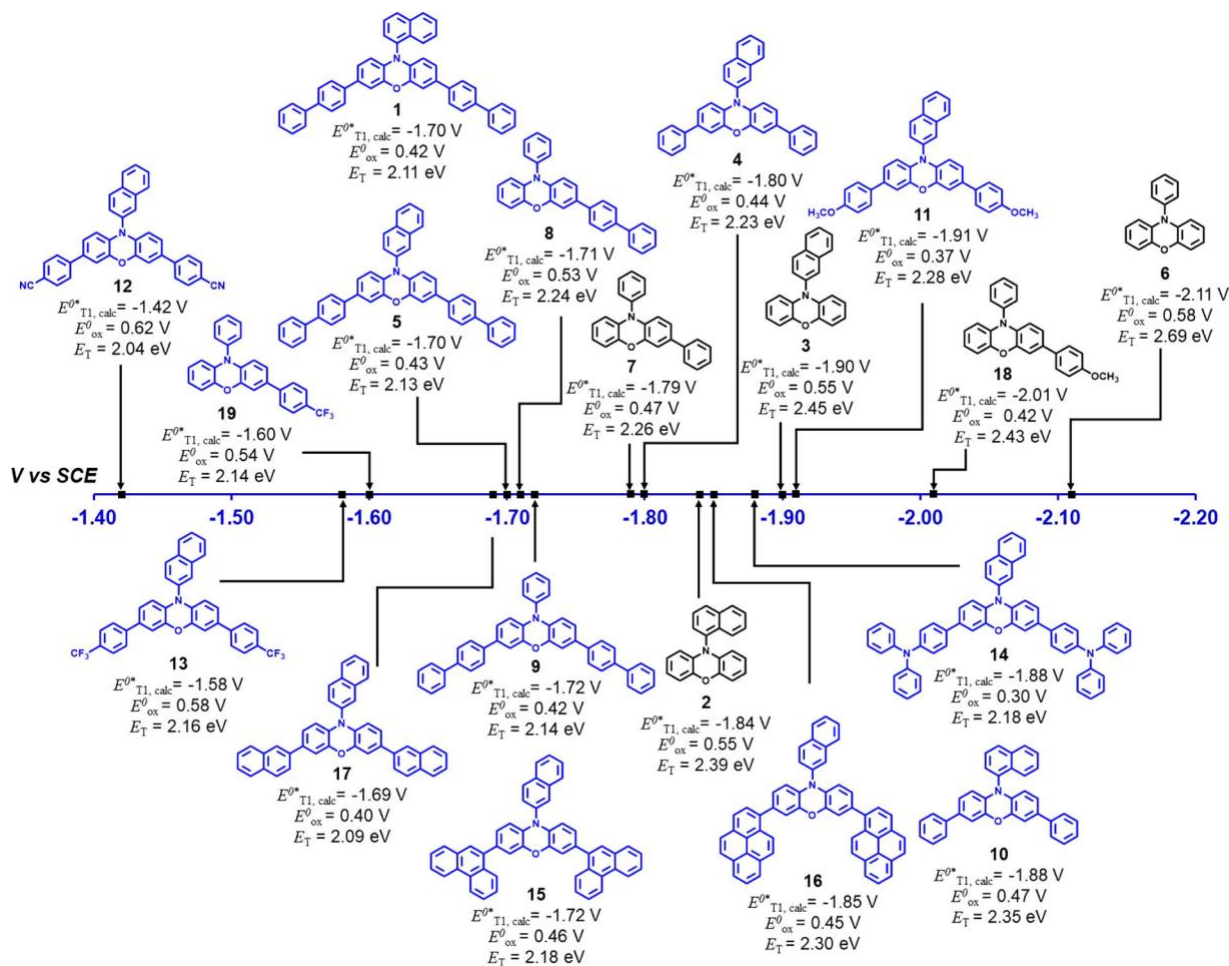


Figure 6.1. Figure adapted from ref 1, designed by Blaine McCarthy. Structures, calculated triplet excited state reduction potentials ($E^{0*}T1_{calc}$ [$PC^{\bullet+}/\beta PC^*$]), calculated oxidation potential of $^2PC^{\bullet+}$ ($E^0_{calc} = E^0$ [$^2PC^{\bullet+}/^1PC$]), and calculated triplet energies (E_T) of phenoxazines investigated in this study. Catalysts colored in gray are UVA light absorbing and catalysts colored in blue are visible light absorbing.

Over the past 3 years, additional studies focused on employing these catalysts in flow reactors for the O-ATRP of a myriad of monomers including benzyl methacrylate, di(ethylene glycol) methyl ether methacrylate, and isodecyl methacrylate.⁴ In the case of methyl methacrylate,

residence time of 90 minutes achieved initiator efficiencies of 90%, 71% monomer conversion, and D of 1.27 while 10 times less catalyst than batch reactors. Using a core-first approach to initiation, Buss et. al demonstrated that phenoxazines could synthesize advanced architectures such as 2, 3, 4, 6, and 8 arm stars.⁵ In the same year, McCarthy et. al. reported that phenoxazines could mediate O-ATRP in a controlled fashion in the presence of oxygen, and Rao et al. presented the first report of a organocatalyzed, visible-light-driven conversion of CO₂ to CH₄ using phenoxazine as an organic sensitizer in tandem with an iron porphyrin catalyst.^{6,7} Lastly, in 2019, a similar strategy to modifying the phenoxazine core (a bromination, followed by a cross coupling) was used by Cole et. al. to design core extended *N,N*- diaryl dihydrophenazines.⁸ Similar to when the core π system of the phenoxazines were extended by aryl substituents, the λ_{\max} of absorption was redshifted, the molar absorptivity was increased, and catalyst loadings could be decreased, and in the case of phenazines the loadings decreased from 1000 ppm to 10 ppm with similar control for the O-ATRP of acrylic monomers.

The 3,7-di(4-biphenyl) 1-naphthalene-10-phenoxazine is now being commercialized along with 5,10-di(2-Naphthyl)-5,10-dihydrophenazine by New Iridium (Figure 6.2). Which will hopefully help lead to the next generation of pharmaceutical and chemical manufacturing.

The image shows a screenshot of the Sigma-Aldrich product page for 3,7-Di(4-biphenyl) 1-naphthalene-10-phenoxazine. The page includes the product name, a purity of ≥97%, a synonym, CAS Number 1987900-95-7, Empirical Formula (Hill Notation) C₄₆H₃₁NO, and Molecular Weight 613.74. A chemical structure is displayed on the left. The right side of the page shows a table with columns for SKU-Pack Size, Availability, Price (USD), and Quantity. The table lists SKU 901111-100MG, availability 'Available to ship on 03/31/19 - FROM', a price of 108.00, and a quantity of 0. There are buttons for 'Bulk orders?' and 'ADD TO CART'. To the right of the screenshot is a photograph of a white plastic bottle with a red cap, labeled 'SIGMA-ALDRICH 901111-100MG 3,7-Di(4-biphenyl) 1-naphthalene-10-phenoxazine 97%'. The bottle is sitting on a surface next to a laptop.

Figure 6.2. A picture of the sales page for the 3,7-Di(4-biphenyl) 1-naphthalene-10-phenoxazine catalyst on Sigma-Aldrich (left), a picture of the packaged catalyst (right).

References

- (1) McCarthy, B.; Pearson, R.; Lim, C.; Sartor, S.; Damrauer, N.; Miyake, G. *J. Am. Chem. Soc.* 2018, 140, 5088-5101
- (2) Sartor, S.; McCarthy, B.; Pearson, R.; Miyake, G.; Damrauer, N. *J. Am. Chem. Soc.* 2018, 140, 4778-4781.
- (3) Theriot, J.; Lim, C.; Yang, H.; Ryan, M.; Musgrave, C.; Miyake, G. *Science*, 2016, 352, 1082-1086
- (4) Ramsey, B.; Pearson, R.; Beck, L.; Miyake, G. *Macromolecules*, 2017, 50, 2668-2674
- (5) Buss, B.; Beck, B.; Miyake, G. *Polym. Chem.*, 2018, 9, 1658-1665
- (6) McCarthy, B.; Miyake, G. *ACS Macro Lett.* 2018, 7, 1016-1021.
- (7) Rao, H.; Lim, C.; Bonin, J.; Miyake, G.; Robert, M. *J. Am. Chem. Soc.* 2018, 140, 51, 17830-17834.
- (8) Cole, J.; Federico, C.; Lim, C.; Miyake, G. *Macromolecules*, 2019, 52 (2), 747-754.

Appendix I – List of Publications by RMP
(In Graduate School)

1. Pearson, R.; Cole, J.; Miyake, G. “Synthesis and Characterization of Core-Modified Benzo[ghi]perylene Monoimides” *submitted*.
2. Ryan, M.; Pearson, R.; Miyake, G. “Organocatalyzed Controlled Radical Polymerizations”, in *Organic Catalysis for Polymerization*. Royal Chemical Society, 2018, 584-606
3. Sartor, S.; McCarthy, B.; Pearson, R.; Miyake, G.; Damrauer, N. “Exploiting Charge Transfer States for Maximizing Intersystem Crossing Yields in Organic Photoredox Catalysts” *J. Am. Chem. Soc.*, 2018, *140*, 4778 – 4781.
4. McCarthy, B.; Pearson, R.; Lim, C.; Sartor, S.; Damrauer, N.; Miyake, G. “Structure-Property Relationships for the Design of Visible Light, Strongly Reducing Phenoxazine Photoredox Catalysts and their Application in Organocatalyzed Atom Transfer Radical Polymerization” *J. Am. Chem. Soc.*, 2018, *140*, 5088 – 5101.
5. Du, Y.[†]; Pearson, R.[†]; Lim, C.[†]; Sartor, S.; Ryan, M.; Yang, H.; Damrauer, N.; Miyake, G. “Strongly Reducing, Visible-Light Organic Photoredox Catalysts as Sustainable Alternatives to Precious Metals” *Chem. Euro. J.*, 2017, *23*, 1 – 8. (*Cover article, one of the most accessed articles in 2017*)
6. Ryan, M.[†]; Pearson, R.[†]; Miyake, G. “The Impact of Light Intensity on Control in Photoinduced Organocatalyzed Atom Transfer Radical Polymerization” *Macromolecules*, 2017, *50*, 4616 – 4622.
7. Ramsey, B.; Pearson, R.; Beck, L.; Miyake, G. “Photoinduced Organocatalyzed Atom Transfer Radical Polymerization Using Continuous Flow” *Macromolecules*, 2017, *50*, 2668 – 2674.
8. Boyle, B.[†]; French, T.[†]; Pearson, R.; McCarthy, B.; Miyake, G. “Structural Color for Additive

Manufacturing: 3D-Printed Photonic Crystals from Block Copolymers” *ACS Nano*, 2017, *11*, 3052 –3058.

9. Pearson, R.[†]; Lim, C.[†]; McCarthy, B.; Musgrave, C.; Miyake, G. “Organocatalyzed Atom Transfer Radical Polymerization Using *N*-Aryl Phenoxazines as Photoredox Catalysts” *J. Am. Chem. Soc.*, 2016, *138*, 11399 – 11407.
10. Theriot, J.; Ryan, M.; French, T.; Pearson, R.; Miyake, G. “Atom Transfer Radical Polymerization of Functionalized Vinyl Monomers Using Perylene as a Visible Light Photocatalyst” *JoVE*, 2016, e53571 – e53571.